Investigation of Renewable, Coupled Solar-Hydrogen Fuel Generation with Thermal Management Systems suitable for Equatorial Regions

**A Dissertation
Submitted to the School of Engineering and Design
of Brunel University
In fulfillment for the Degree of Doctor of Philosophy**

Earle Anthony Wilson

September 2009

ABSTRACT

Solar Energy and Hydrogen (energy carrier) are possible replacement options for fossil fuel and its associated problems of availability and high prices which are devastating small, developing, oil-importing economies. But a major drawback to the full implementation of solar energy, in particular photovoltaic (PV), is the lowering of conversion efficiency of PV cells due to elevated cell temperatures while in operation. Also, hydrogen as an energy carrier must be produced in gaseous or liquid form before it can be used as fuel; but its' present major conversion process produces an abundance of carbon dioxide which is harming the environment through global warming. In search of resolutions to these issues, this research investigated the application of Thermal Management to Photovoltaic (PV) modules in an attempt to reverse the effects of elevated cell temperature. The investigation also examined the effects of coupling the thermally managed PV modules to a proton exchange membrane (PEM) Hydrogen Generator for the production of hydrogen gas in an environmentally friendly and renewable way. The research took place in Kingston, Jamaica.

The thermal management involved the application of two cooling systems which are Gravity-Fed Cooling (GFC) and Solar-Powered Adsorption Cooling (SPAC) systems. In both systems Mathematical Models were developed as predictive tools for critical aspects of the systems. The models were validated by the results of experiments. The results of the investigation showed that both cooling systems stopped the cells temperatures from rising, reversed the negative effects on conversion efficiency, and increased the power output of the module by as much as 39%. The results also showed that the thermally managed PV module when coupled to the hydrogen generator impacted positively with an appreciably increase of up to 32% in hydrogen gas production.

The results of this work can be applied to the equatorial belt but also to other regions with suitable solar irradiation. The research has contributed to the wider community by the development of practical, environmentally friendly, cost effective Thermal Management Systems that guarantee improvement in photovoltaic power output, by introducing a novel way to use renewable energy that has potential to be used by individual household and/or as cottage industry, and by the development of Mathematical Tools to aid in photovoltaic power systems designs.

ACKNOWLEGEMENTS

TABLE OF CONTENTS

LIST OF TABLES

LIST OF FIGURES

NOMENCLATURE

Variable	Definition
A	area (m^2)
c_o	orientation factor (W/m^2K^e)
c_p	specific heat capacity (J/kgK)
$c_\mathbb{P}$	combined specific heat of charcoal and methanol (J/kgK)
e	electronic charge (Coulombs)
E_c	conduction band energy (J)
E_f	Fermi level energy (J)
E_g	band gap energy (J)
f(x)	temperature of slab at time zero (^oC)
F_n	transient temperature parameter (^oC)
h	1. Enthalpy (J/kg)
	2. Planck's constant (J·s)
I_o	saturation current (A)
I_{sc}	short circuit current (A)
J_o	current density (A/m^2)
J_o/J_1	Bessel functions of order zero and one
k	1. Boltzmann constant (J/K)
	2. thermal conductivity (W/mK)
L	thickness of (PV cell) Silicon slab (m)
L_p	diffusion length (m)
$\mathcal{L}$	latent heat of vaporization of methanol (J/kg)
M	combined mass of charcoal and methanol (kg)
m	mass (kg)
m_n^*	effective mass of electrons (kg)
n	free electrons per unit volume (m^{-3})
q	elementary charge (coulombs)
q_o	solar irradiance on cell (position x = 0) (W/m^2)
R	radius of copper tube (m)
r	arbitrary radius (m)
T(t)	function of time only
t	time (s)
T	temperature (K)

U	1. temperature of cell (^{o}C)
	2. overall copper tube heat-loss coefficient (W/m^{2}K)
U_L	temperature of cooling water (^{o}C)
U_T	thermal voltage (volts)
V	transient cell temperature (^{o}C)
x	position along cell thickness (m)
x_m	mass fraction of methanol (kg/kg)
X(x)	function of direction(x) only
z	Zero of J_o

Greek	**Definition**
α	thermal diffusivity of Silicon (m^2/s)
ά	Absorptance coefficient
ε	Porosity
λ	Eigenvalues
φ	steady state cell temperature (^{o}C)
ρ	density of Silicon (kg/m^3)
$ρ_n$	electrical resistivity (ohm-cm)
τ	Transmittance coefficient
μ	mobility of charge carrier (m^2/(V.s))

Abbrev	**Definition**
AWE	Alkaline Water Electrolyzer
eq /kg	equivalent per kilogram
MEA	Membrane-Electrode Assembly
PEM	Proton Exchange Membrane
PV	Photovoltaic
SMR	Steam-Methane Reforming
SOE	Solid Oxide Electrolyzer
BOP	Balance of Plant

Subscripts	**Definition**
char	charcoal
con	condenser
cu	copper

des   desorption

m   methanol

n   1. electron

             2. total number of an arbitrary item

p   hole

s   solid

f   fluid

st   store

t   time

x   position in x-direction

T   temperature

Constants	**Definition**
Đ	charcoal specific
ń	system power specific

CHAPTER 1

INTRODUCTION

Across the globe peoples' ways of life are threaten by insufficiency and un-affordability of energy. The race is on to find answers to what comes next after the "oil age" and also if the planet can be prevented from overheating due to greenhouse gases from the burning of fossil fuel. In light of these concerns this thesis examines proposed solutions to the problems by looking at possible alternatives to fossil fuel. This chapter starts with the impact of elevated oil prices on oil- imported economies, and goes on to the possible renewable energy sources that can replace oil. The chapter also delves further in the motivation for this research and the contribution the research seeks to add to the pool of knowledge.

1.1   Background

Sound the alarm, another country is dying under the weight of high oil bill! In July 2008 oil was trading at US$145 per barrel. With an expenditure budget of US$3.17 billions, and revenue being only US$2.85 billions, the oil bill for Jamaica accounts for nearly US$1 billion (CIA - World Fact – Jamaica 2006) of the budget. The constant rise in oil prices has brought to the fore, once again (oil embargo, 1970's), the need for the world and in particular oil importing countries, such as Jamaica, to find alternative energy sources.

Jamaica, an island located latitude: 18.15 degrees north, has a serious problem. While it needs to accelerate development, it also needs more energy to progress with its developmental plans in regard to industry and infrastructure. But the cost for this energy reduces the country's ability to sustain the said development. Given this non-productive cycle, the country looks with great anticipation at all the emerging new and renewable energy technologies for possible solutions. It has installed 22 megawatt of Hydro Power and 20 megawatt of Wind Power as renewable energy. In addition it proposes to use Liquefied Natural Gas (LNG) and Coal for base load generation in the power sector (The Jamaica Energy Policy Analysis, 2005).

There is not much more scope for further increases in the hydro and wind plants in Jamaica. Hydro is limited by the availability of suitable water sources due to the lack of reasonable elevations and wind is lacking in sustainabe speed in most of the sites that have been tested. While LNG is available from Trinidad and Venezuela, and at cheaper prices than crude oil, there is nothing to stop the price from rising as oil did, if the world demand for it increases. Jamaica's best bet therefore for sustainable energy is coal. Coal however comes with its own problems. It can be very costly to the environment with its dust and ash, and also, as with LNG, produces green house gases in the form of carbon dioxide when burnt.

The above scenario is not limited to Jamaica. Throughout the world it is being played out in oil importing countries, especially those with small developing economies. This leads to the question of long term, environmentally friendly and sustainable energy solutions for such countries. One possible solution which can address the issue globally is Solar Energy, especially along the Equatorial belt. The Equatorial belt is defined as the region around the globe which lies between Tropic of Cancer: latitude 23.5 degrees north, and Tropic of Capricorn: latitude: 23.5 degrees south, of the Equator. This region runs like a belt around the middle of the globe. In this region the sun can appear directly overhead at noon. This occurs at the June solstice for Cancer and the December solstice for Capricorn. Hence the equatorial belt has the highest influx of solar energy year round (Tropics, nd).

With this abundance of 'clean' energy along the equatorial belt, it is prudent for further investigations into the utilization of this energy with the expressed aim of replacing, or at least supplementing, the fossil fuel requirements of oil importing developing countries.

1.1.1   Photovoltaic as a Power Source

Solar energy is utilized in various ways for many years, so the technology is very mature. It is used internationally in crop dryers, water heaters and solar cookers, among other domestic applications. For industrial applications, Parabolic Dish Collectors (where the sun's radiation impinges on the parabolic shaped dish and is then reflected on to an absorber which is located at the focal point of the parabola where the radiation is now concentrated for high temperature heating) and Solar Power Towers (where a system of tracking mirrors, called heliostats, focuses the radiation to a fixed point for high temperature usage) are two such examples. But just as important is the use of the sun's energy in the field of Photovoltaic

Technology. For example, photovoltaic technology can be utilized for a large conventional power plant or it can be used as a simple stand alone power source for an Electrolyzer in the production of hydrogen where hydrogen can be used as a fuel in general, as a fuel in the emerging field of Fuel Cell Technology, and in particular, as fuel for Domestic Cooking.

Photovoltaic is the conversion of light energy directly to electrical energy with the use of photovoltaic cells which, in essence, are semiconductors. These cells absorb light energy and output a voltage which is then used for electrical power applications. The application of photovoltaic as a standalone power source is worldwide and the technology is very mature. Notwithstanding its worldwide usage, photovoltaic has not rivaled traditional power sources due to its inherent problems of low conversion efficiency and the intermittency of sunlight. The results of low conversion efficiency and limited sun-hours translate into a higher cost per kilo-watt-hour when compared with traditional fossil-fuel power generation. The irregularity of sunlight forces the system to utilize batteries, which have very limited life spans, as a means of storing the solar energy for the dark periods. This adds to the overall cost.

While the kilo-watt costs may not be a true comparison since environmental concerns are not factored in, it is this straight cost-matching between the fuel types that the international market is using as the determinant for its choice in a power generation system. Therefore, the conclusion is clear. For photovoltaic to come to the fore on the world stage, its conversion efficiency needs improvement and a suitable storage medium must be found to make it more cost effective as a power system.

1.1.2 Hydrogen as an Energy Carrier

Another possible alternative fuel source (energy carrier) to fossil fuel is Hydrogen. Hydrogen is the most abundant element in the universe. It has the potential to become the preferred fuel in the future, and the literature abounds with suggestions of the world moving towards a "Hydrogen Economy" (Hydrogen Economy Factsheet, 2003; Rifkin, 2003; Crabtree et al., 2004). While hydrogen may not, for the foreseeable future, be the fuel of choice for base load power generation, its niche is definitely in the area of transportation (fuel cell) and domestic energy consumption such as cooking and heating. Transportation consumes fifty percent of the world's petroleum products (Panorama, 2005) and 20 percent of total energy supplied in developing countries is from wood-fuel (EarthTrends, 2001). Not

only does the transportation sector utilize a lot of energy and wood-fuel contributes to deforestation, but their emissions are major contributors to Global Warming.

With the advent of Fuel Cell Technology which can possible replace the internal combustion engines of motor vehicles by employing the burning of hydrogen with oxygen and produces only water as a 'waste', the world became excited about the prospect of this technology which can radically change the negative impact of the transport sector on the environment. But there is a hitch. Hydrogen does not exist naturally on its own as an element. It always exists as a compound substance such as the hydro-carbons or in the compound molecule of H_2O which is water. Therefore, to acquire hydrogen as a fuel some form of processing must take place, and this processing needs some form of energy to power it.

Currently fossil fuel is used to produce hydrogen through Steam Reforming. In this process hydrocarbon feedstock is broken down to release the hydrogen gas. The major problem with this process, apart from the fact that fossil fuel is used to power it, is that for each kilogram of hydrogen produced, over eight kilogram of Carbon Dioxide is also produced (Dahl, et al., 2002; Spath & Mann, 2001). This is an environmental nightmare. A clean way to produce hydrogen gas is by Electrolysis where water molecules are broken down by electricity to produce hydrogen and oxygen. But if conventional power is used in the electrolysis process, then the "cleanness" of the process is compromised.

1.2   Motivation for this Research

In examining two of the cleanest possible replacements for fossil-fuel two constraints exist. The first is, for photovoltaic power to challenge fossil-fuel-base power its conversion efficiency and storage medium need improvement; and the second is, for hydrogen to come into its own as a fuel its production process must be cleaner for a world that is demanding minimum environmental impact processes. Research is ongoing in alleviating the individual constraints mentioned above, and there are also Solar-Hydrogen plants in existence. The aim of this current work seeks to improve the Conversion Efficiency of the photovoltaic system so that an improved system may be used to simultaneously power a conventional plant and an Electrolysis process for hydrogen production in which hydrogen becomes the 'storage-medium' for excess solar energy. This could give a totally green power plant which runs on *Photovoltaic Power by Day and Hydrogen Power by Night.* Achieving totally green power is the motivation for this research.

1.2.1 Significance of the Study

While many research focus on device-level improvement in conversion efficiency for photovoltaic system, the system-level optimization using existing technology can prove to be a more effective approach towards practical implementation. This study focuses on System-level Design and Optimization of Direct Photovoltaic Hydrogen-Generation by adopting Thermal Management Systems such as Gravity-Fed and Solar-Powered Adsorption cooling techniques to improve system efficiency. This investigation seeks to contribute to the pool of knowledge by concentrating on ways to improve the conversion efficiency of a photovoltaic system, couple it to an Electrolyzer, and then optimize the overall system for the production of Hydrogen specifically as Domestic Cooking Gas (for a niche market), and as a source of totally 'green' Renewable Fuel in general.

1.2.1.1 <u>*Hypothesis*</u>

The aim of providing hydrogen-fuel in its 'greenest' form, for small to medium domestic markets (e.g. domestic cooking gas application), rest on an efficient PV system. The hypothesis therefore is: employing Gravity-Fed Cooling (GFC) and Solar Powered Adsorption Cooling (SPAC) techniques for the cooling PV cells, the cells conversion efficiency would improve and also the resulting solar-hydrogen production system would achieve a higher production rate.

1.2.1.2 <u>*Objectives*</u>

The broad objectives of this thesis are:

1. To propose methods which would lead to an improvement of photovoltaic cell efficiency and hydrogen production rates for small (domestic type) systems and test these experimentally. Preliminary research had formulated two such methods, termed Gravity Fed (GFC) and Solar–Powered Adsorption (SPAC) systems.

2. To develop mathematical models which can predict specific aspects of the proposed systems. Preliminary research has indicated that temperature distribution in a PV cell and the time taken for a cylindrical adsorption bed to reach the desorption temperature are the important parameters.

3. To construct an experimental rig to enable measurements to determine the cooling effect on photovoltaic cell conversion efficiency of the Gravity Fed (GFC) and Solar –Powered Adsorption (SPAC) systems.

4. To further develop the experimental rig to enable measurements to establish the effects of coupling an Electrolyzer to a PV power system with GFC/SPAC thermal management by examining changes in hydrogen production rates.

5. To compare the developed mathematical models with experimental results and carry out parametric analysis to generalize results.

1.2.1.3   Original Outcomes

The original outcomes of the thesis are:

1. To confirm by experimentation that both proposed cooling systems improve the conversion efficiency of PV cells.

2. To demonstrate that the proposed coupled system, PEM Solar-Hydrogen plant with GFC/SPAC thermal management, is a practical way of producing hydrogen as:
    a) a renewable fuel source from a renewable energy source, in general
    b) a domestic cooking gas, in particular,
 by utilizing matured, enhanced, system-level devices.

Overall, the project seeks to demonstrate (by experimentation and targeted theoretical calculations) the feasibility of self-sustained, small to medium, solar-hydrogen plants with thermal management, suitable to the Equatorial Belt regions of the world.

1.3   Structure of Thesis

The development of the thesis is presented by chapters:

Chapter 2:

This chapter focuses on the review of the literature. It highlights issues regarding the Solar-Hydrogen production processes and shows the contribution of other researchers in addressing some of these issues. Particular emphasis is placed on understanding the temperature related problem of silicon-based photovoltaic (PV) modules and the proposed solutions given in the literature. The chapter ends with the strategies employed by this investigation in addressing the temperature related problem.

Chapter 3:

This chapter explains the theoretical (mathematical) and experimental models developed in order to test the hypothesis described by this investigation. It shows the development of the analytical solutions to the heat equations for the cooling techniques employed. The theoretical results will be matched against experimental data.

Chapter 4:

The execution of the experiments and the instruments utilized are described here. The chapter explains the test arrangements for the simulations of the cooling techniques applied to the PV cells and also gives the format for hydrogen production under normal environmental conditions.

Chapter 5:

This chapter gives the results obtained and the calculations from the data gathered. Samples of graphs and major findings are presented here.

Chapter 6:

Parametric analyses are performed on the mathematical models to establish degrees of sensitivities, further probes are carried out on fuel plant productivity and cost, and the overall contributions made to the body of knowledge.

Chapter 7:

This chapter compares the stated objectives of the research with the experimental results and gives the conclusions of the study along with recommendations for further investigations.

CHAPTER 2

LITERATURE REVIEW

The production processes of Solar-Hydrogen are reviewed in this chapter as well as contribution of other researchers in addressing some of the issues raised in the processes. In addition, focus is placed on the temperature related problem of silicon-based photovoltaic (PV) panels and the solutions, with their inadequacies, as given in the literature. The chapter ends with the hypothesis and proposed solutions to be investigated, with their limitations, in addressing the temperature related problem.

2.1   Hydrogen Production Processes

Even though hydrogen is the most abundant element in the universe, it does not exist in free form so it has to be extracted. Most of the world's current supply of hydrogen is derived from fossil fuels, and therefore most hydrogen production does not eliminate the emission of green house gas (GHG) pollutants that are connected to climate change. One of the main production processes is steam reforming of fossil fuel feed stock, which is mainly natural gas comprised of methane, CH_4,(Momirlan and Veziroglu, 2002). In this process steam at high temperature and pressure (700 – 1000 ^{o}C/ 3 -25 bar) reacts with the fossil fuel feed stock in the presence of a catalyst to produce hydrogen (Natural Gas Reforming, 2006: HFCIT). According to Spath and Mann (2001), their analysis of the life cycle assessment of hydrogen production by steam reforming of natural gas shows that 74.8% of the GHG emissions, (carbon dioxide equivalent, CO_2-eq), of the entire plant comes from the hydrogen production operation. From their data this translates to 8.9 kg CO_2-eq per kilogram hydrogen produced. Rosen and Scott's study (1992), as cited in Momirlan and Veziroglu, 2002, showed that of the eleven main hydrogen production processes only five are of mature status, namely, steam reforming of natural gas, catalytic decomposition of natural gas, partial oxidation of heavy oil, coal gasification and water electrolysis.

Steam reforming of natural gas is generally referred to steam methane reforming (SMR) because natural gas (fossil fuel based) consists mainly of methane, with addition of some heavier hydrocarbons and carbon dioxide. The reforming is a two step process.   The

first step involves methane reacting with steam at elevated temperatures (750-800 ^{o}C) to produce synthesis gas (syngas) which is primarily hydrogen and carbon monoxide. This first step is called reforming of natural gas. The second step, known as water gas shift reaction, takes the carbon monoxide produced in the first step and reacts it with steam over a catalyst, forming hydrogen and carbon dioxide. This reaction is accomplished in two stages; a high temperature shift (HTS) at 350 ^{o}C and a low temperature shift (LTS) at 200 ^{o}C. In the overall process more carbon dioxide (global warming gas, GWG) is produced than hydrogen (Hydrogen Fact Sheet-Hydrogen Production, n.d)

The catalytic decomposition of natural gas uses Palladium as a catalyst to break down the gas to hydrogen and carbon. According to Poirier and Sapundzhiev (1997), in this process natural gas is decomposed over Palladium, using an external heat source, according to the reaction $CH_4 \leftrightarrow C + 2H_2$. The carbon amasses on the catalyst and the hydrogen exits the reactor. As time passes the catalyst is covered with carbon and must be regenerated by burning off the carbon with air. This produces carbon monoxide and dioxide.

Partial oxidation of heavy oil involves a 3-step process (synthesis gas generation, water-gas shift reaction, gas purification) at high temperature and pressure. It may be catalytic, operating at 600 ^{o}C and using feedstock ranging from methane to naphtha, or non-catalytic, with temperature range of 1150-1315 ^{o}C with feedstock ranging from methane, heavy oil to coal. The process sees hydrocarbon feedstock being partially oxidized with oxygen to produce carbon monoxide. The CO is then shifted with steam to carbon dioxide and hydrogen, and in the final step the gas is purified (Yurum, 1995).

Coal gasification is a process where coal is converted to gaseous products by feeding it to a gasification reactor and the temperatures and pressures are then elevated. The gasification is carried out in the presence of oxygen at purity greater than 95%. The reactions are presented as:

$$2C + O_2 \leftrightarrow 2CO + heat \tag{1}$$

$$C + H_2O + heat \leftrightarrow CO + H_2, \tag{2}$$

where C represents pyrolysis products (Yurum, 1995)

Since this research is focusing on matured and non-fossilized fuel feedstock processes along with zero carbon by-products in the production of hydrogen, of the five processes mentioned only water electrolysis is therefore considered.

2.1.1 Water Electrolysis

Water electrolysis is the decomposition of water into hydrogen and oxygen by means of an electric current. The literature shows that water electrolysis is one of the most important, matured, but more expensive, industrial processes for hydrogen production. But while electrolysis systems are more expensive than other forms of hydrogen production, the technology, according to Solomon and Banerjee (2006), is well suited for small scale production. In support, Rosen and Scott (1998) showed that in an Energy efficiency/Exergy efficiency comparison, for non-hydrocarbon based processes using electricity and/or high temperature heat for the efficiencies, the following obtains:

- Steam-Methane Reforming (SMR)   86%/78%
- Thermochemical Water Decomposition   21%/16%
- Current-Technology Water Electrolysis   77%/67%
- Advanced-Technology Water Electrolysis 92%/83%

(It must be noted that both Rosen (2009) and Ni et.al (2007) confirmed that in some processes, it is indeed proven that energy efficiencies are higher than those of exergy. For example, Ni et.al found that in an energy/exergy analysis of the thermodynamic-electrochemical characteristics of hydrogen production by a solid oxide steam electrolyzer (SOSE) plant, the energy losses which were due mainly to inefficiencies of the heat exchangers were less than those of the exergy. They stated that the high exergy destruction due to the over-potentials in the SOSE operation led to considerable exergy losses since electricity has 100% exergy.)

The Energy/Exergy efficiencies ratings demonstrate why water electrolysis ranks high among the other established processes as a viable technology. The literature further shows that the major technologies (electrolyzers) employ for electrolytic hydrogen production are Solid Oxide, Alkaline Water, and Polymer Membrane Electrolyzers (Momirlan and Veziroglu, 2002; Electrolytic Processes, 2006: HFCIT).

2.1.1.1   Solid Oxide Electrolyzer

The literature highlights that hydrogen production with solid oxide electrolytes (SOE) is more efficient because thermodynamically, the electrolysis process operates better at elevated temperatures (Wang, et al., 2006 quoting Doenitz, et al., 1980). The normal operating temperature of current SOE's is cited as ranging from 873 K - 1273 K (Ni, et al. 2007; Wang, et al. 2006; Wen & Mason, 1978).

This high temperature requirement eliminates SOE from consideration in this investigation as this requirement makes it unsuitable for small to medium size domestic plants on which focus is being placed. Figure 2.1 is a graphical presentation of the operation of a Solid Oxide Electrolyzer.
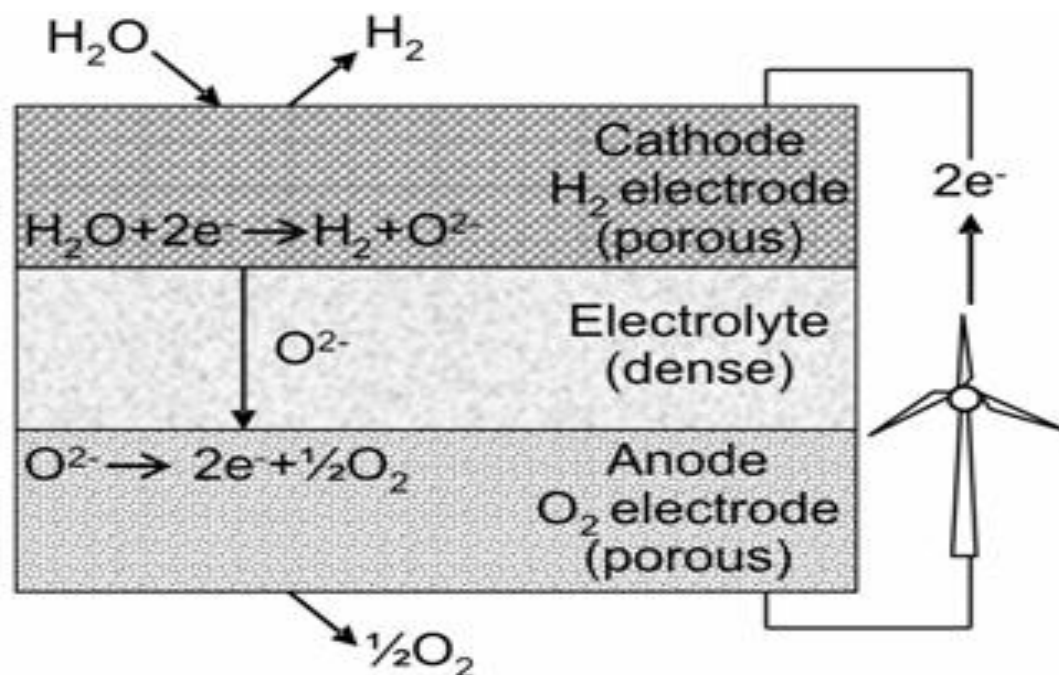
Figure 2.1   Schematics of a Solid Oxide Electrolyzer (after Hauch et al, 2008)

(Figure 2.1 shows steam and electrical energy from an external source entering at the porous cathode. Thermal dissociation in conjunction with electrocatalysis split the water into hydrogen and oxygen.)

2.1.1.2   Alkaline Water Electrolyzer

Bourgeois (2006) and the Hydrogen Production Lecture #6 (2005) show that for alkaline electrolyzers the following obtains:

- Operation Conditions: 70-100 ^{o}C and 1-30 bar
- Can utilize cost effective electrode materials (iron, nickel, nickel compounds)
- Most mature of the processes
- Easy to maintain if it is unipolar
- Difficult to maintain if it is bipolar

Notwithstanding some of the above positive attributes of alkaline water electrolyzer (AWE), both Lehman (2005) and data obtained from Hydrogen Production-Lecture #6 (2005) noted drawbacks to AWE. The negative feedbacks given are:

- Caustic liquid electrolytes and other hazardous materials
- High energy content for mechanical compression to achieve storage pressure
- Maintenance regime required

These negatives, and in particular the caustic liquid electrolytes which are of environmental concerns, are not in line with the concept of a domestic 'green-energy' system; hence the non-consideration of this type of electrolyzer. Figures 2.2a and 2.2b show the basic layout of Alkaline Water Electrolyzer.
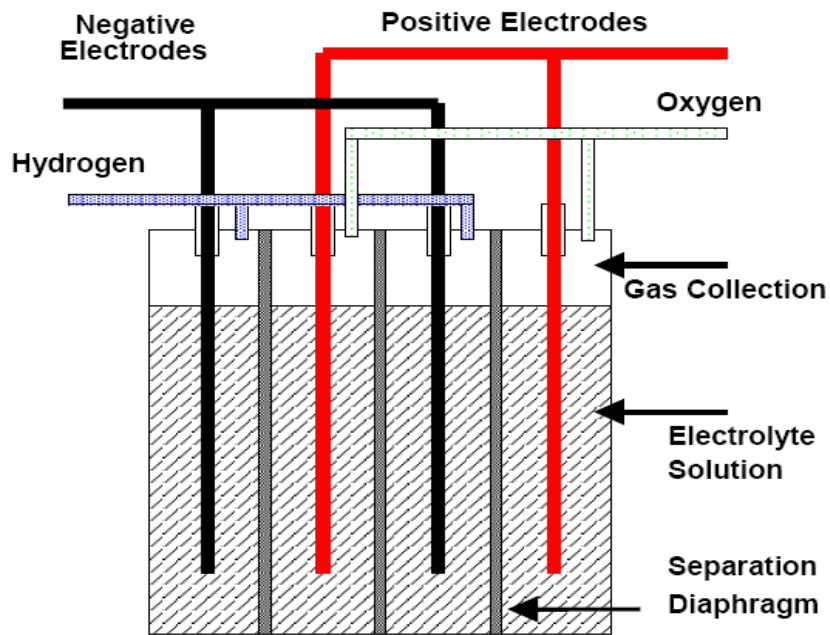
(a) Uni-Polar Alkaline Electrolyzer
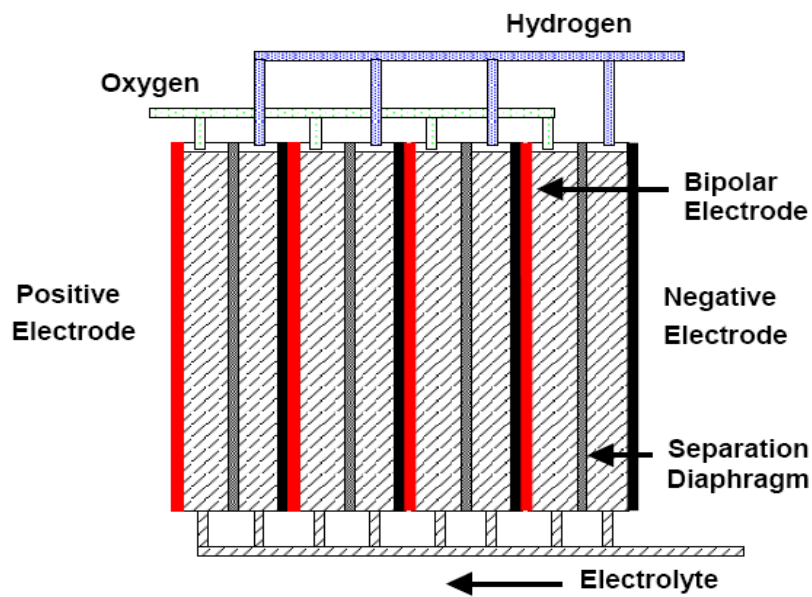
(b) Bi-Polar Alkaline Electrolyzer

**Figure 2.2 Schematics of Uni-Polar & Bi-Polar Alkaline Electrolyzers
(after Kroposki et al, 2006)**

(The schematics show the positive (red) and negative (black) electrodes in the electrolyte solution. Hydrogen is liberated at the negative sides of the cells. The bipolar has individual electrodes that are separated by insulators so that one side acts as a cathode for one cell and the other as an anode for another cell.)

2.1.1.3   Polymer Electrolyte /Proton Exchange Membrane (PEM) Electrolyzer

PEM electrolyzers, graphically represented in Figure 2.3, according to the literature (Badwal et al., 2006; Hydrogen Production Lecture #6, 2005) have the following characteristics:

- Modular and all solid state system
- Electrochemical compression to storage requirement
- Fast response time: start-up/shut-down
- Hydrogen generation starts immediately at ambient conditions
- High current density at higher efficiency

These characteristics satisfy the domestic 'green-energy' system under consideration. The major advantage of PEM electrolyzer is its ability to generate hydrogen at pressures ready for storage and therefore negates the need for a mechanical compressor. This not only greatly reduces system and energy costs but also leads to the possibility of storing the gas at low pressure for domestic cooking application. The major drawback to the use of PEM electrolyzer however, is the high cost associated with the membrane-electrode assembly (MEA), and so the major part of continuing research is to address this cost issue.
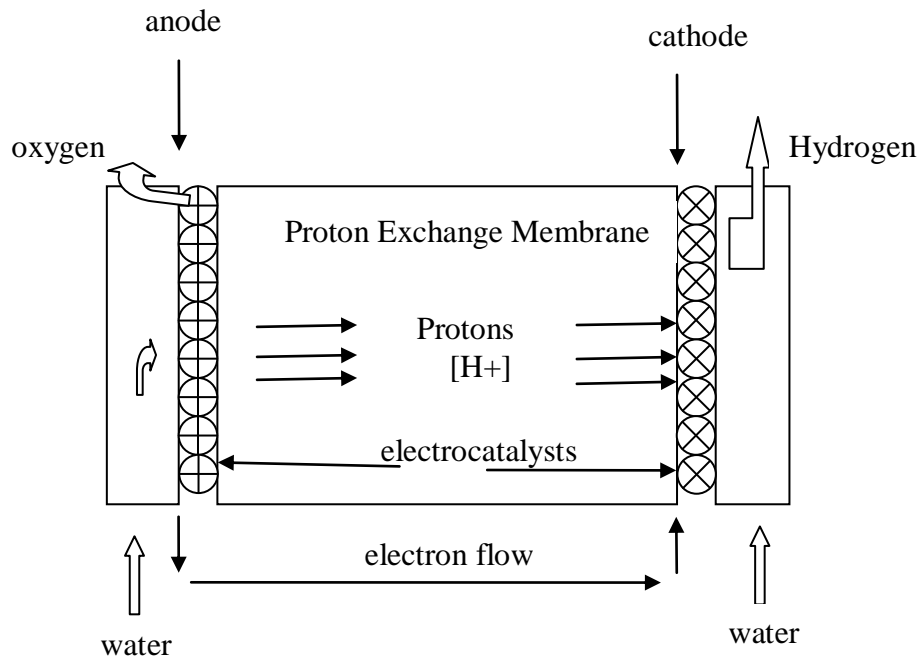
Figure 2.3   **Schematic of a PEM Electrolyzer**

(Figure 2.3 shows water entering the electrolyzer and is broken down at the surface of the membrane to form protons, electrons and oxygen. The protons travel across the membrane due to the influence of the electric field, and recombine with the electrons at the cathode to form hydrogen).

To date, some of the major milestones in addressing the cost issue for PEM electrolyzers have being reached by Giner Electrochemical Systems, LLC (GES)/US Department of Energy, as outlined in the DOE Hydrogen Program Progress Report, (2005). The outstanding achievements are:

- Up to 75% production cost reduction by the development of an oxygen anode side membrane support structure (ASMSS)
- Up to 40% production cost reduction by the development of a fabrication method for a thermoplastic cell frame.
- Cost reduction by utilizing thinner membranes resulting in higher current densities hence higher efficiency.

Other manufacturers, such as 3M, report cost reduction in MEAs. 3M reports 'low-cost MEAs' by employing nanostructured thin-film catalyst support system ("Low-Cost Membrane Electrode Assemblies", 2001). The reduction in cost is not stated so a price

comparison is not possible here. Huslage, et al. (2002) stated that by utilizing radiation grafting as a production methodology, they have obtained MEAs that are less costly than the commercialized Nafion®-112 MEAs, yet with comparable operating characteristics.

The conclusion is that PEM electrolyzers are fast approaching affordable commercialization. With their compactness, durability, and very low maintenance, this augurs well for small to medium size hydrogen generation plants which are the focus of this investigation. On the issue of Electrolysis/Electrolyzer the United States Department of Energy (US-DOE) Hydrogen Program 2007 Projects Review states: *"The reviewers identified electrolysis using renewable energy as 'one of the two most viable options for hydrogen production in the near term.'"*(Hydrogen Production and Delivery, 2007).

The comment from the experts implies that it is worthwhile to continue the drive to find a breakthrough in Renewable Energy-Hydrogen Development. Therefore, this investigation seeks to contribute to this undertaking by demonstrating that utilizing water electrolysis, through a PEM electrolyzer powered by **improved photovoltaic technology**, is practical for small to medium size hydrogen farms, especially along the equatorial belt (the tropics) where water and sunlight are ubiquitous.

2.2 Photovoltaics

As stated in Sections 1.1.1 and 1.1.2, along with Hydrogen, the other Renewable Energy source to rival or replace fossil fuel is Photovoltaic. Photovoltaic (PV) is the use of certain types of 'doped' material called semiconductors which convert light energy, such as sunlight, directly into electricity. These materials exhibit a property known as the photoelectric effect that causes them to release electrons after absorbing photons of light energy. These free electrons are directed as an electric current for PV electricity generation. Gallium arsenide (GaAs), cadmium sulfide (CdS), silicon (Si) and germanium (Ge) are examples of semiconductor materials use to fabricate photovoltaic cells. Photovoltaic system entails no moving part, is totally environmentally friendly, silent, a reliable technology and has the potential of addressing a significant portion of the world's electricity generation.

The first practical usage of the PV technology started in the 1960s by the space industry to power onboard systems in spacecrafts and isolated communication stations, and

also to aid in certain defense needs. The initiatives of the space programmmes saw to the development, reliability and the beginning of cost reduction of the technology. It took the energy crisis in the 1970s to usher in the photovoltaic technology as a source of general electrical power generation; and the constant rise in oil prices in this first decade of the twenty-first century see the photovoltaic technology attempting to usurp the dominance of fossil-fuel power generation (Power Trip Energy Corp, n.d.).

PV power generation system has not yet fully rivaled its fossil fuel counter part because of the relatively high production cost of PV panels and the low conversion of the light energy into electricity (low conversion efficiency) of the PV cells. The major thrust of the research in this field is to improve the conversion efficiency of PV cells, and reduce the associated production costs.

2.2.1 Types of Photovoltaic Cells

2.2.1.1 Single and Multiple Junctions PV Cells

Knier (2002) stated that the most common PV systems use single junction cells (Figure 2.4a). In these types of cells the photovoltaic effect is restricted to only the portion of the light spectrum that has photons with energy, equal to or greater than that of the band gap energy (E_g) of the semiconductor material, to free electrons for an external electric circuit. The band gap energy, with units of electron volts (eV), is the energy needed for an electron to 'jump' from the top of the valence band to the bottom of the conduction band, as shown in Figure 2.5. The remaining portion of the light energy goes into increasing the cell temperature, which further reduces the conversion efficiency of the cell. The literature also showed that the conversion efficiency of silicon single junction cell, without light concentration, reaches only 17% (Centurioni et al. 2004).

(a) single junction cell   (b)   multi-junction cell
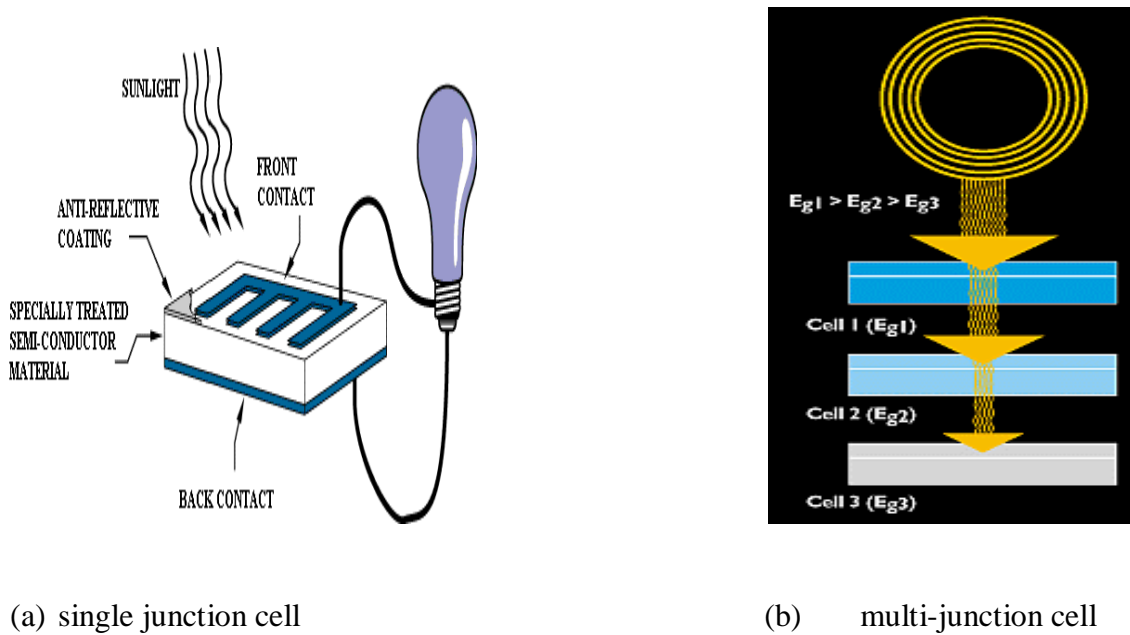
Figure 2.4 Schematics of single & multiple junctions PV cells (after Knier, 2002)
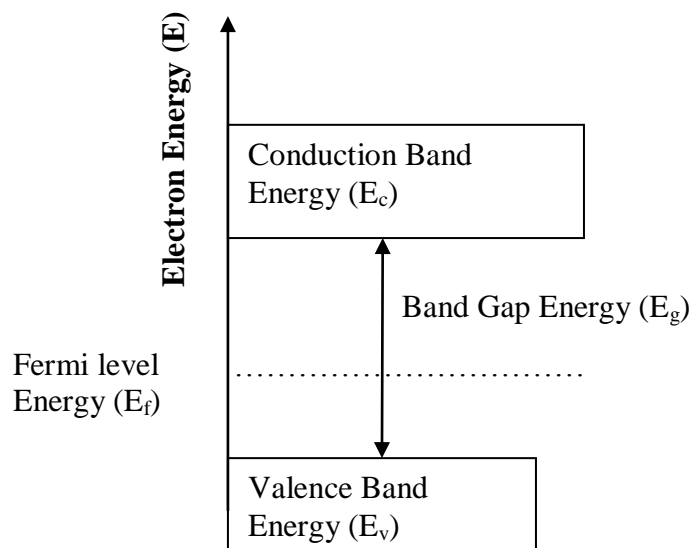
Figure 2.5   Context of Electron Energy for Semi-conductor

In order to improve the single junction cell efficiency, research has led to novel innovations such as Tandem Cell (multi-junction stacked cell) technology. Muti-junction cells increase PV conversion efficiency by optimizing the utilization of the light spectrum in individual cell (Figure 2.4b). This improved efficiency is achieved by using two or more different cells, with different band gap energies (E_g) and multiple junctions, in generating a voltage. In this arrangement individual single-junction cells are stacked in descending order of band gap energy (E_g). The top cell absorbs the highest energy photons and the remaining cells absorb the remaining photons in descending order.

Tandem cells have shown conversion efficiencies ranging from 31% to 40.35% (Conibeer, et.al, 2008; Hamzaoui, et al. 2005) but the improved efficiency is negated by increase in production and material costs (chiefly gallium arsenide- GaAs). Therefore, since material cost is a major factor in the fabrication of PV cells, in order to reduce cost, most researchers have turned to improving the conversion efficiency of single junction cells made of Silicon (Carabe & Gandia, 2004; Radziemska, 2003).

The chief reason for Silicon being the material of choice in PV manufacture is that Silicon abounds in nature in the form of silica (high grade sand, quartz rock). Having a cheap source of raw material the next step is therefore to improve the conversion efficiency of the cell.

2.3   Temperature Dependence of Conversion Efficiency in PV Cells

It has been established that the conversion efficiency, which translates to power output of PV cells, falls as the cell temperature is elevated. It is only a portion of the sun-light that enters the cell which is converted to electricity, so as the cell operates the remaining portion of the sunlight converts to heat and elevates the cell temperature. This increase in operating temperature reduces the conversion efficiency of the cell. This phenomenon, according to Maycock and Stirewalt (1985), is more pronounced in Silicon cells than other cells such as Gallium arsenide. The phenomenon, though, seems puzzling if one assumes power output is solely dependent on electrical conductivity (P=IV). In addition, quantum physics shows that the increase in conductivity of a semiconductor is directly proportional to temperature.

To further make the point, Goetzberger et al. (1998) stated that electrical conductivity in the form of free electrons per unit volume, n, in the conduction band of a semiconductor, depends decisively on temperature as demonstrated by the formula

$$n = 2 \left(\frac{2\pi m_n^* kT}{h^2} \right)^{3/2} exp \left(\frac{E_f - E_c}{kT} \right) \tag{1}$$

where the term $\left(\frac{2\pi m_n^* kT}{h^2} \right)$ is the effective density of state of the electrons in the conduction band, and m_n^* is the effective mass of electrons, h is Planck's constant, T is absolute

temperature and k is Boltzmann's constant. The Fermi level energy (E_f) is less than the conduction band energy (E_c), as depicted in Figure 2.5, which shows that the exponential term is greatly influenced by temperature.

Goetzberger et al. (1998) further pointed to the fact that at absolute zero semiconductors become insulators and conductivity is seen only as temperature increases. This fact seems to suggest that the conductivity of a PV cell, as a function of temperature, would be limited only by how high a temperature a PV cell can sustain; and by implication so too its power output. But Maycock and Stirewalt (1985) asserted that power output of PV cells is not solely dependent on electrical conductivity but also, at a given insolation, is inversely proportional to temperature.

This inverse relationship of power output (conversion efficiency) to temperature is due to the dependence of the open circuit voltage, V_{oc}, on temperature (Angrist, 1982; Goetzberger, et al., 1998; Graff & Fischer, 1979, and Hu & White, 1983). Goetzberger, et al. (1998) cited the development of the open circuit voltage as

$$V_{oc} \approx U_T ln\left(\frac{I_{sc}}{I_o}\right) \tag{2}$$

[updated by Markvart and Castaner (2003) to $V_{oc} = \frac{kT}{q} Ln\left(\frac{I_{sc}}{I_o} + 1\right)$] $\tag{2.1}$

($U_T = kT/q$ thermal voltage, q = elementary charge, I_{sc} = short circuit current) and stated that the efficiency of a PV cell is essentially reducing the saturation current, I_o.

Graff and Fischer (1979) further explained that in a cell, the current-voltage characteristics obtain in the dark is of equal importance as that of the photocurrent. They added that this is due to the fact that when power is drawn from a cell the 'dark current' which exists across the junction opposes the photocurrent. The most important contribution to the 'dark current', they stated, is that of the saturation current, I_o, which comes from the injection of minority carriers crossing the p-n junction.

In establishing the impact of the saturation current, I_o, on conversion efficiency (power output), Angrist (1982) showed that current density, $J_o = I_o/A$, which is saturated current per unit area, is given by

$$J_{o(p)} = 2.23*10^{31} T^4 \rho_n \mu_n \mu_p ke L_p^{-1} exp[- E_g/(kT)] \tag{3}$$

[updated by Markvart and Castaner (2003) to $J_o = 1.5 \cdot 10^5 exp(-E_g/kT)$] $\tag{3.1}$

(ρ_n = electrical resistivity, μ = mobility of charge electron(n)/hole(p), e = electronic charge, L_p = diffusion length). The equation highlights the strong dependence of current density, J_o, on temperature since the term before the exponential is influence by the fourth power of temperature. Likewise, the exponential varies according to temperature fluctuations for a given semiconductor material. Angrist noted that the smaller J_o is the more efficient the cell becomes. He then concluded that the lower the operating temperature of a PV module, the better its performance.

In general the literature shows a decrease in open circuit voltage, V_{oc}, of -0.41%/K to - 0.65%/K and reduction in conversion efficiency of the same order of -0.08%/K to - 0.4%/K at temperatures above 298 K (Hu & White, 1983; King, et al., 1997; Radziemska, 2003; Sweelem, et al., 1999). Therefore in addressing the problem of reduction in conversion efficiency of PV cells due to elevated operating temperature, some form of cooling mechanism has to be employed for the cells.

2.4   Techniques Employed in Cooling PV Cells to Improve Conversion Efficiency

Various techniques have been employed by researchers in an attempt to cool PV cells. The following are some of those techniques used:

1. A string module with the cells laminated on copper fin absorber with water tube welded on the back (Brogren & Karisson, 2002).

2. A heat spreader made of 3mm thick aluminum plate attached to a module (Araki, et.al., 2002).

3. Evaporative cooling based on the theory of heat pipes (Farahat, 2004).

4. Increasing thermal mass of modules by attaching them to small water filled tanks (Ronnelid, et al., 1999, and Krauter, 2004). Krauter found, though, that this technique greatly increases the weight of the module, 200 kg/module.

5. Blowing air across the back of the cell through an adjustable air-gap (Sweelem, et al., 1999).

6. Circulating water over cell (Brogren & Karisson, 2002).

From the literature, of all the techniques adapted to cool PV cells, circulating water over the cell, usually at the back, proves to be the most effective (Brogren & Karisson, 2002). Krauter (2004), and Abdolzadeh and Ameri (2009), however, circulated water over the front of the cell with very good effect, but this technique runs the risk of depositing scales on the face of the cell and thus reducing its effectiveness. The circulating water technique has one major downside and that is the 'parasitic' power required to run the pumps. This means that part of the power gained in cooling the cell is "lost" in running the pump.

In an attempt to negate the 'parasitic' power problem, Furushima and Nawata (2006) devised a system which utilizes siphonage. By using the city mains to get water to the supply tank on top of the building, they bypassed the use of a pump. In order to circulate the water over the back of the cells, they employed a piping system with a controller for valves openings which induced siphonage in the piping from the top level to the ground level of a building. This technique, apart from being complex with controllers and synchronizing valves, will also require the maintenance of air-tight seals in the piping.

Therefore, in assessing the effectiveness of any cooling system, simplicity of design and net power gains (increase power from cooling minus parasitic power for circulating pump) are issues to be considered.

2.5   Proposed Cooling Techniques

The aim of providing hydrogen-fuel in its 'greenest' form, for small to medium domestic markets (e.g. domestic cooking gas application), rest on an efficient PV system. This investigation has proposed two cooling techniques that will improve the conversion efficiency of PV cells while achieving design simplicity and maximizing power gains.

2.5.1 Gravity-Fed Cooling (GFC) Technique

This investigation theorizes that the conversion efficiency of PV cells can be improved without the loss of any parasitic-power by the employment of a gravity-fed water-cooled system, where water is allowed to flow across the back of the cell ('wet' PV cell) under the force of gravity. The system uses water that is being diverted from an upstream source, such as a river or any elevated position including catchments for rain water, channels the water across the back of a PV cell ('wet' cell) to cool the cell, and returns the water downstream (Figure 2.6).

The power required to drive the water through the system comes from the hydraulic head of the flow stream under gravity, due to the difference in elevation. No circulating pump is required. It is envisioned, therefore, that the system will be coupled to remote or semi-remote PV power generation since the cooling technique limits the system to regions that have water supply.
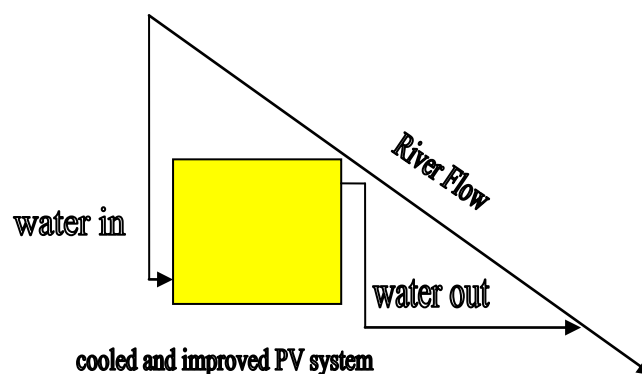
Figure 2.6   Schematics of a Gravity-Fed Cooling (GFC) System

2.5.2 Solar-Powered Adsorption Cooling (SPAC) Technique

In order to remove the constraints of a cooling system that is restricted to only regions that have water, this investigation also theorizes that the conversion efficiency of a PV cell can be improved, while minimizing parasitic-power loss, by incorporating a Solar-Powered Adsorption Cooling (SPAC) system (Figure 2.7). The adsorption cooling system is used to

chill water below ambient temperature. This chilled water is then circulated across the back of the PV cells for cooling of the cells. The fact that the water is chilled means that less water is required for the same degree of cooling and hence a reduced pumping rate. The reduced pumping rate minimizes the 'parasitic-power' needed to drive a circulating-water pump.

2.5.2.1   *Solar-Powered Adsorption Cooling (SPAC)*

Solar-powered adsorption cooling (refrigeration) is comprised of a 2-phase cycle (Fig 2.7a&b). The first phase is the heating-desorption-condensation phase (1-2-3) and the second is the cooling-evaporation-adsorption phase (3-4-1). The first phase utilizes solar radiation for heating an adsorbent bed made up of activated charcoal with an adsorbate (refrigerant), usually methanol, adsorbed into its pores (Jing & Exell, 1993). As the bed temperature rises to the condensing temperature and pressure of the adsorbate, the adsorbate desorbs (evaporates) from the charcoal and migrates to the condenser. In the condenser it gives up its heat of vaporization, liquefies and flows by gravity into a water-jacketed evaporator. During the night (second phase) the adsorbent bed cools to ambient temperature hereby reducing the entire system pressure. When the bed pressure falls to the saturated vapor pressure of the adsorbate, the liquid adsorbate vaporizes in the evaporator by absorbing heat from the surrounding water. This is the adsorption cooling/refrigeration effect. The adsorbate vapor then migrates to the adsorbent bed where it is re-adsorbed. Description of the adsorption cooling systems and associated thermodynamic related issues such as the isotherms are presented extensively in the literature (Anyanwu, 2003; Li, et al., 2004; Sakoda & Suzuki, 1984; Wang, et al., 2005).

Solar-powered adsorption cooling systems have no moving parts (Fig 2.7b), only three main components (adsorption bed, condenser, evaporator), simple controls, simple design and material requirements, and is powered by an extensive temperature range: 50 ^{0}C – 500 ^{0}C (Wang & Oliveira, 2005).

The major shortcomings of this cooling system are low coefficient of performance (COP) and low specific cooling power (SCP). But where this investigation is concerned, the disadvantage of a low COP is of small consequence since the energy (sunlight) required to drive the process is totally free. Likewise, the drawback of a low SCP is of consequence only as much as it affects the physical size of the bed required for a given cooling capacity.

(mBar)Ln P

X_max(0.5 kg/kg)

X_min (0.12 kg/kg)

(10.1)P_con

2

3

.... isoster

━━▶ heating

→ cooling

⇒ desorption-condensation

⇒ adsorption-evaporation

1

4

(9.7)P_ev

(-3.4)T_ev
21 °C

(-3.3)T_con
30 °C

(-3.1)T_des,min
50 °C

(-2.8)T_des,max
80 °C

-1/T x 10³ (K⁻¹)

(-3.35)T_ads,min
25 °C

(-3.25)T_ads,max
35 °C
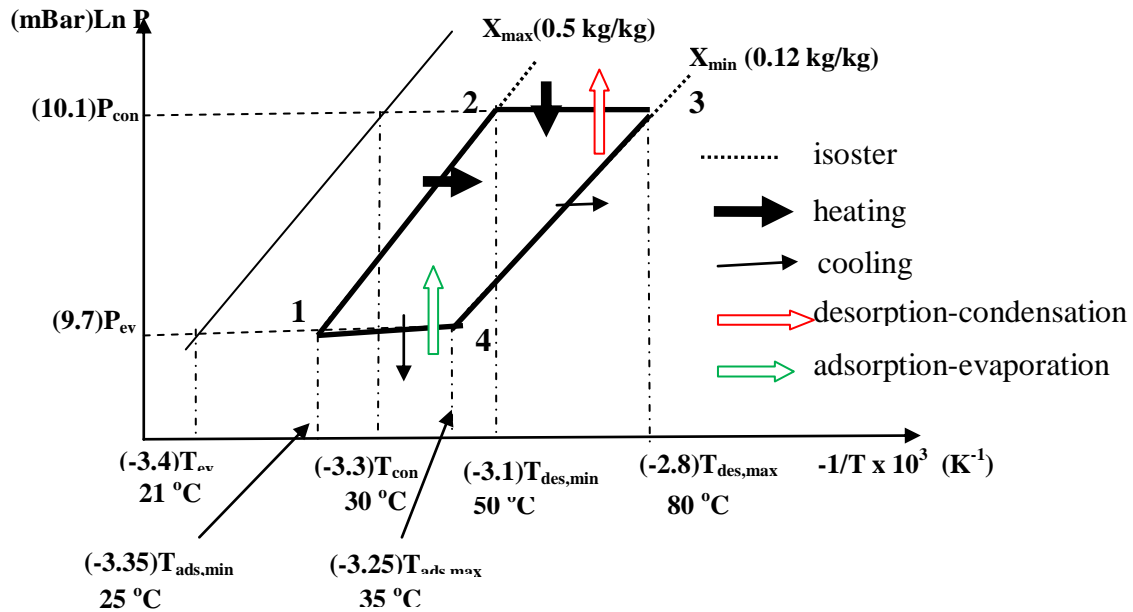
1-2: (Bed) HEATING AND PRESSURISATION
During this period, the adsorber receives heat. The adsorbent temperature increases (isosteric)
along the line of maximum concentration (X_max), inducing pressure increase from evaporation
pressure to condensation pressure.

2-3: (Condenser) HEATING AND DESORPTION plus CONDENSATION
During this period the adsorbent temperature continues increasing, which induces desorption
of vapour. This desorbed vapour is liquified in the condenser.

3-4: COOLING AND DEPRESSURISATION
During this period the adsorbent releases heat. The adsorbent temperature decreases, which
induces pressure decrease from the condensation pressure down to the evaporation pressure.

4-1: (Evaporator) COOLING AND ADSORPTION plus EVAPORATION
During this period the adsorbent temperature continues decreasing, which induces adsorption
of vapour . This adsorbed vapour is vaporized in the evaporator. The evaporation heat is
supplied by the heat source at low temperature.

Figure 2.7a   Adsorptive/Desorptive Cycles in the Clapeyron Diagram
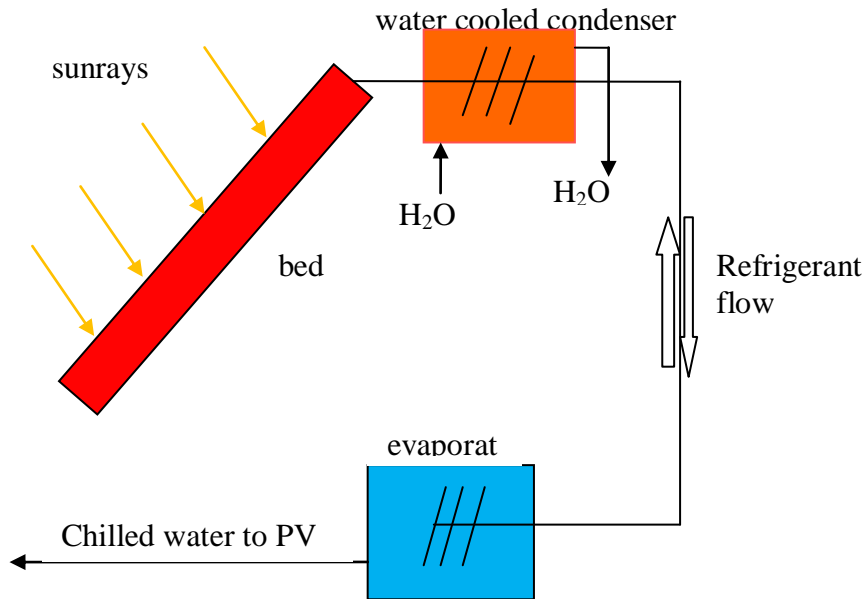
Figure 2.7b   Schematics of Solar Powered Adsorption Cooling (SPAC) System

2.6   Summary

Chapter two examined the Solar-Hydrogen production processes and highlighted the Proton Exchange Membrane (PEM) Electrolyzer as the preferred method for hydrogen production because of its 'simple' and environmentally friendly production system. The issues relating to Solar-Power, specifically Photovoltaics, were scrutinized and the temperature related problems were analyzed. The chapter closed with the premise that photovoltaic temperature problems can be addressed by the employment of either Gravity-Fed Cooling (GFC) or Solar-Powered-Adsorption Cooling (SPAC) system.

CHAPTER 3

MATHEMATICAL AND EXPERIMENTAL MODELS

This chapter outlines the theoretical (mathematical) and experimental models developed in order to test the hypothesis described in chapter two. It presents the development of the analytical solutions to the heat equations for the cooling techniques employed. The mathematical models are developed to be used as predictive tools in the study of specific aspects of the temperature profiles in the PV Cells and Adsorption/Desorption Bed. It is 'predictive' to the extent that they will accurately represent the real systems. On the other hand, the experimental models are seen as scaled versions of any real system. The theoretical results will be matched against the experimental data for validation.

The research evidence has shown (Radziemska, 2003) that the performance of silicon-based photovoltaic (PV) panels is strongly affected by the operating temperature. In warm climates like Jamaica and the other parts of equatorial belt regions where the solar irradiation is the highest on earth and the difference between the normal mean temperatures of the warmest and coldest months at some places is 3 °C or less (Waugh, 1998, p.196), this effect could become more pronounced. It has been reported that the temperature coefficient of a typical PV panel could be –0.65%/K for power output (Radziemska, 2003) and –0.4%/K for conversion efficiency (King, et al., 1997). This would translate to a 32.5% increase in power output and a significant 20% increase in conversion efficiency if the panel temperature is reduced from 80 $^{\circ}$C to 30 $^{\circ}$C.

3.1 Gravity-Fed Cooling (GFC) Theoretical Postulation

In Section 2.5, this research postulated that PV cells conversion efficiency can be improved by employing a cost-effective gravity-fed (no pump) water cooling system. To test this hypothesis a theoretical (mathematical) model of the system is developed and this is matched against experimental results. The mathematical model is to be used as a 'predictive tool' that should accurately represent the temperature profile of a PV cell with solar irradiance on the front surface and cooling water on the back surface.

3.1.1 Gravity-Fed Cooling Mathematical Model

Various mathematical models for heat transfer through PV cells have been shown in the literature. Royne, et al. (2005) modelled heat transfer through a PV cell under concentrated sunlight as a composite material, using a one dimensional equivalent resistance (R) circuit approach (Figure 3.1a). The accuracy of this model is dependent on the R- values used. As they pointed out, values of R should be used with caution since they fluctuate with temperature. Luque, et al. (1998) modelled their system, under concentrated sunlight, by applying the Heat Equation to a one dimensional heat-conduction through a silicon wafer with a thick aluminum plate attached to the back surface as heat sink (Figure 3.1b). On close examination of the model it seems likely that heat flow will be reduced across the silicon/electrical insulator/aluminum interface resulting in a slower temperature drop in the cell.
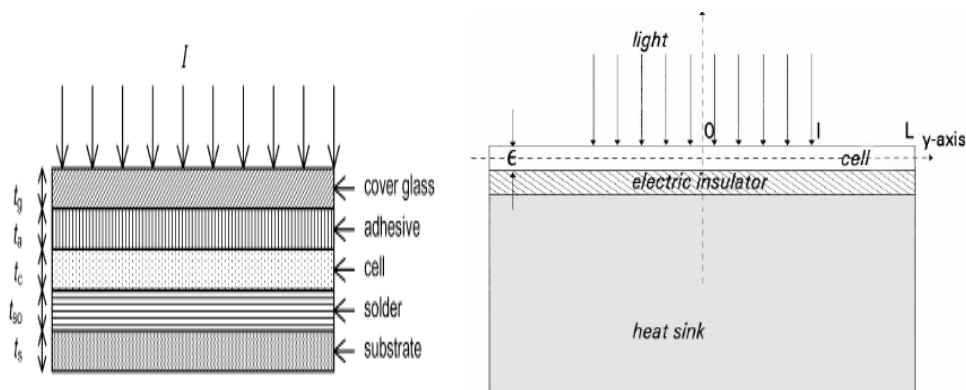
(a) Schematic of a composite material model (Royne, et al., 2004)

(b) Schematic of cell-electrical insulator-heat sink model (Luque, et al., 1998)

Figure 3.1   **Models of heat transfer through PV Cells**

In this investigation the PV cell is modelled as a Silicon slab with non-concentrated solar irradiance on the front surface and running water on the back surface (hence 'wet' PV cell), as shown in Figure 3.2. The assumptions for this model are:

(a)   Silicon is the predominant material in a PV cell, hence the silicon slab.

(b)   A worst case scenario where all the incident irradiance is absorbed as heat energy.

(c)   The thinness of the module makes it reasonable to consider a one-dimensional heat flow.

(d)   The flow rate of water at the back of the slab is high enough to keep the surface temperature constant and equal to the temperature of the water. (This is a Dirichlet

boundary condition, and as explained by Incropera and DeWitt (2002), Dirichlet conditions are close approximations of surfaces in contact with melting solids or boiling liquids. Heat is transfer at the surface but the surface stays at the temperature of the phase change process, thus setting the boundary condition at the surface. Therefore, since the analysis is the heat conduction within the boundaries of the slab, the heat transfer between surface and cooling medium is not explicitly included. This conclusion is verified, through examples, by both Incropera and Dewitt (2002) and Trim (1990)).
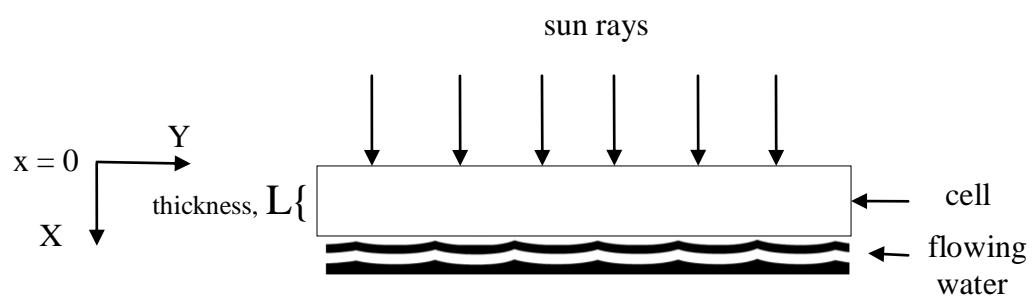
Figure 3.2   **Schematic of a 'wet' PV cell model**

The resulting second order one-dimensional heat conduction equation for the model is solved analytically as follows:

Heat Conduction Equation

$$\frac{\partial U}{\partial t} = \alpha \frac{\partial^2 U}{\partial x^2} \tag{4}$$

U is the temperature of the (silicon) slab and is dependent on position, x, and time, t.
α is the thermal diffusivity, $k/\rho c_p$, of silicon; with k, ρ and c_p being thermal conductivity, density and specific heat of the silicon material, respectively.

The Boundary and Initial Conditions are:

$$\frac{\partial U}{\partial x}(0, t) = -\frac{q_o}{k} \quad t > 0 \tag{4.1}$$

$$U(L, t) = U_L \qquad t > 0 \tag{4.2}$$

$$U(x, 0) = f(x) \qquad 0 < x < L \tag{4.3}$$

q_o is the solar irradiance on front surface of slab; U_L is the temperature of the back surface of the slab, ie the water temperature; $f(x)$ is the initial (time zero) temperature distribution in slab.

Let:

$$U(x, t) = V(x, t) + \varphi(x) \tag{5}$$

$V(x,t)$ is the transient portion of the temperature profile and $\varphi(x)$ is the steady state portion.

Developing the steady state portion:

$$\Rightarrow \frac{\partial^2 \varphi}{\partial x^2} = 0 \tag{6}$$

and

$$\frac{\partial \varphi}{\partial x} = -\frac{q_o}{k} \tag{6.1}$$

Integrating eqn 6 twice and applying BC:

$$\Rightarrow \varphi(x) = Ax + B \tag{6.2}$$

(A and B are arbitrary constants)

$$\frac{\partial \varphi}{\partial x} = A = -\frac{q_o}{k} \tag{6.3}$$

$$\varphi(L) = U_L = -\frac{q_o L}{k} + B \tag{6.4}$$

$$B = U_L + \frac{q_o L}{k} \tag{6.5}$$

Steady State portion, *φ(x)*, of the temperature profile is:

$$\varphi(x) = U_L + \frac{q_o}{k}(L - x) \tag{7}$$

For the transient portion, *V(x,t)*, of the temperature profile, let:

$$V(x,t) = X(x)T(t) \tag{8}$$

X(x) is a function of position, *x*, only and *T(t)* is a function of time, *t*, only.

$$\Rightarrow \frac{\partial V}{\partial t} = \alpha \frac{\partial^2 V}{\partial x^2} \tag{9}$$

$$\Rightarrow X(x) \frac{\partial T}{\partial t} = \alpha T(t) \frac{\partial^2 X}{\partial x^2} \tag{9.1}$$

$$\Rightarrow \frac{1}{\alpha} \frac{\frac{\partial T}{\partial t}}{T(t)} = \frac{\frac{\partial^2 X}{\partial x^2}}{X(x)} = -\lambda^2 \tag{9.2}$$

(*λ* is an arbitrary non-zero constant)

The solution to the differential equation (9.2) gives:

$$X(x) = A Cos(\lambda x) + B Sin(\lambda x) \tag{9.3}$$

and

$$T(t) = D Exp(-\alpha \lambda^2 t) \tag{9.4}$$

This gives the transient temperature profile as:

$$V(x,t) = \{[ACos(\lambda x) + BSin(\lambda x)]DExp(-\alpha\lambda^2 t)\}$$
$$= \{[FCos(\lambda x) + GSin(\lambda x)]Exp(-\alpha\lambda^2 t)\} \tag{9.5}$$

(A, B, C, D, F, G are arbitrary constants)

Differentiating eqn (9.3) and applying boundary conditions:

$$\frac{\partial V(0)}{\partial x} = \frac{\partial U(0)}{\partial x} - \frac{\partial \varphi(0)}{\partial x}$$

$$= -\frac{q}{k} - \left(-\frac{q}{k}\right) = 0 \tag{9.6}$$

$$V(L) \quad = U_L - \varphi(L) = U_L - U_L = 0 \tag{9.7}$$

$$\Rightarrow \frac{dX(o)}{dx} = -A\lambda Sin(\lambda x) + B\lambda Cos(\lambda x) \tag{9.8}$$

$$\Rightarrow B\lambda = 0; \quad \Rightarrow B = 0 \tag{9.9}$$

$$\Rightarrow X(L) = 0 = ACos(\lambda L) \quad \text{(A is non-zero constant)} \tag{9.10}$$

$$\Rightarrow Cos(\lambda L) = 0 \tag{9.11}$$

$$\Rightarrow \lambda = \frac{(2n-1)\pi}{2L} \tag{9.12}$$

eqn (9.5) becomes:

$$V(x,t) = [FCos(\lambda x)]Exp(-\alpha\lambda^2 t) \tag{9.13}$$

F is an arbitrary constant and λ represents the Eigen-values.

Fourier analyzing equation (9.13) gives the transient temperature profile as:

$$V(x,t) = \sum_{n=1}^{\infty} \left\{ \left[F_n Cos \frac{(2n-1)\pi x}{2L} \right] Exp \left[-\frac{\alpha(2n-1)^2\pi^2 t}{4L^2} \right] \right\} \tag{9.14}$$

and @ t = 0

$$V(x,0) = f(x) - \varphi_{(x)} = \sum_{n=1}^{\infty} \left[F_n Cos \frac{(2n-1)\pi x}{2L} \right] \tag{9.15}$$

$$\Rightarrow F_n = \frac{2}{L} \int_0^L [f(x) - \varphi(x)] Cos \frac{(2n-1)\pi x}{2L} \tag{9.16}$$

The "predictive" tool that can show how the temperature profile, U, in the silicon slab varies at any position/time (x/t) is given by the sum of the steady and transient temperature conditions [eqns (7) + (9.14)], which translates to:

$$U(x,t) = \left[U_L + \frac{q_o}{k}(L-x) \right] + \sum_{n=1}^{\infty} \left\{ \left[F_n Cos \frac{(2n-1)\pi x}{2L} \right] Exp \left[-\frac{\alpha(2n-1)^2\pi^2 t}{4L^2} \right] \right\} \tag{10}$$

Fn is given by equation 9.16.

Equation (10) is solved using MATLAB codes. (See appendix A for codes).

Equation (10) will be validated by analyzing the temperature profiles it produces with those obtained from the experimental model which is described in Section 3.1.2.

3.1.2 Gravity-Fed Cooling (GFC) Experimental Model

The proposed GFC system is as shown in Figure 3.3a. To simulate the proposed system, the experimental 'wet' PV cell model is replicated by gravity feeding water from an overhead tank to the back of a PV module, as illustrated in Figure 3.3b and Figure 3.4; and

the temperature, voltage and water flow-rate relationships are then analyzed. The temperature profiles obtained will be used to validate the mathematical model described in Section 3.1.1.

(a) Proposed GFC System   (b) Simulated GFC System
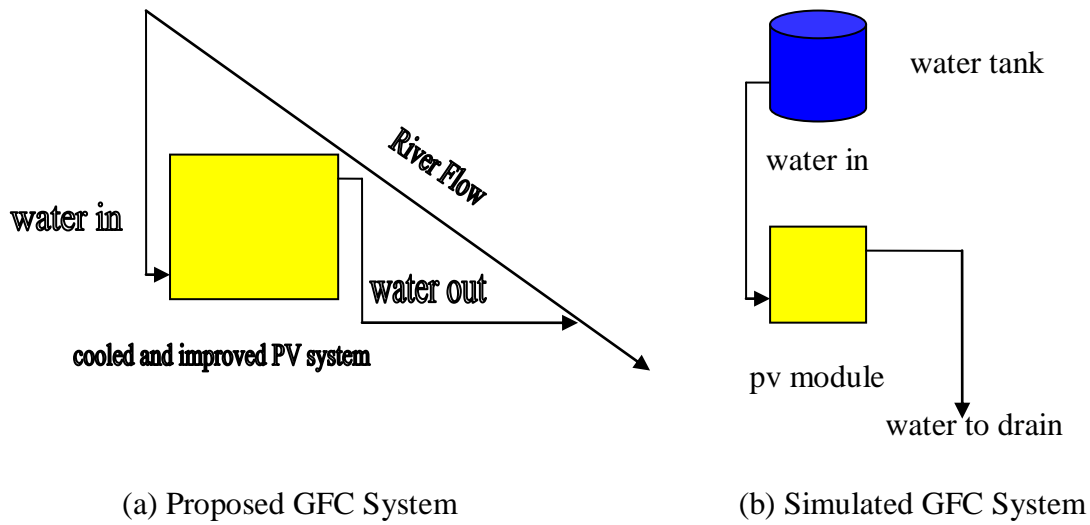
Figure 3.3   Schematics of Proposed and Experimental Simulated GFC Systems
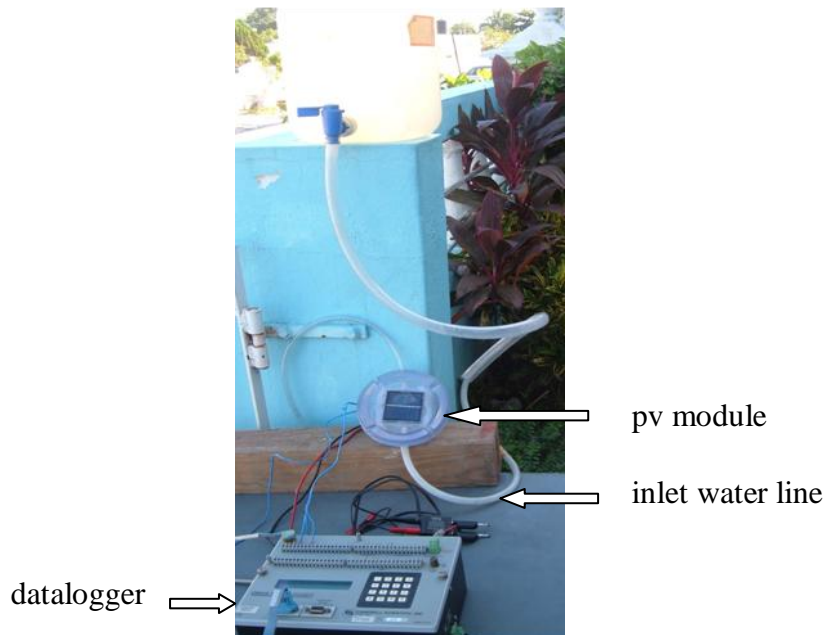
Figure 3.4   Layout of Apparatus for Gravity-Fed Cooling (GFC) Experiment

More details on the experiment procedures and apparatus are given in chapter 4.

3.2   Solar-Powered Adsorption Cooling (SPAC) Theoretical Postulation

Section 2.5.2 postulated that the constraint that limits the Gravity-Fed Cooling (GFC) technique to regions with water supplies can be removed. This can be achieved by employing a solar-powered adsorption cooling (SPAC) system to reduce the temperature of stored water below ambient temperature. The stored water is then circulated over the back surface of the PV cells. The chilled water minimizes the power require to run the circulating pump as less water is required to keep the system cool. The result is improved conversion efficiencies of the PV cells with minimum loss of 'parasitic- power'. To test the hypothesis a theoretical (mathematical) model of the SPAC is created and this is matched against experimental results. (The purpose of the mathematical model is to have a predictive tool that can accurately represent the degree of cooling that will be obtained from the SPAC system).

While a SPAC system is a compound system comprising the adsorption/desorption bed, condenser and evaporator; the focus is placed on the adsorption/desorption bed because the proper functioning of the bed is critical to the efficiency of the SPAC system. This means that it is crucial that the bed is able to reach the desorption temperature (boiling point) of the adsorbate to enable it to desorb (evaporate) from the adsorbent. Modelling of the adsorption/desorption rate, which is temperature dependent, is therefore considered as a function of heat conduction through the bed; and thus heat conduction through the bed constitutes the major theoretical engagement for SPAC systems (Li & Wang, 2003; Sakoda & Suzuki, 1984; Wang & Oliveira, 2005).

In general, adsorption/desorption bed modelling is based on heat and mass transfer through the porous bed and the balancing of the general energy-equation. The models are based mainly on a flat bed (to a lesser degree on a cylindrical bed) configurations, and in almost all cases they employed the Dubinin-Astakhov (D-A) equation for the adsorption/desorption isotherms (Aghbalou et al. 2004; Li & Wang, 2003). While the D-A equation is important in giving the amount of adsorbate (Methanol) desorbed from the pores of the charcoal bed, the predictive accuracy of any model, though, is highly dependent on what is used as the Effective Thermal Conductivity, K_e, of the bed (Critoph & Turner, 1995).

3.2.1 Modelling of Desorption Process in a Charcoal Bed

The desorption process takes place in a Charcoal Bed which comprises of activated granular charcoal which is saturated (adsorbed) with Methanol and is encased in a 19mm diameter by 1 metre long copper tube. The model formulated in this investigation for the desorption process differs mainly in the treatment of its effective thermal conductivity, K_e, for the bed (equation 14.2) and is developed along the following stages and assumptions:

1. Solar Energy (irradiation) over a period of time heats up copper tube and conducts through the charcoal bed.
2. Average temperature (T_1) of the copper tube over the time period becomes the boundary temperature of the bed (system).
3. Energy conducted increases the Bed (system) temperature to the Desorption temperature, T_{des}. (isosteric/sensible heating of the bed. No concentration change).
4. Additional energy goes to the Desorption (evaporation) of Methanol from the bed (isobaric heating accompanied with concentration change of Methanol).
5. The mass of methanol desorbed is given by the Dubinin-Astakhov (D-A) equation

The main assumptions here are that the specific heat of adsorbed methanol is the same as that of bulk liquid methanol and that the bulk of desorption takes place after the bed reaches the desorption temperature, T_{des}.

Governing Equation

The general equation that governs the energy balance of the Desorption Process is:

$$E_{net} + E_{gen} - \Delta E_{st} = E_{out} \qquad (11)$$

(E_{net} = net input energy to system, E_{gen} = energy generated bed, ΔE_{st} = energy stored in bed, E_{out} = energy leaving bed).

(Note: only some terms are explained here for clarity, but the full explanations of terms can be found in the nomenclature).

Net Input Energy, E_{net}

The energy to the system (bed) is composed as follows: E_{in} is the net direct solar irradiation (I) received by the Tube. This energy increases the temperature of the tube, a portion is re-

radiated (lost) due to temperature difference between tube and ambient, and the remaining portion, E_{net}, is then conducted to the charcoal bed.

$$E_{in} = \acute{\alpha} A_{cu} I t \tag{12}$$

$$E_{lost} = A t U (T_{tube} - T_{amb}) \tag{12a}$$

$$E_{net} = E_{in} - E_{lost} \tag{12b}$$

$\acute{\alpha}$ is the absorptance coefficient of copper, A_{cu} is the area of copper tube exposed to the solar irradiation, I, and U is the tube heat-loss coefficient ($W/m^2 K$).

Generated Energy, E_{gen}

No energy is generated in the bed, hence:

$$E_{gen} = 0 \tag{13}$$

Stored Energy, E_{st}

The energy stored will be reflected as an increase in both the tube and bed temperatures.

$$E_{st} = M_{bed} c_{\mathbb{P}} \Delta T_{bed} + m_{cu} c_p \Delta T_{tube} \tag{14}$$

where M_{bed} and $c_{\mathbb{P}}$ are the combined charcoal/methanol mass and specific heat, respectively; m_{cu} = mass of copper tube, T_{bed} and T_{tube} = bed and tube temperatures ^{o}C.

$$C_{\mathbb{P}} = [\varepsilon C_p]_f + [(1 - \varepsilon) C_p]_s \tag{14a}$$

(sub-scripts f and s are fluid and solid, respectively and ε = porosity of bed)

In this research, the sensible heating temperature profile of the bed, T_{bed}, (heating the bed to the point where it reaches the desorption temperature), is modelled as one dimensional (radial) heat conduction in an Infinite Cylinder. But, whereas the general heat equation for the bed is given as

$$\frac{\partial T}{\partial t} = \frac{k_e}{\rho C_{\mathbb{P}}} \left[\frac{\partial^2 T}{\partial r^2} + \frac{1}{r}\frac{\partial T}{\partial r} \right] - \dot{Q} \tag{14.1}$$

where $\dot{Q} = h_{des}\rho \frac{dX_m}{dt}$ is the heat source term for the heat of desorption (Li and Wang, 2003; Demir et al. 2008). Anyanwu et al. (2001) pointed out that during isosteric (sensible) heating of the bed $\frac{dX_m}{dt} = 0$ (no phase change of Methanol), hence the heat source term, $\dot{Q}$, vanishes. The isosteric heating temperature profile of the bed, T_{bed}, model is then reduced to:

$$\frac{\partial T}{\partial t} = \frac{k_e}{\rho C_{\mathbb{P}}} \left[\frac{\partial^2 T}{\partial r^2} + \frac{1}{r}\frac{\partial T}{\partial r} \right] \tag{14.1a}$$

where effective thermal conductivity, $k_{e,}$ is developed as:

$$k_e = k_s \left[1 + \frac{3\varepsilon\left(1 - \frac{k_s}{k_f}\right)}{(1-\varepsilon) + \left(\frac{k_s}{k_f}\right)(2+\varepsilon)} \right] \tag{14.2}$$

(k_s and k_f are thermal conductivity of solid (charcoal) and fluid (methanol), respectively)

This treatment of the effective thermal conductivity is adopted from Kaviany (1995) as one of the predictive equations for effective thermal conductivity for packed (porous) beds. Kaviany stated that this particular formulation is given by Hashin and Shtrikman (1962) variational formulation: upper bound, and its effectiveness is dependent on the ratio of the thermal conductivities of the solid (charcoal), k_s, to that of the fluid (methanol), k_f, being equal to or greater than one ($k_s/k_f \geq 1$). This formulation is chosen because its configuration is dependent on the porosity, ε, of the charcoal bed.

For this research, the charcoal particles used are assumed to be spherical and also that the arrangement of the particles in the bed is Simple Cubic. For such an arrangement,

Kaviany (1995) gives the porosity, ε, as 0.476. The effective thermal conductivity is reduced to simply a matter of geometry for a given solid/fluid combination.

Output Energy, E_{out}

The energy out of the bed, E_{out} , is comprised of the evaporation (desorption) of the methanol from the charcoal. This takes place when the temperature of the bed reaches the desorption temperature of Methanol. That is, $T_{bed} = T_{des}$.

So:

$$E_{out} = h_{des} m_{char} x_m \qquad (15)$$

where h_{des} is desorption energy, m_{char} is mass of charcoal and x_m is the mass concentration of methanol desorbed from the charcoal (kg methanol per kg charcoal). The heat of desorption given by Zhang and Wang (2002) as:

$$h_{des} = L_m \frac{T_{des}}{T_{con}} \qquad (15.1)$$

where L_m is the latent heat of vaporization of methanol. x_m is given by the renowned Dubinin-Astakhov (D-A) equation (Jing & Exell, 1993):

$$x_m = x_o exp\left[-Đ\left(\frac{T_{des}}{T_{con}} - 1\right)^{ń}\right] \qquad (15.2)$$

x_o is the maximum mass concentration of methanol for the adsorption space (kg methanol per kg charcoal), T_{des} and T_{con} are the desorption and condenser temperatures, respectively. Đ and ń are system parameters relating to the desorbing of the methanol/charcoal pair.

While the energy balance equation (11) enables a proper accounting of all energies associated with the system, the equation of import is the Dubinin-Astakhov equation (15.2) which gives the mass of methanol desorbed from the bed and goes to the evaporator. This is so because it is the mass of methanol desorbed (x_m) that determines the effectiveness of the SPAC system. In that, the degree of cooling given by the system is contingent on the mass of methanol leaving the evaporator; and on leaving it draws energy from the water in the evaporator, thus dropping the water temperature. Mathematically, this means:

$$m_w c_{p_w} \Delta t_w = m_{char}\, x_m L_m \tag{16}$$

Therefore, the degree of cooling (change in water temperature, Δt) is given as:

$$\Delta t_w = \frac{m_{char} x_m L_m}{m_w c_{p_w}} \tag{16.1}$$

The COP (efficiency) of the system is then given as the change in the energy of the water in the evaporator E_{evap} (eqn 16) to that of the energy input to the system E_{in} (eqn 12):

$$COP_{sys} = \frac{\text{useful energy}}{\text{input energy}} = \frac{E_{evap}}{E_{in}} = \frac{m_w c_{p_w} \Delta t_w}{\acute{\alpha} A_{cu} It} \tag{16.2}$$

3.2.2 Development of Bed Temperature Profile ($T_{bed} = T_{(r,t)}$)

Heat Conduction in Infinite Cylinder

Due to the ratio of Length to Diameter (1000/19) the heat flow through the tube can be assumed as one dimensional in the radial direction.

Heat Conduction Equation

$$\frac{\partial T}{\partial t} = \frac{k_e}{\rho C_{\mathbb{P}}} \left[\frac{\partial^2 T}{\partial r^2} + \frac{1}{r}\frac{\partial T}{\partial r} \right]$$
$$\tag{17}$$

$$0 < r < R; \quad t > 0$$

T is the temperature of the adsorption bed and is a function of radius, r, and time, t; with k_e, ρ and $C_{\mathbb{P}}$ being the combined-effective: thermal conductivity; density; and specific heat of the bed, respectively. "Combined" here refers to the composition of the solid, s, and fluid, f, phases of the bed.

Where effective thermal conductivity

$$k_e = k_s \left[1 + \frac{3\varepsilon \left(1 - \frac{k_s}{k_f}\right)}{(1-\varepsilon) + \left(\frac{k_s}{k_f}\right)(2+\varepsilon)} \right] \qquad (17.1)$$

and effective density

$$\rho C_{\mathbb{P}} = \left[\varepsilon (\rho C_p)_f + (1-\varepsilon)(\rho C_p)_s \right] \qquad (17.2)$$

and specific heat $C_{\mathbb{P}}$ is given by equation 14a. ε is the porosity (void fraction) of the bed.

The boundary conditions are:

$$T(R,t) = T_1 \qquad t > 0 \qquad (17.3)$$

$$\frac{dT(r_o,t)}{dr} = 0 \qquad t > 0 \qquad (17.4)$$

$$T(r,0) = T_0 \qquad 0 < r < R \qquad (17.5)$$

R is the outer radius of the cylinder, T_1 the average temperature of the tube over the given time period and T_0 the initial (time zero) bed temperature. [Note, T_1 is comprised of the average values of the top and bottom surface temperatures of tube (T & B) as shown in Table 5.6 on page 70].

Let:
$$T(r,t) = V(r,t) + \Psi(r) \qquad (18)$$

V(r,t) is the transient portion of the temperature profile and Ψ(r) is the steady state portion.

Developing the steady state solution:

$$\Rightarrow \frac{\partial^2 \Psi}{\partial r^2} + \frac{1}{r}\frac{\partial \Psi}{\partial r} = 0 \qquad (18.1)$$

And applying boundary conditions

$$\Psi(R) = T_1 \qquad (18.2)$$

$$\frac{d\Psi(r_o)}{dr} = 0 \qquad (18.3)$$

By Reduction Formulation, let:

$$\frac{\partial \Psi}{\partial r} = P \qquad (18.4)$$

$$\Rightarrow \frac{dP}{dr} + \frac{1}{r}P = 0 \qquad (18.5)$$

$$\frac{dP}{dr} = -\frac{P}{r} \qquad (18.6)$$

$$\frac{dP}{P} = -\frac{dr}{r} \qquad (18.7)$$

integrating

$$lnP = -ln(r) + lnC_1 = ln\left(C_1/r\right) \qquad (18.8)$$

$$\Rightarrow ln\left(\frac{Pr}{C_1}\right) = 0 \qquad (18.9)$$

$$\Rightarrow Pr = C_1 \qquad (18.10)$$

$$P = \frac{c_1}{r} = \frac{d\Psi}{dr} \qquad (18.11)$$

$$d\Psi = \frac{c_1}{r}dr \qquad (18.12)$$

$$\Psi(r) = c_1 \ln(r) + c_2 \tag{18.13}$$

from boundary conditions

$$C_1 = 0 \tag{18.14}$$

Therefore, at steady state:

$$\Psi(r) \Rightarrow \Psi(R) = T_1 \tag{19}$$

The transient portion of the temperature profile of the porous bed is developed as follows:

$$\frac{\partial V(r,t)}{\partial t} = \alpha^2 \left[\frac{\partial^2 V}{\partial r^2} + \frac{1}{r}\frac{\partial V}{\partial r}\right] \tag{20}$$

where $\alpha^2 = k_e / \rho C_{\mathbb{P}}$
with boundary conditions

$$V(R,t) = T(R,t) - \Psi(R) = T_1 - T_1 = 0 \tag{20.1}$$

$$\frac{dV(r_o,t)}{dr} = \frac{dT(r_o,t)}{dr} - \frac{d\Psi(r_o)}{dr} = 0 \tag{20.2}$$

$$V(r,0) = T(r,0) - \Psi(r) = T_o - T_1 \tag{20.3}$$

Now let

$$V(r,t) = F(r)\mathfrak{I}(t) \tag{20.4}$$

$F(r)$ is a function of radius, r, only and $\mathfrak{I}(t)$ is a function of time, t, only

Differentiating eqn (20.4)

$$\frac{\partial V}{\partial r} = \mathfrak{I}(t)\frac{\partial F}{\partial r} \tag{20.5}$$

$$\frac{\partial^2 V}{\partial r^2} = \Im(t)\frac{\partial^2 F}{\partial r^2} \tag{20.6}$$

$$\frac{\partial V}{\partial t} = F(r)\frac{\partial \Im}{\partial t} \tag{20.7}$$

Substituting in eqn (20)

$$F(r)\frac{\partial \Im}{\partial t} = \alpha^2\left[\Im(t)\frac{\partial^2 F}{\partial r^2} + \frac{1}{r}\Im(t)\frac{\partial F}{\partial r}\right]$$

$$= \alpha^2 \Im(t)\left[\frac{\partial^2 F}{\partial r^2} + \frac{1}{r}\frac{\partial F}{\partial r}\right] \tag{20.8}$$

$$\frac{1}{\Im(t)\alpha^2}\frac{\partial \Im}{\partial t} = \frac{1}{F(r)}\left[\frac{\partial^2 F}{\partial r^2} + \frac{1}{r}\frac{\partial F}{\partial r}\right] = -\lambda^2 \text{ (where } \lambda \text{ is a non-zero constant)} \tag{20.9}$$

Analyzing $\Im$ from eqn (20.9), gives

$$\frac{\partial \Im}{\partial t} + \lambda^2 \alpha^2 \Im(t) = 0 \tag{21}$$

$$\Rightarrow \frac{d\Im}{\Im} = -\lambda^2 \alpha^2 dt \tag{21a}$$

With solution:

$$\Im(t) = C exp(-\lambda^2 \alpha^2 t) \tag{22}$$

C is an arbitrary constant. Analyzing F from eqn (20.9) gives

$$\left[\frac{\partial^2 F}{\partial r^2} + \frac{1}{r}\frac{\partial F}{\partial r}\right] + \lambda^2 F = 0 \tag{23}$$

With solution

$$F(r) = DJ_o(\lambda r) + GY_o(\lambda r) \tag{24}$$

D and G are arbitrary constants

Now as r→0, Y_o →-∞, implying, from boundary conditions, that G = 0.

So

$$F(r) = DJ_o(\lambda r) \tag{24.1}$$

and hence

$$V(r,t) = DJ_o(\lambda r)C \, exp(-\lambda^2 \alpha^2 t)$$

$$= AJ_o(\lambda r)exp(-\lambda^2 \alpha^2 t) \tag{24.2}$$

From boundary conditions

$$V(R,t) = 0 = AJ_o(\lambda R)exp(-\lambda^2 \alpha^2 t) \tag{24.3}$$

This implies that

$$J_o(\lambda R) = 0 \tag{24.4}$$

So that

$$\lambda_n = \frac{zeros \, of \, J_o}{R} \tag{24.5}$$

Thus, the transient temperature profile of the porous bed is:

$$V_n(r,t) = \sum_{n=1}^{\infty} A_n F_n(r)exp(-\lambda^2 \alpha^2 t) \tag{25}$$

Where the normalized Eigen functions are:

$$F_n(r) = \frac{\sqrt{2}J_o(\lambda_n r)}{RJ_1(\lambda_n R)} \tag{25.1}$$

$$\Rightarrow V_n(r,t)$$

$$= \frac{\sqrt{2}}{R} \sum_{n=1}^{\infty} A_n \frac{J_o(\lambda_n r)}{J_1(\lambda_n R)} \exp(-\lambda^2 \alpha^2 t) \tag{26}$$

J_o and J_1 are Bessel Function of orders zero and one, respectively.

At t = 0,

$$V_n(r) = T_o - T_1 = \sum_{n=1}^{\infty} A_n F_n(r) \tag{26.1}$$

Where A_n is derived as (Trim,1990):

$$A_n = \int_o^R r(T_o - T_1) F_n(r) dr$$

$$= (T_o - T_1) \int_o^R r \frac{\sqrt{2} J_o(\lambda_n r)}{R J_1(\lambda_n R)} dr$$

$$= \frac{\sqrt{2}}{\lambda_n} (T_o - T_1) \tag{26.2}$$

Therefore the predictive tool for the porous bed temperature-profile (T_{bed}) is the sum of the steady state (Ψ) and transient state (V) temperature-profiles [eqns (19) + (26)]:

$$T(r,t) = T_1 + \frac{2(T_o - T_1)}{R} \left[\sum_{n=1}^{\infty} \exp(-\lambda^2 \alpha^2 t) \frac{J_o(\lambda_n r)}{(\lambda_n) J_1(\lambda_n R)} \right] \tag{27}$$

where T_o and T_1 are temperatures at zero time and tube surface, respectively. J_o and J_1 are Bessel Function of orders zero and one, respectively. The above system of equations is programmed in Matlab (see appendix B for codes) and the experimental model, described in Section 3.2.3, will be used to validate this system of equation by comparing the data gathered from the experiment with those derived from the equations.

Again, the aim in the development of this system of equations is to obtain a 'tool' that can predict the temperature profile of the porous bed with some degree of accuracy. This is necessary as it is difficult to measure the temperature across the bed in practical applications. Hence this tool, if found accurate, should remove uncertainties as to what is happening in any given practical adsorption cooling system with this type of configuration.

3.2.3 SPAC Experimental Model

The SPAC system is modelled as a 19mm dia. x 1000 mm long copper tube bed with 12mm copper tube coil as both condenser and evaporator. The system is designed with no valves (Figure 3.5), and is similar to the no-valve solar ice maker found in the literature (Li et al., 2004), so that minimum supervision is required. The bed comprises activated granular charcoal/methanol pair. The system is analyzed for the degree of cooling given by the evaporator and the data gathered will be used to validate the system of equations derived in Section 3.2.1.
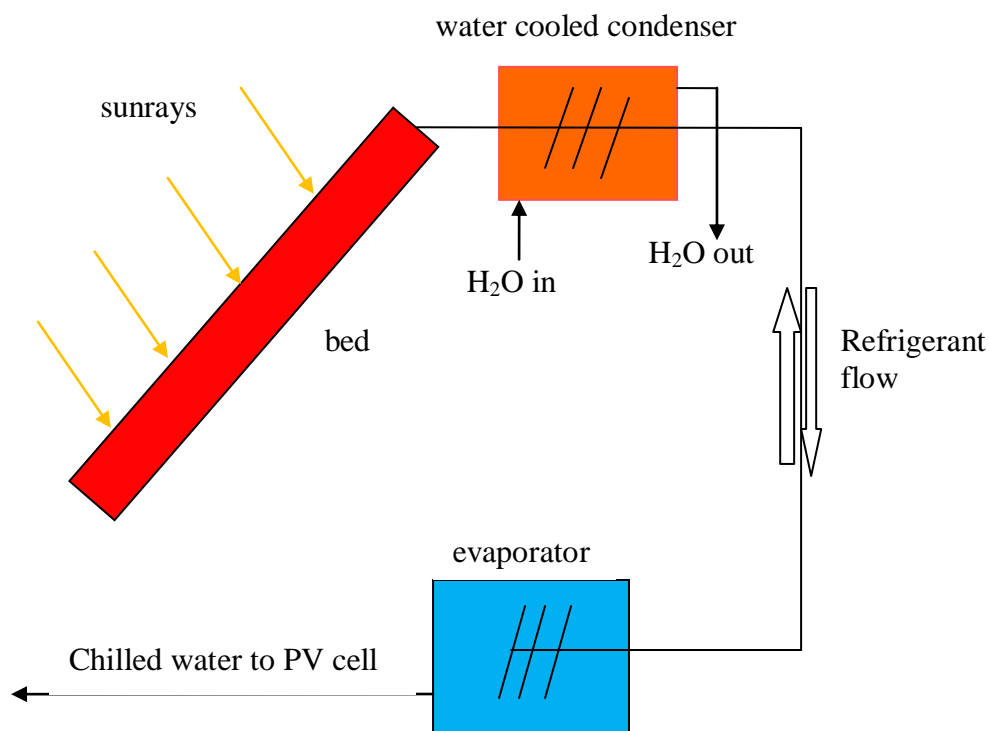
Figure 3.5   Schematics of Solar Powered Adsorption Cooling (SPAC) System

More details of the experimental procedures and apparatus are given in chapter 4.

3.3   Summary

Chapter 3 showed the development of the mathematical and experimental models, along with all governing equations, for the Gravity-Fed Cooling (GFC) and Solar Powered Adsorption Cooling (SPAC) systems. It gave, in mathematical terms, a formulation that is be able to determine (predict) how the temperature, U(x,t) (eqn 10), varies in a PV cell using Gravity-Fed Cooling (GFC) as:

$$U(x,t) = \left[U_L + \frac{q_o}{k}(L-x) \right] + \sum_{n=1}^{\infty} \left\{ \left[F_n Cos \frac{(2n-1)\pi x}{2L} \right] Exp \left[-\frac{\alpha(2n-1)^2 \pi^2 t}{4L^2} \right] \right\}$$

Likewise it established a similar 'predictive tool' for the desorption temperature, $T_{(des)}$ (eqn 27).

$$T(r,t) = T_1 + \frac{2(T_o - T_1)}{R} \left[\sum_{n=1}^{\infty} exp(-\lambda^2 \alpha^2 t) \frac{J_o(\lambda_n r)}{(\lambda_n)J_1(\lambda_n R)} \right]$$

This temperature is required for the generation of the Dubinin-Astakhov (D-A) equation, which in turn determines the effectiveness of the SPAC system.

Chapter 3 also set the stage for the description of the experimental procedures and instrumentation which follows in Chapter 4.

CHAPTER 4

EXPERIMENTS and INSTRUMENTATION

Having developed in Chapter 3 the theoretical (mathematical) and experimental models on which the objectives and specific outcomes for the thesis are predicated, this chapter outlines the procedures for the execution of the required experiments which will validate (or not) the hypotheses and also the findings from the theoretical calculations.

As mentioned in Section 1.2.1.2, a major objective of the research is to establish the effectiveness of both Gravity-Fed Cooling (GFC) and Solar-Powered Adsorption Cooling (SPAC) on Photovoltaic power-output, and also as mentioned in Section 1.2.1.3, a specific outcome is to demonstrate that hydrogen can be utilized for domestic cooking. The chapter also describes the procedures for the experiments which will aid in accomplishing the objectives. These experiments are as listed in Table 4.1

The Instruments used in the experiments are described at the end of the chapter.

Table 4.1   Summary of Experiments and Types of Tests

Experiments	Nature of Tests	Number of Test Runs	Time (days)
Gravity Fed Cooling System	(1) Effects of temperature variations on PV module voltage & power	10	3
	(2) Effects of cooling water flowrates on temperature variations	4	2
Solar Powered Adsorption Cooling (SPAC) System	(1) Determination of affinity of charcoal for methanol	2	2
	(2) Determination of degree of cooling given by system	5 (cycles)	5
	(3) Effects of sub-cooled temperature variations on PV module voltage & power	7	3
	(4) Effects of sub-cooled water flow rates on temperature variations	4	2

Hydrogen Production	Impact of temperature variations in PV module on Electrolyzer power and hydrogen outputs	8	8
Burning/Cooking Hydrogen Gas	(1) Burning hydrogen gas directly from electrolyzer	6	1
	(2) Cooking with low pressure hydrogen gas	5	3

4.1   Procedure for the Experimentation of the GFC System

An eight-cell PV module, measuring 6cm x 6cm x 0.3cm, with rated voltage of 4.5 volts at 25 ^{o}C and 1000 W/m^2 was used in the experiment (Figures 4.1& 4.2). The back of the module was enclosed and the terminals sealed against water intrusion with silicone sealant (Figure 4.3). Inlet and outlet ports were installed for water flow. The water entered at the bottom of the module and left at the top. The water was supplied under gravity from an overhead tank with a hydraulic head of 1.2m. Flow rates ranging from 0.03 litre/min to 2 litre/minute were investigated to establish optimum conditions.

The water was not circulated (simulating the return to source downstream, Figure 3.3) so as to ensure a constant supply-temperature. A thermocouple was placed at the centre of the back surface of the PV module and sealed against water intrusion. Another was placed in the water stream. The water flowed through a gap of 3cm (Figure 4.3).
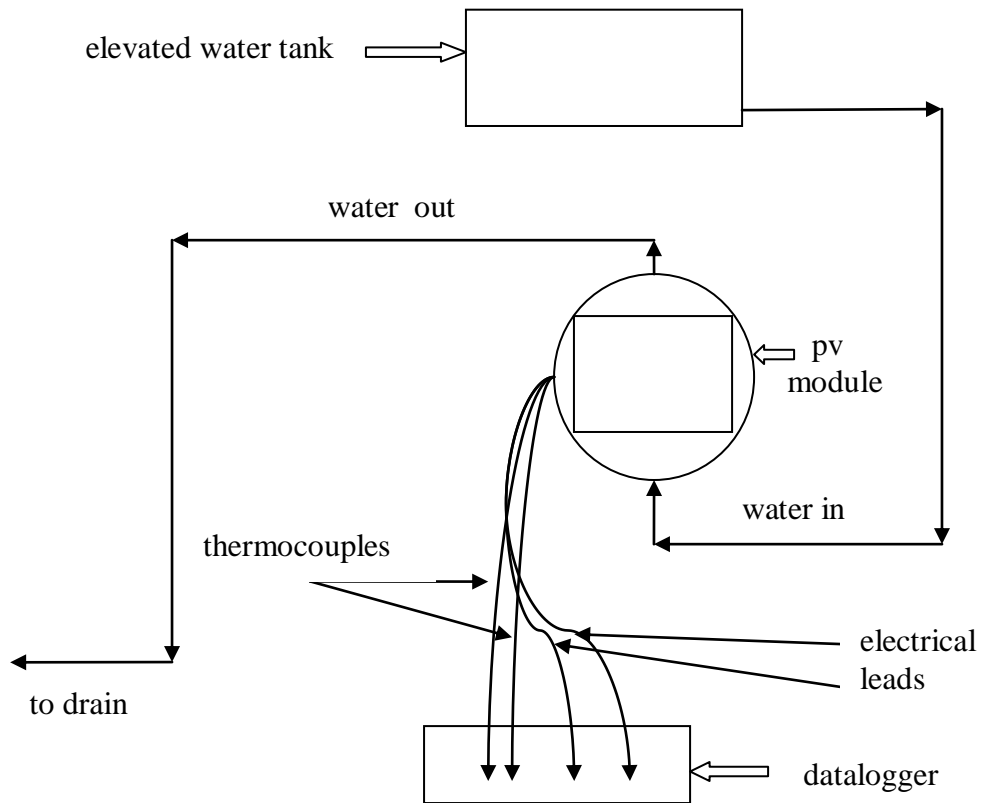
Figure 4.1   Schematics of Gravity-Fed Cooling Apparatus and Experiment
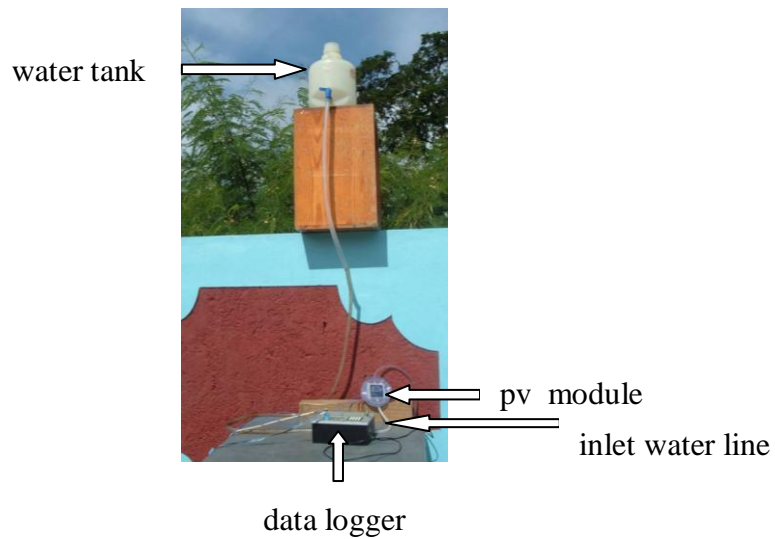
Figure 4.2   Layout of Gravity-Fed Cooling (GFC) Experiment

Figure 4.3 **Back View of of PV Module**

The module was placed outdoors, free of all shade, and monitored for one week between the hours of 6am – 6pm. This was to ascertain its operational temperature range under the prevailing conditions. On the days of the actual tests the cooling water was turned on as soon as the module reached the maximum temperature of 62 - 68 ^{o}C. The water was kept on for half an hour and then turned off. The module was then allowed to return to the maximum temperature and the water was again turned on. This on/off operation was repeated for three to four times per day as long as the solar irradiance was sufficient to raise the module to the maximum temperature and remained in the range of 900 – 1050 W/m^2. The procedure was repeated for three consecutive days and all data were recorded by a Campbell's CR23X data-logger (Figure 4.4).

Figure 4.4 **Campbell CR23X Data-Loggers**

4.2   Procedure for Experimentation of the SPAC System

4.2.1 System Construction

The Solar-Powered Adsorption Cooling (SPAC) system was constructed as a 19mm (diameter) x 1000 mm long copper tube bed with 12mm diameter copper tube used to build both the condenser and the evaporator. The system was designed for minimum supervision and so it incorporated no valves between bed-condenser-evaporator as shown in Figure 4.5. This design is similar to the no-valve solar ice maker used by Li et al. (2004). The design removed the need to monitor the system to accommodate valve opening and closing in the evenings and mornings.

The bed comprised of activated granular charcoal/methanol pair. The condenser and evaporator were encased in thermally insulated containers. The condenser had cooling water circulating through it. Figure 4.6 shows the schematics of the Solar-Powered Adsorption Cooling experiment and Figure 4.7 shows the actual SPAC experimental set up.
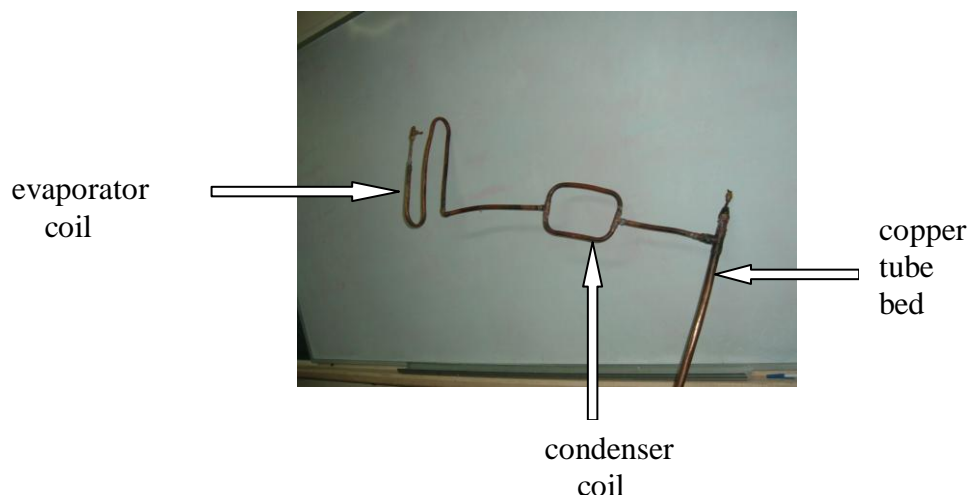
Figure 4.5   **Construction of SPAC system**
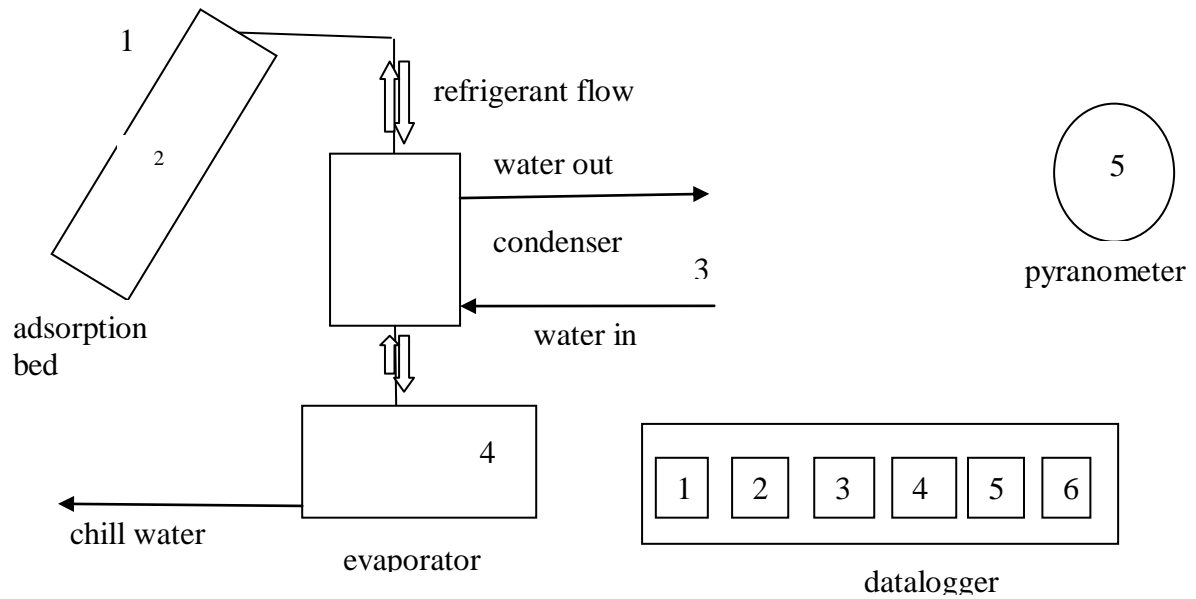
Figure 4.6   Schematic of the Experimental Apparatus for the SPAC System

1-Copper tube temp probe(T_1)   2-Bed-centre temp probe(T_{bed})   3-Water outlet temp probe(T_{con})
4-Chill water (evap) temp probe(T_{evap})   5-Pyranometer probe   6-Ambient temp probe, T_{amb}
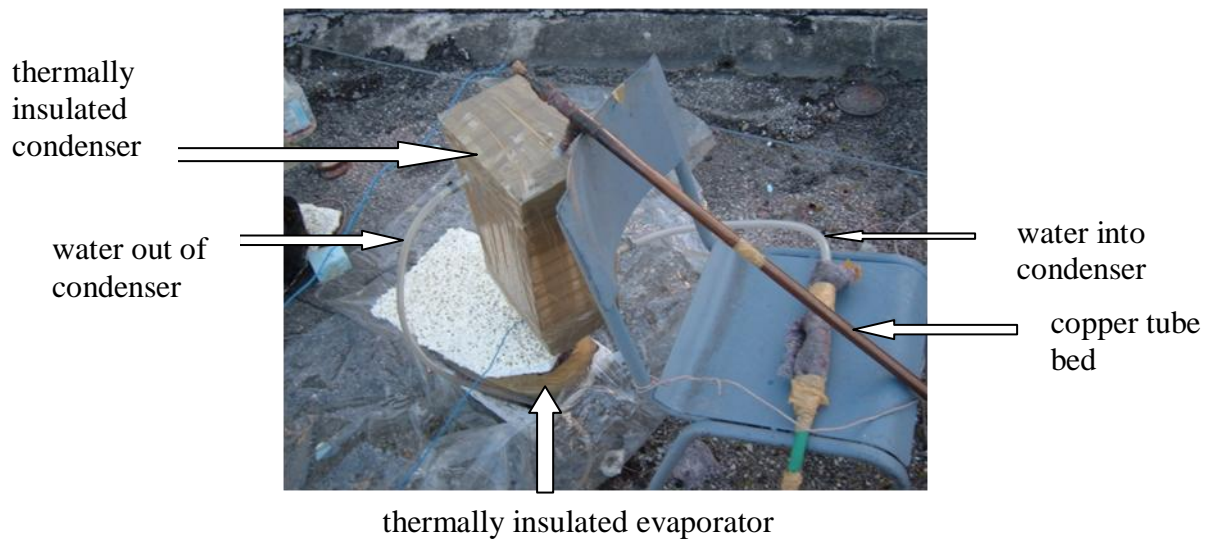
Figure 4.7   Experimental setup of SPAC System

(The figure shows copper-tube bed methanol/charcoal inside supported by chair while exposed to solar radiation. Thermally insulated condenser with circulating water and evaporator are shown at the side).

4.2.2 Determination of the Affinity of the Charcoal for Methanol

The activated carbon used was a granular type, under the brand name AquaClear, for aquariums. It was characterized only as 'premium research grade' and the average diameter of the grains was 1.2 mm. (The average diameter was obtained by shaking the grains through calibrated sieves of American Society of Testing and Material (ASTM) specifications). This type of activated charcoal was used instead of the powdered type because of the grain size. The literature shows that grain size averaging 1.0 mm diameter gives the best adsorptive capacity (Jing and Exell, 1993).

To determine the adsorptive properties of the AquaClear charcoal the following steps, adopted from Jing and Exell (1993), were undertaken:

Step 1: Twenty- two (22) grams of charcoal were encased in a 150mm long by 19mm diameter copper tube.

Step 2: The tube was placed in an oil bath and heated to 120 ^{o}C while at the same time subjected to a vacuum of 710 mm(28") Hg. This condition was held for one hour to ensure the removal of moisture from the charcoal.

Step 3: After one hour both the vacuum and oil bath were switched off and the charcoal was exposed to the methanol. The system was left overnight (for convenience) and the amount of methanol adsorbed was recorded. This procedure was carried out twice and in both instances the amount of methanol adsorbed was 11grams. This gives a concentration ratio (adsorptive capacity) of 1:2 (kg methanol/kg charcoal).

4.2.3 Determination of Coefficient of Performance (COP) of SPAC System

To determine the effectiveness of the SPAC system in terms of the degree to which it can lower (sub-cool) the circulating water temperature below that of the ambient, the following procedure was executed. The metre long copper tube was charged with 120 gram of the activated charcoal and placed under vacuum for four hours after which 60 gram of methanol was drawn into the tube. This amount of methanol was to satisfy the 1:2 ratio established as the adsorptive capacity of the charcoal (Section 4.2.2). The system stabilized at 405mm (16") Hg vacuum. At this level the boiling point of methanol drops from 65 $^{\circ}$C at one atmosphere to 52 $^{\circ}$C (Properties of Fuel, n.d).

The complete system (bed, condenser, evaporator), supported by a chair, was placed on the roof of the lab (Figure 4.7). Thermocouple probes were attached and connected to the data logger for analyses of the various temperatures (Figure 4.6). The thermocouple probes were located:

- On the surface of the copper tube, shielded from direct sunlight (tube temperature, T_1)
- In the centre of the charcoal/methanol bed (bed temperature, T_{bed})
- In the outlet water stream of the condenser (condenser temperature, T_{con})
- In the water which covered the evaporator coil (evaporator temperature, T_{evp})
- In the ambient air, shielded from sunlight and wind velocity (T_{amb})

It was found that during the sunlit hours the bare copper tube of the bed, when exposed to the ambient conditions especially wind speed, had a high rate of heat re-radiation back to ambient resulting in a slow temperature rise in the bed. In order to minimize the overall heat loss (re-radiation) from the copper tube to the ambient, the metre long bed was covered with clear plastic to give a green house effect, as shown in Figure 4.8. The overall heat loss coefficient, U(W/m^{2}K), which included both convective and radiative losses was calculated from the following formulation developed by Klein (1979) and reported by Duffie and Beckman (1991):

$$U = \left[\frac{n_{pls}}{\frac{C_o}{T_{tube}}\left(\frac{T_{tube}-T_{amb}}{n_{pls}+f}\right)^e} + \frac{1}{h_w} \right]^{-1} +$$

$$\left[\frac{\sigma(T_{tube}+T_{amb})(T_{tube}^2+T_{amb}^2)}{(E_{tube}+0.00591n_{pls}h_w)^{-1}+\frac{2n_{pls}+f-1+0.133E_{tube}}{E_{pls}}-n_{pls}} \right] \qquad \text{eq4.1}$$

n_{pls}= # plastic wrap; E_{tube}= copper emissivity; E_{pls}=plastic emissivity;

h_w= wind heat transfer coefficient; σ = Stefan-Boltzmann constant

f = (1 + 0.089h_w - 0.1166$h_w E_{tube}$)(1 + 0.07866n_{pls})

C = 520(1 – 0.000051β^2); for $0^o < \beta < 70^o$. For $70^o < \beta < 90^o$, use $\beta = 70^o$

β = tube tilt angle (degrees)

e = 0.430[1 – (100/T_{tube})]

The range of values for U obtained by Jing and Exell (1994) using the formulation is 5.5 – 20 (avg 10.25) $Wm^{-2}K^{-1}$. Our calculation gave a value of 10.4 $Wm^{-2}K^{-1}$. The plastic cover did not affect the night cooling of the bed. Finally the condenser cooling water was switched on. A pryranometer was also attached to the logger to record the solar irradiation.
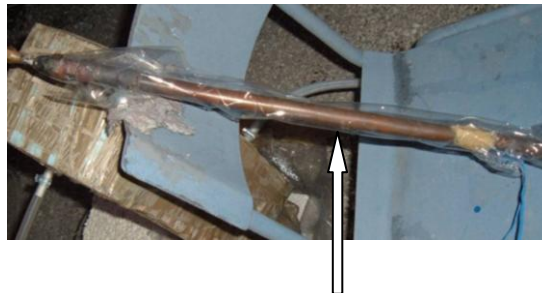
copper-tube bed covered with plastic

Figure 4.8   Copper-Tube Bed covered with plastic to reduce daylight heat re-radiation to ambient

4.2.4 Impact of the SPAC System (a simulation)

To ascertain the impact of the SPAC system, the equipment described in Section 4.1 was again utilized (Figure 4.9); that is, the eight-cell PV module, measuring 6cm x 6cm x 0.3cm with rated voltage of 4.5 volts at 25 ^{o}C and 1000 W/m^2, was re-engaged. As described before, the back of the module was enclosed and the terminals sealed against water intrusion with silicone sealant. Inlet and outlet ports were installed for water flow.

The difference in this simulation was that the water being circulated over the back of the PV module was kept at the same temperature, T_{evap}, that was obtained in the evaporator of the SPAC system. The effects of this chilled water given by the SPAC system on voltage

generated by the PV module were investigated. Also investigated were the impacts of varying flow rates of the cooling water, in order to establish the optimum operating conditions.
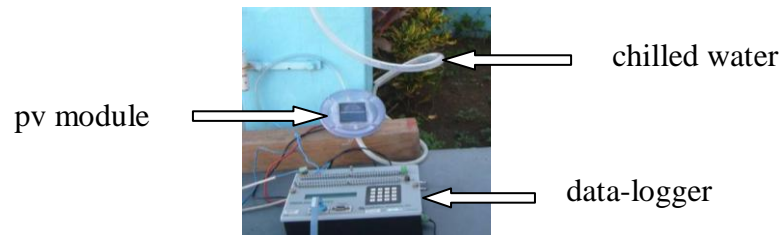
Figure 4.9   Simulation of Solar-Powered Adsorption Cooling (SPAC) System

4.3   Hydrogen Production versus Temperature Variation of PV Panel

One of the objectives given in Section 1.2.1.2 is to establish the rate of hydrogen production from an electrolyzer, for each cooling system. In other words, in what ways do the degrees of cooling of a PV module, given by each cooling system (GFC and SPAC), affect the production rate of an electrolyzer that is powered by the said PV module.

In order to establish the relationship between hydrogen production of an Electrolyzer and temperature variation of a PV module, a double-cell PEM electrolyzer, rated at 65 mL/min, was coupled to a 13watt PV module measuring 33 cm by 33 cm by 0.5 cm thick. The module was modified in a fashion similar to that described in Section 4.1. The back of the module was enclosed and the terminals sealed against water intrusion with silicone sealant (Figure 4.10). Inlet and outlet ports were installed for water flow. Water entered at the bottom of the module and left at the top (Figure 4.1). The water was also supplied under gravity from an overhead tank with a hydraulic head of 1.2m. Figures 4.11 and 4.12 show the complete experimental set up.
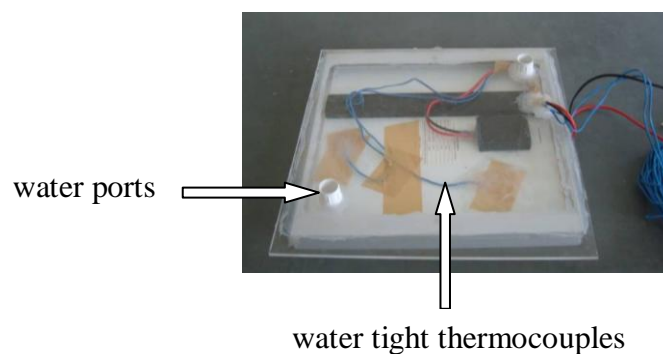
Figure 4.10   Back View of PV Module Fitted for Water Flow
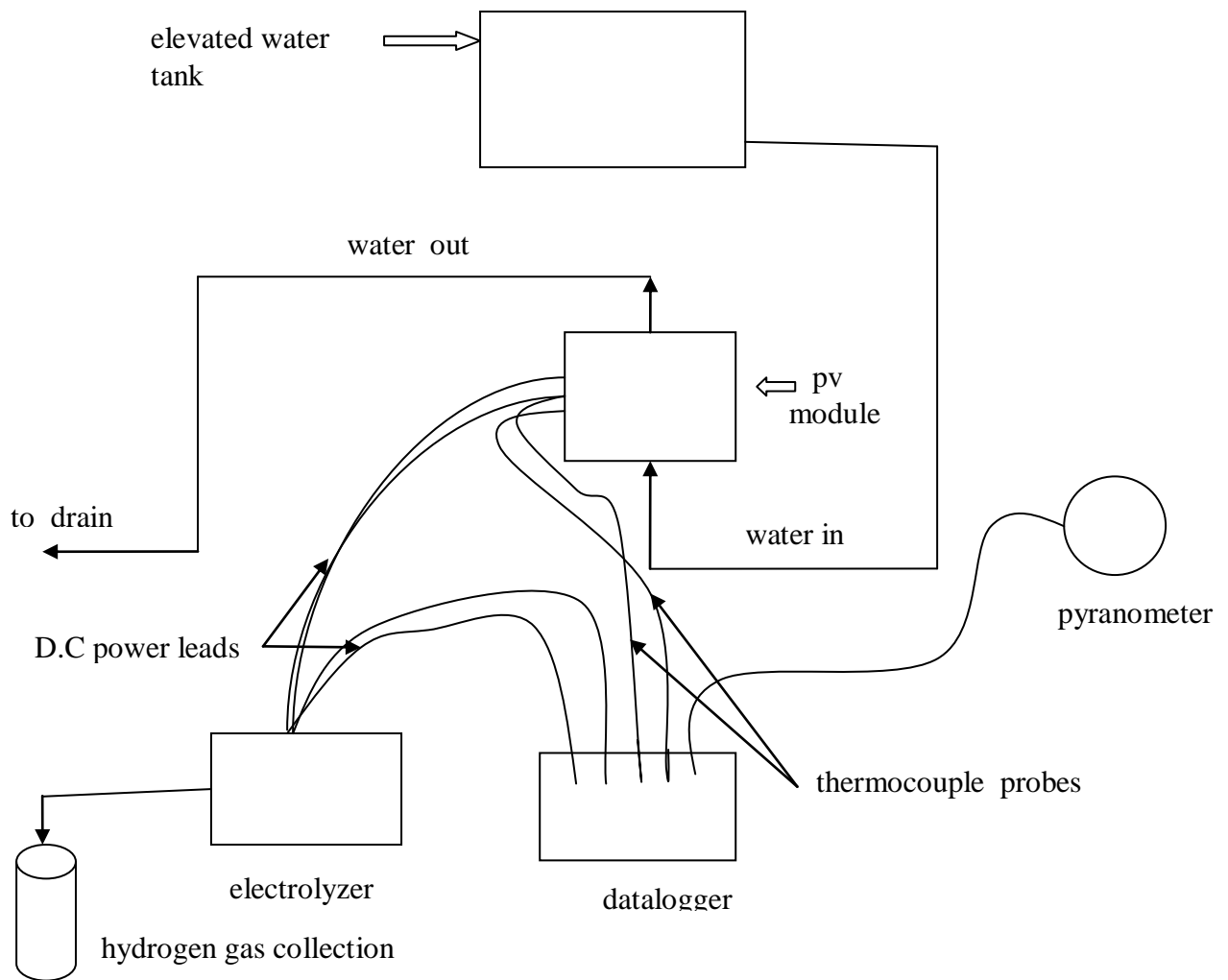
Figure 4.11　　　**Schematics of Hydrogen Production Experiment**
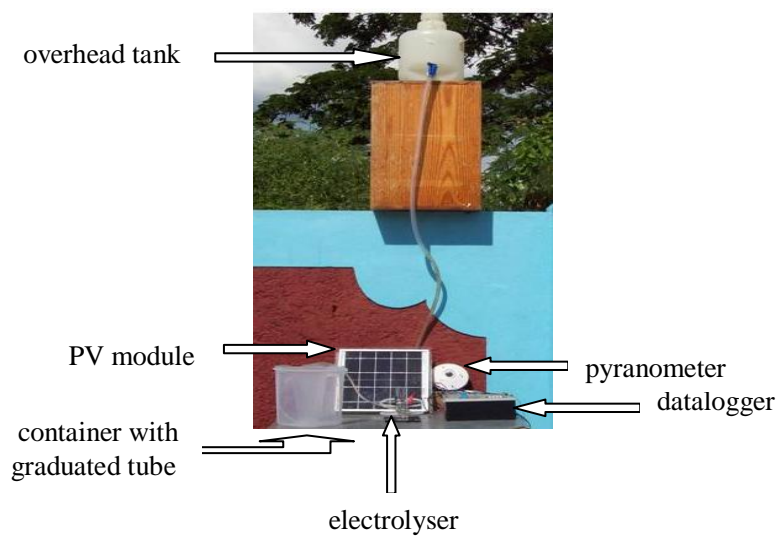
Figure 4.12　　**Layout of Apparatus for Hydrogen Production vs Temperature Variation of PV Panel Experiment**

The hydrogen output from the electrolyzer was measured by means of an inverted graduated tube, as shown in Figure 4.13. The graduated tube was filled with water and then inverted into a water-filled container. The outlet end of the plastic tubing that transports the hydrogen gas from the electrolyzer was then placed in the inverted tube. At this stage the graduated tube was completely filled with water and devoid of all bubbles. The electrical connections from the PV module were then attached to the electrolyzer and the stop-watch started on the appearance of the first bubble at the top of the graduated tube.

This procedure for the production rate of hydrogen was repeated for PV module-temperatures ranging from 25 $^{\circ}$C – 60 $^{\circ}$C in steps of 5 degrees. Production rates of hydrogen and also output power drawn from the PV module by the electrolyzer were logged and then plotted against temperature.
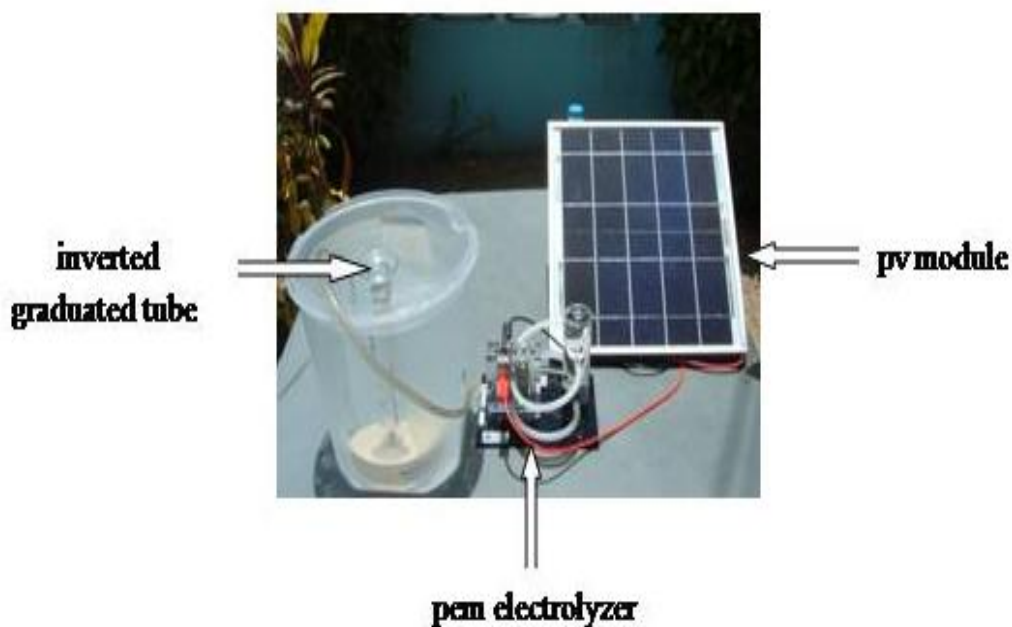
Figure 4.1   Measuring production of hydrogen from Electrolyzer/PV Module System

4.4   Hydrogen as a Cooking Gas

4.4.1 Burning of Low Pressure Hydrogen Gas

One of the specific outcomes of this research (Section 1.2.1.3) seeks to demonstrate, after all general safety precautions are taken into consideration, that low pressure hydrogen gas can be used for cooking and also that it is as safe as any other domestic gas such as propane and petrol. Hydrogen gas is safer than the regular propane gas because it being so much lighter than air dissipates very rapidly and hence unable to form any degree of concentration which is necessary for an explosion to occur; provided that it is not in a very confined space. On the other hand, propane, which is denser than air, settles in the vicinity of a leak and thus creates an explosive concentration.

The following tests were carried out to demonstrate the relative ease in using low pressure hydrogen gas.

4.4.1.1   *Igniting Low Pressure Hydrogen Gas from Electrolyzer*

A Bunsen burner was modified by removing the barrel and exposing the needle valve at the base. It was observed that low compression (pressure) and flow of hydrogen gas from the electrolyzer was insufficient to support a flame when the barrel was on the burner. The burner was then directly attached to the hydrogen hose on the electrolyzer and the electrolyzer was then powered by the PV module. At the start of gas flow the burner was lit. The set up is shown in Figure 4.14.
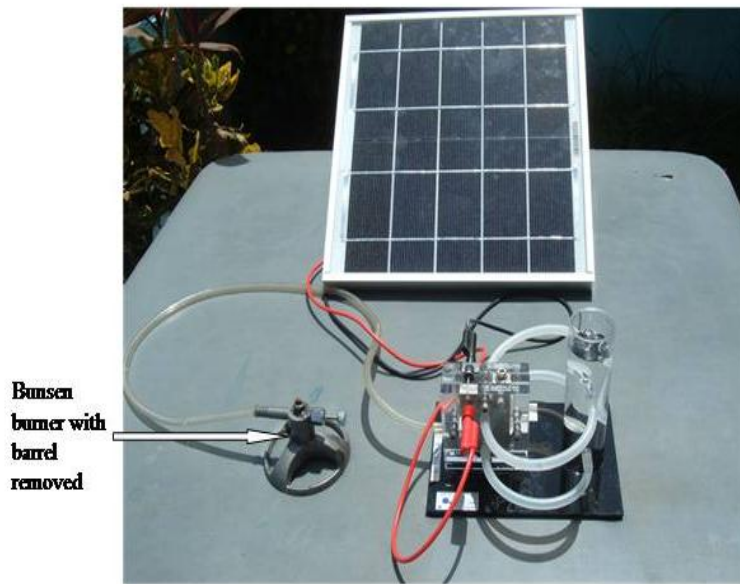
Figure 4.2 **Burning of hydrogen gas directly from electrolyzer**

4.4.1.2 *Cascading Storage System (CSS) for Hydrogen Gas*

To compensate for the low compression/flow of gas from the electrolyzer (note, there are PEM electrolyzers that can produce gas at 10 bar and 30 litres per hour (Heliocentris Energy Systems@ www.heliocentris.com)) a Cascading Storage System (CSS) was developed for the demonstration of hydrogen as a cooking gas. This system was developed because Metal Hydride Canisters, the preferred medium for storing hydrogen, are too expensive for consideration in this investigation.

The Cascading Storage System (CSS) consists of a high pressure cylinder with hydrogen gas at 34 bar connected to a regular cooking gas (low pressure) cylinder at a pressure of 4 bar, via a pressure regulator. A standard cooking gas regulator (0.03 bar output) was then attached to the low pressure cylinder. This Cascading Storage system was then connected to a modified Bunsen burner that acted as a 'one-burner-stove'. Figures 4.15 and 4.16 show the Cascading Storage system attached to a stove/burner.

The Bunsen burner was modified by completely sealing the air vent at the bottom of the barrel. The reason for the modification was that, unlike propane gas, premixing of the hydrogen gas with air before ignition creates a weak mixture (excess oxygen) that is unable to support a flame.
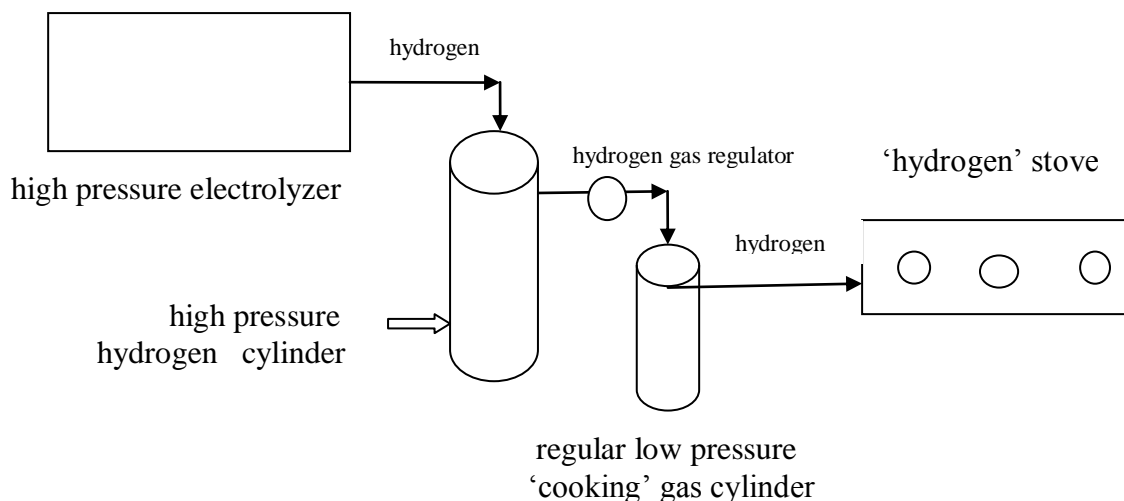
Figure 4.15   Schematics of Cascading Storage System (CSS) for Hydrogen Gas
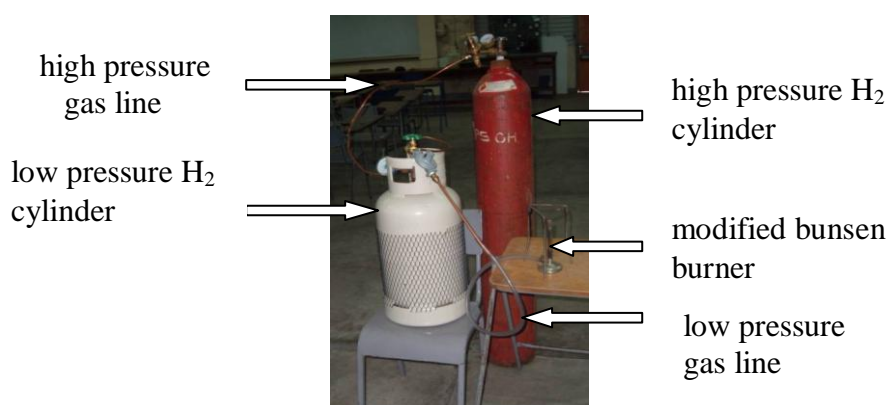
Figure 4.16   Hydrogen Gas Cascading Storage System (CSS) attached to Burner

4.4.2 Cooking with Low Pressure Hydrogen Gas

Having developed the Cascading Storage System (CSS) for hydrogen gas, which now puts the handling of hydrogen in the same realm as that of propane, this allowed the researcher to put the specific objective of utilizing hydrogen as a cooking gas to the test.

After transferring the hydrogen gas from the high pressure cylinder to the low pressure cylinder, a demonstration of the use of hydrogen as a cooking gas was carried out. An egg was placed in a pot on the 'one-burner-stove', the regulating valve on the cylinder

was opened and the hydrogen gas lit. Figure 4.17 shows the demonstration of cooking with hydrogen gas.

low pressure H$_2$ gas

pot with egg

modified Bunsen burner
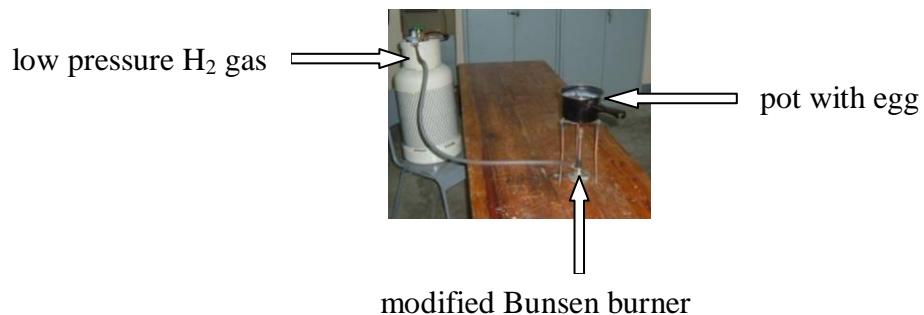
Figure 4.17   Demonstration of Cooking with Low Pressure Hydrogen Gas

4.5   Instrumentation

The Instruments used in the experiments are given in Table 4.2. A complete description of these instruments and the degree of accuracy given by each is given in Appendix D.

Table 4.2   List of Instruments used in Experiments

INSTRUMENT	TYPE/BRAND
Pyranometer	Kipp and Zonen CM1
Data-Logger	Campbell CR23X
Electrolyzer	PEM/StaXX2
PV Module	(1) Eight Cells (2) SUN-13

Sieves	(1) A.S.T.M (2) Canadian: Tyler Equivalent
Electronic Scale	Sartorius CP2202S
Multimeter	Kosmos RE30B
Voltage Divider	Campbell
Current Shunt	Fluke 80J-10

4.6 Summary

Chapter 4 described the procedures for the experiments required to achieve the objectives of the research and listed the instruments used. The major procedural descriptions that the chapter outlined are those for:

- Gravity-Fed Cooling (GFC) system
- Solar-Powered Adsorption Cooling (SPAC) system
- Determination of the adsorptive capacity of charcoal for methanol
- Hydrogen production rates
- Demonstration of hydrogen as a cooking gas

CHAPTER 5

RESULTS and CALCULATIONS

This chapter gives the results obtained from the experiments carried out as described in Chapter 4. And as the objectives in Section 1.2.1.2 stated, the experiments were to determine the effects of Gravity-Fed Cooling (GFC) and Solar Powered Adsorption Cooling (SPAC) on PV modules and systems. Therefore the results are examined in light of these objectives. The chapter looks firstly at the findings from experimentations and then matches them against the findings from the mathematical models. Samples of Raw Data, Major Calculations, Regression and Uncertainty Analyses, and Graphs are also presented.

In terms of calculations the following are covered:

1. Mathematical Modelling of Gravity-Fed Cooling system
2. Mathematical Modelling of a Cylindrical Desorption Bed
3. Energy Balance for Solar-Powered Adsorption Cooling (SPAC) system
4. Hydrogen Production versus Temperature Variation of PV Panel

5.1   Typical Measured Data from Experiments

Table 5.1 presents typical raw data obtained from the experiments on cell temperature versus voltage. It highlights the effects that elevated cell-temperature has on the operational voltage of a PV module. The table shows that as the cell temperature increases the output voltage decreases. This effect translates itself in increased cost for PV systems. In that, to compensate for the voltage drop PV systems have to be oversized.

Table 5.1   Typical Measured Data showing the Effects of Elevated Cell Temperature on Voltage

(from Nature of Test #1 in Table 4.1)

Solar Irrad (W/m²)	Cell Volts (V)	Cell Temp (deg C)	Solar Irrad (W/m²)	Cell Volts (V)	Cell Temp (deg C)	Solar Irrad (W/m²)	Cell Volts (V)	Cell Temp (deg C)
rror± 10 W/m	0.1% error	0.1% error	rror± 10 W/m	0.1% error	0.1% error	rror± 10 W/m	0.1% error	± 0.1% error
1038	4.368	34.18	953	4.363	34.25	973	4.358	34
1038	4.35	35.78	948	4.332	35.85	981	4.34	35.57
1038	4.291	37.41	955	4.272	37.3	994	4.286	37.2
1046	4.284	38.37	1008	4.3	38.48	1007	4.279	38.3
1046	4.273	39.88	1009	4.288	40	1019	4.271	40.04
1046	4.266	41.98	1013	4.263	41.47	1023	4.261	41.77
1046	4.281	42.83	1015	4.239	42.77	1019	4.249	42.66
1046	4.263	44.15	1017	4.216	44.01	1040	4.238	44.08
1046	4.244	45.06	1018	4.197	45.13	1051	4.23	45.09
1046	4.225	46.32	1022	4.177	46.23	1065	4.194	46.21
1047	4.21	47.2	1023	4.158	47.34	1070	4.183	47.37
1047	4.193	48.22	1019	4.137	48.23	1067	4.173	48.21
1046	4.176	49.05	1019	4.122	49.09	1063	4.16	49.11
1045	4.157	49.8	1020	4.111	49.95	1062	4.137	50.06
1045	4.135	50.49	1024	4.097	50.79	1073	4.109	50.81
1044	4.117	51.53	1026	4.086	51.5	1052	4.093	51.57
1042	4.099	52.24	1028	4.076	52.16	995	4.082	52.3
1040	4.082	52.87	1029	4.067	52.73	939	4.077	52.82
1040	4.069	53.29	1028	4.057	53.21	1016	4.071	53.28
1039	4.061	53.75	1031	4.052	53.72	1035	4.065	53.77
1039	4.057	54.01	1031	4.045	54.08	1036	4.066	54.16
1040	4.055	54.43	1032	4.04	54.44	985	4.06	54.45
1039	4.055	54.75	1032	4.031	54.72	992	4.052	54.79
1039	4.054	55.18	1033	4.026	55.01	1009	4.048	55.11
1039	4.048	55.31	1035	4.021	55.23	1013	4.04	55.3
1040	4.039	55.4	1035	4.016	55.46	1017	4.033	55.51
1040	4.031	55.69	1035	4.01	55.7	1017	4.029	55.7
1040	4.029	55.89	1035	4.004	55.95	1017	4.021	56.01
1038	4.027	56.18	1035	3.997	56.17	1007	4.017	56.19
1038	4.026	56.49	1034	3.994	56.43	1022	4.018	56.45
1037	4.02	56.6	1036	3.988	56.71	1022	4.018	56.67
1036	4.018	56.87	1036	3.98	56.99	1022	4.016	56.92

**Table 5.2 Typical Measured Data showing the Effects of Gravity Fed Cooling (GFC)
System on PV Module Temperature and Voltage**
(from Nature of Test #1 in Table 4.1)

		Effects of Gravity Fed Cooling						
DAY 1: Test Run #1			DAY 2: Test Run #4			DAY 3: Test Run #9		
Solar Irrad (W/m^2)	Cell Volts (V)	Cell Temp (deg C)	Solar Irrad (W/m^2)	Cell Volts (V)	Cell Temp (deg C)	Solar Irrad (W/m^2)	Cell Volts (V)	Cell Temp (deg C)
error± 10 W/m	± 0.1% error	± 0.1% error	rror± 10 W/m	± 0.1% error	± 0.1% error	rror± 10 W/m	± 0.1% error	± 0.1% error
1045	3.979	61.93	1045	3.892	62.04	1042	3.925	61.94
1044	3.99	59.1	1045	3.938	59.28	1040	3.979	59.04
1044	4.041	55.41	1045	4.018	55.6	1040	4.022	55.32
1043	4.139	49.86	1047	4.141	50.21	1040	4.135	50.11
1043	4.223	43.44	1047	4.253	44.03	1040	4.217	43.27
1044	4.355	36.01	1047	4.361	35.94	1042	4.333	35.54
1044	4.375	32.56	1048	4.372	32.46	1042	4.383	33.14
1044	4.46	30.1	1047	4.45	30.19	1040	4.44	30.08
1044	4.471	29.72	1048	4.465	29.81	1040	4.43	30.06
1044	4.473	29.81	1050	4.475	29.67	1040	4.43	30.1
1038	4.47	29.71	1051	4.482	29.57	1035	4.468	29.98
1038	4.468	30.02	1051	4.484	29.51	1035	4.471	29.96
1035	4.47	29.99	1052	4.488	29.52	1038	4.472	30.05
1036	4.472	29.98	1052	4.488	29.49	1035	4.469	30.06
1040	4.472	29.95	1052	4.49	29.49	1035	4.47	30.01
1040	4.472	29.96	1050	4.493	29.46	1035	4.468	29.99
1041	4.471	29.98	1049	4.495	29.48	1028	4.468	30.02
1044	4.47	30.01	1049	4.496	29.39	1030	4.47	29.97
1044	4.471	29.98	1048	4.497	29.3	1030	4.471	29.96

Table 5.2 shows the effects of operating a PV module with a GFC system. The values
in the table demonstrate that the cooling system lowers the module temperature down to 30
^{o}C. This is only five degrees above the manufacturer's specification. The table values also
highlight the increase in the module output voltage due to the reduced operating temperature.
The cooling water temperature was 28 ^{o}C.

Table 5.3   Typical Measured Data showing the Effects of Solar Powered Adsorption Cooling (SPAC) System on PV Module Temperature and Voltage
(from Nature of Test #5 in Table 4.1)

Effects of Solar Powered Adsorption Cooling								
DAY 1: Test Run #2			DAY 2: Test Run #5			DAY 3: Test Run #7		
Solar Irrad (W/m²)	Cell Volts (V)	Cell Temp (deg C)	Solar Irrad (W/m²)	Cell Volts (V)	Cell Temp (deg C)	Solar Irrad (W/m²)	Cell Volts (V)	Cell Temp (deg C)
rror± 10 W/m	0.1% error	0.1% error	rror± 10 W/m	0.1% error	0.1% error	rror± 10 W/m	0.1% error	0.1% error
1045	3.848	67.58	1043	3.882	66.11	1030	3.862	67.33
1045	4.171	48.18	1043	4.182	47.83	1030	4.158	47.35
1045	4.229	43.73	1043	4.218	44.15	1036	4.225	43.66
1045	4.304	38.84	1045	4.301	38.42	1036	4.271	39.29
1044	4.361	33.38	1045	4.358	33.98	1036	4.382	32.96
1044	4.423	28.75	1045	4.441	28.79	1036	4.427	28.21
1044	4.493	25.91	1039	4.476	26.12	1038	4.485	26.31
1044	4.511	23.96	1039	4.518	23.43	1038	4.511	24.04
1040	4.539	22.51	1039	4.537	22.32	1030	4.521	22.41
1040	4.576	21.73	1040	4.552	21.67	1030	4.562	22.32
1040	4.601	21.54	1039	4.598	21.48	1030	4.603	21.55

Table 5.3 shows the effects of operating a PV module with a SPAC system. With this cooling system, the values in the table demonstrate that the module temperature was kept below the manufacturer's referenced temperature of 25 ^{o}C. The table values also highlight the greater increase in the module output voltage over those obtained in Table 5.2. The cooling water temperature was 21 ^{o}C.

Table 5.4   **Typical Measured Data showing the Effects of GFC Water Flow
Rates on Module Voltage and Temperature**
(from Nature of Test #2 in Table 4.1)

	Effects of GFC Water Flow Rates on Module Parameters							
	Day 1				Day 2			
	Run #1		Run #1		Run #2		Run #4	
Time	0.03 L/min		0.06L/min		1.0L/min		2.0 L/min	
(min)	(V)	(deg C)	(V)	(deg C)	(V)	(deg C)	(V)	(deg C)
	± 0.1% error	± 0.1% error	± 0.1% error	± 0.1% error	± 0.1% error	± 0.1% error	± 0.1% error	± 0.1% error
0	3.884	66.06	3.888	65.23	3.882	67.98	3.893	65.78
0.25	3.887	65.35	3.915	62.44	4.216	44.23	4.45	33.26
0.5	3.891	63.25	4.066	56.28	4.371	33.85	4.447	29.98
0.75	3.974	57.18	4.216	45.13	4.44	30.42	4.45	30.04
1	4.086	51.42	4.259	41.32	4.447	30.34	4.451	30
1.25	4.222	44.39	4.283	37.65	4.443	30.45	4.448	29.99
1.5	4.288	40.1	4.301	35.43	4.443	30.21	4.451	29.97
1.75	4.281	37.45	4.382	33.76	4.447	30.33	4.451	29.99
2	4.335	35.69	4.404	32.87	4.451	30.41	4.447	30.01
2.25	4.362	34.46	4.418	32.26	4.452	30.37	4.449	30
2.5	4.375	33.65	4.423	31.81	4.448	30.41	4.453	29.99
2.75	4.391	33.02	4.436	31.42	4.452	30.35	4.451	29.99
3	4.401	32.54	4.447	31.11	4.451	30.41	4.451	29.99
3.25	4.398	32.16	4.448	30.92	4.451	30.43	4.453	30.01
3.5	4.403	31.82	4.452	30.81	4.451	30.39	4.451	30
3.75	4.401	31.56	4.449	30.55	4.449	30.34	4.451	29.99

Table 5.4 highlights the impact of the GFC system on the PV module parameters. The values in the table demonstrate that increased cooling water flow rates resulted in less time taken for the module temperature to reach steady state. The module temperature reached within three degrees of the cooling water temperature of 28 $^{\circ}$C for all flow rates.

Table 5.5   **Typical Measured Data showing the Effects of SPAC Water Flow Rates on Module Voltage and Temperature**
(from Nature of Test #6 in Table 4.1)

Effects of SPAC Water Flow Rates on Module Parameters							
Day 1				Day 2			
Run #2		Run #2		Run #2		Run #3	
0.02 L/min		0.03 L/min		0.06 L/min		0.8 L/min	
Time (min) — (V)	(deg C)	(V)	(deg C)	(V)	(deg C)	(V)	(deg C)
	± 0.1%error	± 0.1%error	± 0.1%error	± 0.1%error	± 0.1%error	± 0.1%error	± 0.1%error
0 / 3.869	66.11	3.818	67.58	3.882	65.64	3.742	67.49
0.5 / 4.175	48.18	4.218	43.73	4.338	36.23	4.556	22.05
1 / 4.283	38.84	4.354	33.38	4.478	27.14	4.599	21.52
1.5 / 4.358	33.98	4.453	30.75	4.503	24.04	4.601	21.38
2 / 4.414	30.93	4.467	27.91	4.521	23.13	4.603	21.31
2.5 / 4.471	28.79	4.489	25.96	4.557	22.07	4.605	21.26
3 / 4.479	27.23	4.496	24.82	4.595	21.55	4.605	21.24
3.5 / 4.485	26.41	4.507	23.67	4.603	21.42	4.605	21.25

In Table 5.5, the speed at which the SPAC system cools the PV module is quite evident. The table underscores the higher voltage values and lower module temperatures achieved through the SPAC system.

Table 5.6 Typical Temperature Measurements for the Solar Powered Adsorption Cooling Experiment

(from Nature of Test #4 in Table 4.1)

TIME	Amb T (deg C) ± 0.1% err	Evap T (deg C) ± 0.1% err	Day 2: Cycle 2 Bed T (deg C) ± 0.1% err	TubeT (deg C) ± 0.1% err	TubeB (deg C) ± 0.1% err	Cond T (deg C) ± 0.1% err	Sol Rad W/m^2 err ± 10 W/m^2
6am	24.32	21.88	25.62	23.47	23.46	28.13	29
7	24.84	22.17	27.14	29.45	29.44	28.23	53
8	27.65	23.43	35.86	40.48	40.47	28.31	290
9	29.45	24.31	53.17	63.29	63.29	28.27	612
10	30.88	25.08	66.01	73.17	73.17	28.33	785
11	32.01	27.52	72.66	79.25	79.22	28.23	899
12 noon	33.66	28.73	79.05	85.65	85.61	28.29	984
1	34.83	30.07	83.42	84.76	84.72	28.32	896
2	34.72	30.88	76.8	74.81	74.82	28.39	847
3	33.88	29.9	64.28	57.32	57.28	28.31	701
4	32.79	29.03	41.48	33.24	33.25	28.26	320
5	31.98	28.72	33.56	31.27	31.28	28.15	85
6	31.36	28.17	31.71	30.65	30.63	28.19	49
7	30.5	23.73	29.13	30.84	30.85	28.25	
8	29.13	22.47	28.43	28.3	28.28	28.23	
9	28.43	22.29	27.68	27.56	27.52	28.24	
10	27.36	22.09	26.42	25.89	25.88	28.21	
11	26.42	21.59	25.87	25.03	25.05	28.18	
12 midngt	25.87	21.22	25.29	24.87	24.88	28.07	
1	25.29	21.32	25.2	24.24	24.24	28.11	
2	25.2	21.47	25.01	23.96	23.97	28.14	
3	25.11	21.55	24.57	23.51	23.5	28.22	
4	25.23	21.68	24.43	23.49	23.49	28.19	
5	25.13	21.89	24.38	23.04	23.04	28.2	

Legend: **Amb T**: ambient temp; **Evap T:** evaporator temp; **Bed T**: adsorption/desorption bed temp; **Tube T**: copper tube top surface temp; **Tube B**: copper tube bottom surface temp; **Cond T**: condenser temp; **Sol Rad**: solar irradiance

Table 5.6 shows typical temperature data captured from the SPAC system. The averages of these values were used to calculate the system performance criteria such as coefficient of performance (COP) and degree of cooling.

5.2   Results from GFC Experiments and Modelling

Having discussed typical experimental results in the previous section, this section presents and discusses the results from the Gravity Fed Cooling (GFC) experiments described in Section 4.1. It also compared them with results derived from mathematical modelling.
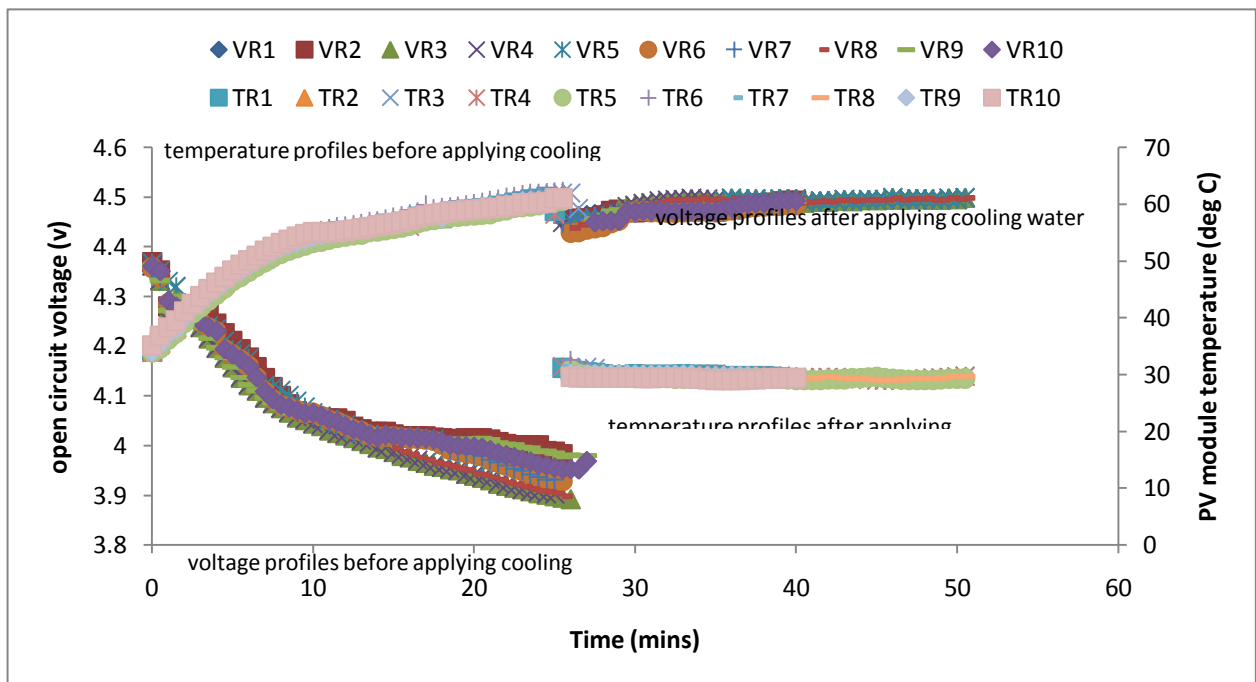
Figure 5.1   Scatterplots of the 10 sets of voltage and temperature measurements for the 10 experimental runs conducted.
(from Nature of Test #1in Table 4.1)

Statistically, the Scatterplot profiles have a standard deviation of 0.012 V for the voltage profiles and 0.488 ^{o}C for the temperature profiles.

Legend: VR1: voltage, run #1
        TR3: temperature, run #3

Figure 5.1 shows the scatter plots of the voltages and temperatures measured for the 10 runs (trials) as the PV module was first heated by exposure to solar irradiance and then cooled by applying water to the back surface. The profiles formed by the scatter plots all show the dramatic changes that took place after the cooling water was applied. Average profiles from these plots are used in subsequent figures.

Regression Analysis

The Scatter plots in Figure 5.1 were statistically analyzed by Regression. Both the Statistics and the ANOVA for Figure 5.2 verified the strong correlation between PV module voltage and module temperature by the 'R Square' and 'Significant F' values, respectively.

SUMMARY OUTPUT

Regression Statistics	
Multiple R	0.995741
R Square	0.9915
Adjusted R Square	0.991311
Standard Error	0.010673
Observations	47

ANOVA

	df	SS	MS	F	Significance F
Regression	1	0.597936	0.597936	5249.353	3.06E-48
Residual	45	0.005126	0.000114		
Total	46	0.603062			

	Coefficients	Standard Error	t Stat	P-value	Lower 95%	Upper 95%
Intercept	4.917321	0.011596	424.0371	1.08E-82	4.893964	4.940677
X Variable 1	-0.01587	0.000219	-72.4524	3.06E-48	-0.01631	-0.01543
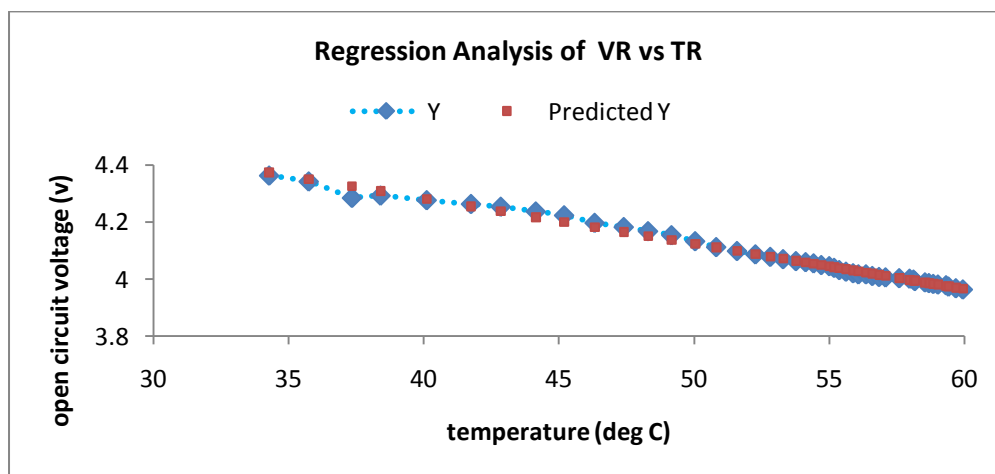
Figure 5.2   Regression analysis of the Correlation of PV module Voltage and Temperature

The 'R Square' value of 0.9915 means that 99.15% of the variance in the observed values of the dependent variable (voltage) is explained by the model, and the lower the significance F value the greater the chance that the relationships between open circuit voltage and PV module temperature in the model are real. The 'Significant F' value presented in the ANOVA is 3.06×10^{-48}.

5.2.1 Un-Cooled PV Module

Having statistically established the strong relationships between the experimental values in Section 5.2, the report took the average profiles and further analyzed them in terms of the objectives of the research.

Open Circuit Voltage(Voc) vs Module Temperature
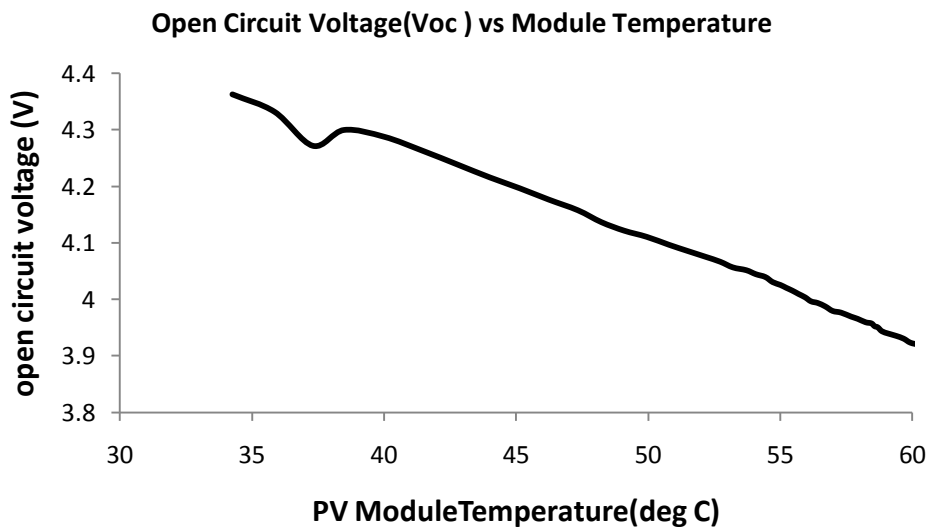
Figure 5.3   Impact of elevated temperature on open circuit voltage of a PV module
(averaged voltage profile extracted from the 0-20 minutes portion of Fig. 5.1)

Figure 5.3 shows the results of the 8-cell PV module described in section 4.1, with rated V_{oc} of 4.5 volts being exposed to a constant (average) solar irradiance of 989 W/m^2 (range: 924 – 1053 W/m^2) incident on the front face. The back face is not cooled. The figure shows the inverse linear relationship between open circuit voltage and module temperature and in particular the negative impact that elevated temperature has on module voltage. This result concurs with the literature, especially Durish, et al. (2007), that the efficiency of a PV module is a linear function of cell temperature with constant irradiance. The figure shows an 11% fall in voltage for a 28°C rise in module temperature. The 'dip' in the graph is due to a couple of low readings in the Scatter Values at 0-3 minutes in Figure 5.1.

5.2.2 *Application of the Gravity-Fed Cooling (GFC) System*

Figure 5.4 represents the results of the same 8-cell PV module mentioned in Section 5.2.1 with rated V_{oc} of 4.5 volts being exposed to the same solar irradiance of 989 W/m^2 incident on the front face. But this time the GFC system was employed, which allowed cooling water to flow over the back face of the PV module, holding it at the cooling water temperature of 28 ^{o}C. The recorded data started when the module temperature was 34 ^{o}C and voltage 4.36 volts. The module temperature was allowed to rise to 62 ^{o}C before the cooling water was switched on at time zero (25.5 minutes in Figure 5.4).
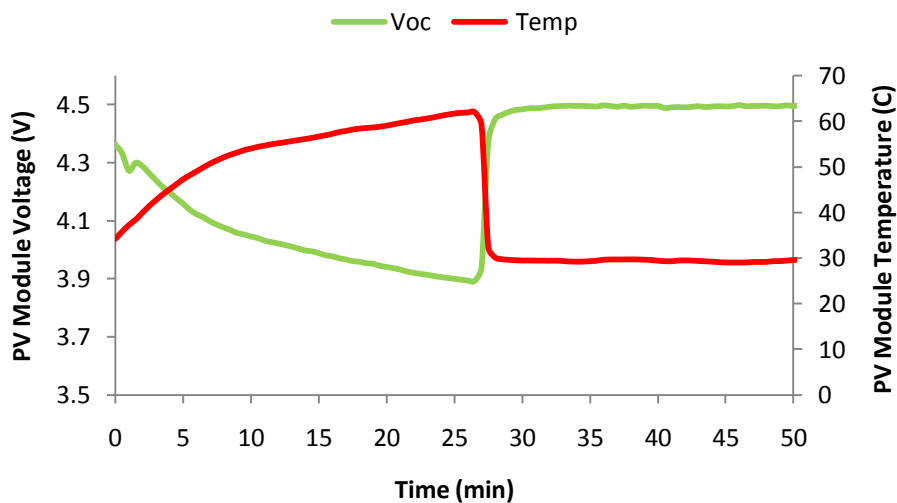
Figure 5.4   Voltage and Temperature profiles of a 'wet' PV module with cooling water switched on at 25.5 minutes.
(averaged line plot of scatter plots in Figure 5.1)

The profiles highlight the rapid cooling of the module after the application of the GFC system. Within a very short period of time the module reached steady state, and a drop in temperature from 62°C to 30°C (within two degrees of the cooling water temperature) was recorded.

The profiles also show the inverse relationship between the voltage and temperature. The voltage fell from 4.4V to 3.9V as the module temperature rose from 34 ^{o}C to 62 ^{o}C. But within seconds of switching on the cooling water (25.5 minutes in Figure 5.4), the module voltage went to the rated voltage of 4.5V and stayed there as long as the cooling water flowed.

With the application of the GFC system, the results of the experiments clearly indicated the positive effects of the system on the module's voltage and temperature. The first

half of the graph (0 – 25 min) is the negative result of temperature rise of the module as was shown in Figure 5.3. But as soon as the Gravity-Fed Cooling system was engaged (25.5 min) the negative effect was reversed as indicated by the rapid fall in module temperature and the equally rapid rise in module open-circuit voltage.

The effects of the Gravity-Fed Cooling system totally reversed the fall in module voltage that is shown in Figure 5.3, and increased the voltage to 100% of its rated value. This resulted in a 12.8% increase in the conversion efficiency of the PV module (Sweelem et al., 1999; Hu & White, 1983) by achieving a 32 degrees (62°C – 30°C) reduction in module temperature. Therefore, in view of the objectives of the research the experimental results from the GFC system showed that the system effectively cooled the PV module.

5.2.3 Results from Gravity-Fed Mathematical Model

As noted in Section 1.2.1.2 that one of the primary objectives of the current work is to ascertain the impact of a Gravity-Fed Cooling (GFC) system on photovoltaic power generation. In so doing, another objective was to develop a mathematical model of the temperature profile across the PV cell. This developed model was given as (Section 3.1.1):

$$U(x,t) = \left[U_L + \frac{q_o}{k}(L - x)\right] + \sum_{n=1}^{\infty}\left\{\left[F_n Cos\frac{(2n-1)\pi x}{2L}\right]Exp\left[-\frac{\alpha(2n-1)^2\pi^2 t}{4L^2}\right]\right\}$$

The model was programmed with Matlab codes (Appendix A). The results from the model are now described.

Figure 5.5 shows the results of the mathematical model for a 3mm thick PV cell (described in Section 4.1) having solar irradiance of 1000 W/m^2 incident on the front surface and the back surface held at the cooling water temperature of 28 $^{\circ}$C. At time zero, the time at which the cooling water was switched on, the temperature of the cell was 62 $^{\circ}$C.
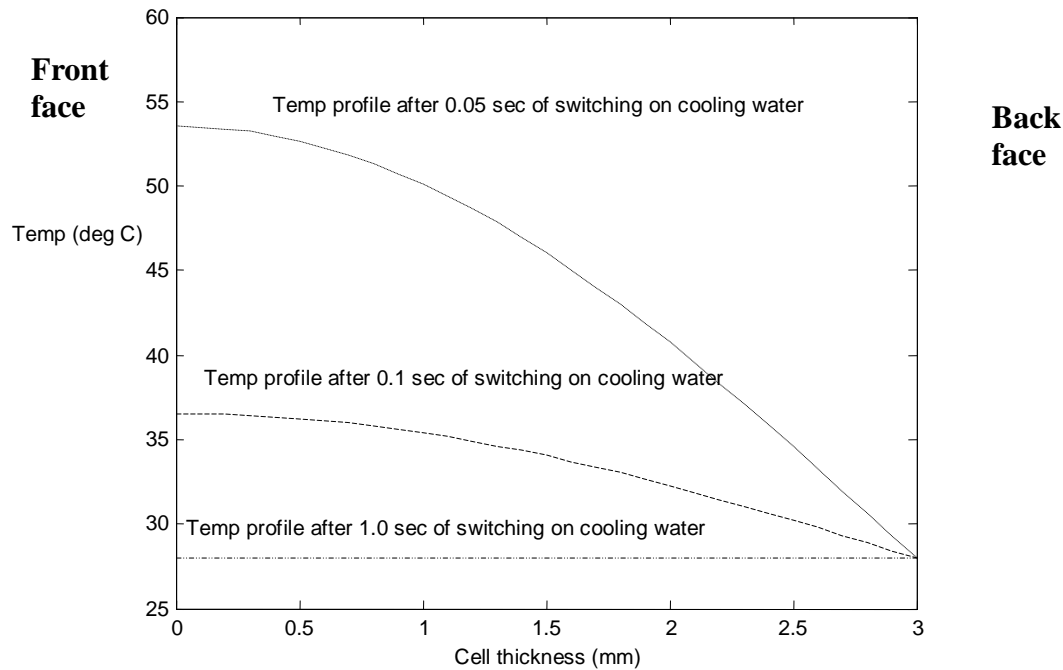
Figure 5.5 **Time-Steps of Temperature profiles for a modelled 3mm thick 'wet' PV cell with irradiance of 1000 W/m^2 incident on front face and back face held at water temperature of 28 ^{o}C**

The model showed that rapid cooling of a PV cell can occur with the application of cooling water. The cell reached steady state within a very short time of the cooling water being switched on. This was a fall in temperature from 62 ^{o}C to 28 ^{o}C, the temperature of the cooling water. This result was similar to those obtained from the GFC experiments as is represented in Figure 5.4. The model therefore implied that, theoretically, a silicon cell can be held at the temperature of the cooling fluid; which further implied that a PV cell can be maintained at its rated efficiency.

In essence, the results from the model were supported by those from the experiments indicating the GFC system was effective. The 34 ^{o}C drop in temperature that the model gave translated to a 13.6% increase in conversion efficiency as stated by Sweelem et al. (1999) and Hu & White (1983). Both researchers showed that the conversion efficiency coefficient for PV cells is in the order of -0.4% for each degree rise in cell temperature. Parametric analyses with this model are carried out in Chapter 6.

5.3   Results from the SPAC Experiments and Modelling

It was noted in Section 2.5.1 that the Gravity-Fed Cooling system has a major limitation, in that it limits the system to places that have water supplies such as rivers, lakes, streams and water-catchments. To remove this limitation so that hot desserts and other places with limited water supply can utilize this improved PV system, the SPAC system is envisioned to ensure that the PV power system has its own chilled-circulating water.

But a major aspect of the SPAC system is the function of the adsorption/desorption process in the bed. For the system to function properly, the temperature of the entire bed needs to rise, and rise quickly, to a value which corresponds to the boiling (desorption) point of methanol.

This section presents the results from the SPAC experiments described in Section 4.2 which is to determine the effectiveness of the bed.

Graphical Representation of Typical Temperature Measurements for SPAC Experiment
(from Nature of Test #4 in Table 4.1)
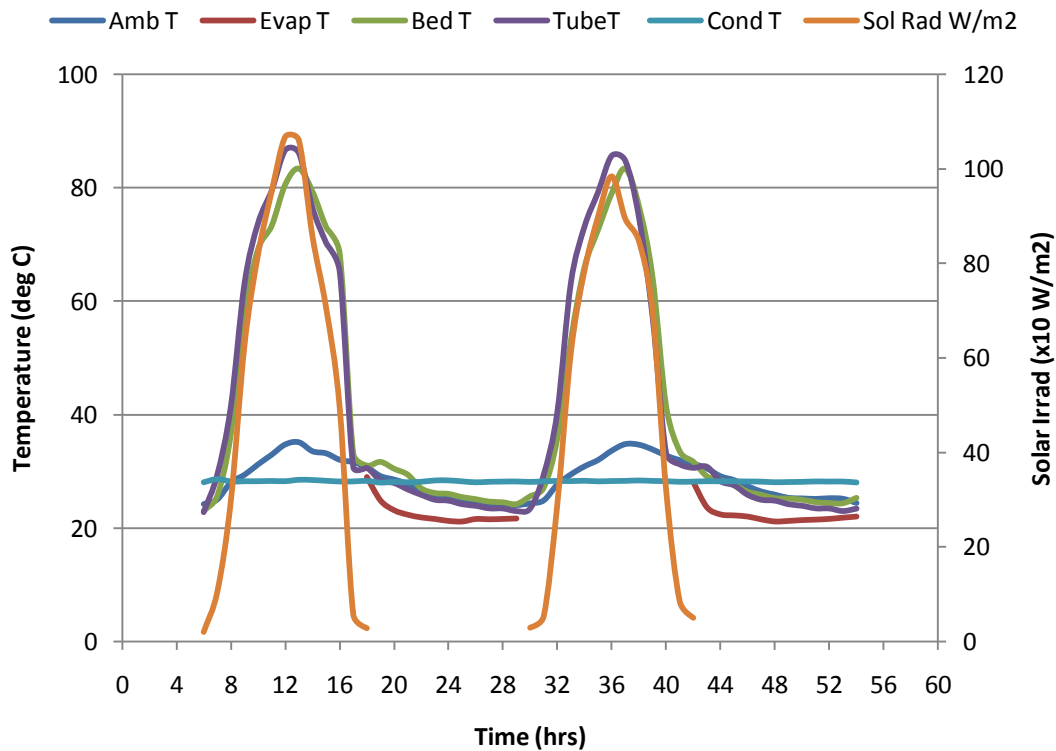
Figure 5.6   Temperature Evolutions of 2 Consecutive Cycles from SPAC Experiment

Figure 5.6 shows that the tube temperature (Tube T) moved in phase with increases in solar irradiance. It also illustrates that the bed temperature (Bed T) was in phase with the climb in tube temperature. As was expected, in the evening the bed temperature lagged the tube temperature in cooling down. Of note was the sudden elevation of bed temperature at the18-20 and 42-44 hour time periods. These time slots also coincided with the steepest drop in evaporator temperature (Evap T). This phenomenon supported the theory that an adsorption process is exothermic.

That is, at the time when the bed temperature and pressure fell sufficiently to create a negative pressure difference between the bed and the evaporator, the Methanol started to migrate from the evaporator to the bed. In the process it drew energy from the water in the evaporator to change its phase from liquid to vapor. In doing this it reduced the water temperature. Simultaneously, the gaseous Methanol on reaching the bed gave up its heat of vaporization to the bed, hence the rise in bed temperature, returned to liquid state to be adsorbed by the charcoal.

These adsorption time slots were similar to the ones obtained by Lemmini and Errougani (2007) in their experimentations.

5.3.1 Results of Experiment on Bed Temperature of the SPAC System
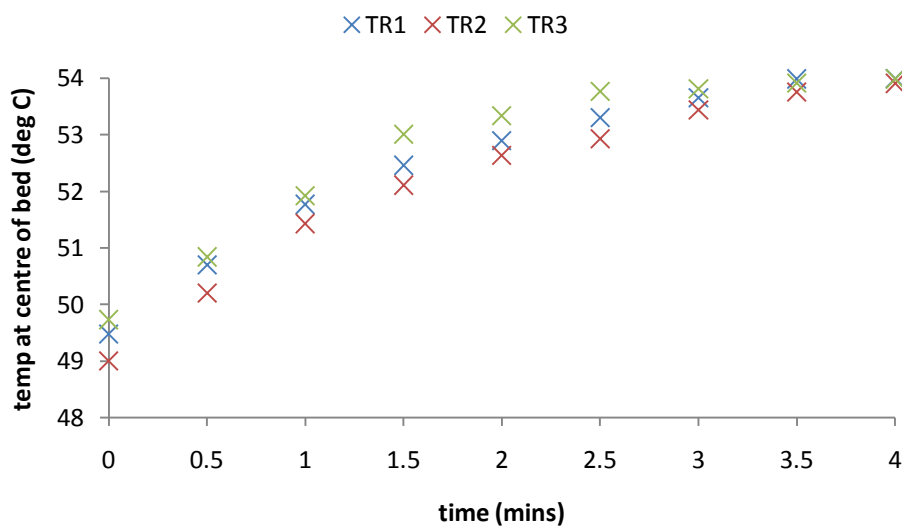
Figure 5.7   Scatter-plots of Temperature changes at centre of bed with respect to time

From the SPAC experiment, described in Section 4.2.3, the charcoal/methanol bed (Figure 4.7) was exposed to an average solar irradiation of 1062 W/m^2 over a 4 minutes period. During this period the average temperature of the copper tube was 54°C. Figure 5.7 shows three trial runs measuring the temperature changes at the centre of the bed under the given conditions. It shows the temperature rising from 49°C to 54°C in four minutes.

The ability of the bed to quickly rise to the desorption temperature of the Methanol (52°C at 405 mm Hg vacuum) gave credence to the treatment of the Effective Thermal Conductivity, K$_e$, of the bed as described in Section 3.2.1, and answered the question about the functionality of the bed design. The bed was designed cylindrically as opposed to the traditional rectangular shape. The quick attainment of steady state of the bed should also aid in the predictive accuracy of the mathematical model developed in Section 3.2.2, as Critoph and Turner (1995) pointed out that the accuracy of any model is very dependent on the composition of the effective thermal conductivity of the bed. The four minutes that were required for the bed to reach the steady state of desorption temperature must be understood as four minutes out of an exposure time of six hours.

5.3.2 *Results from Mathematical Model of Bed Temperature for SPAC System*

To determine if the bed could rise to the desorption temperature and hence be effective, an objective (Section 1.2.1.2) was to develop a mathematical model of the temperature profile of the bed. The developed model of the temperature profile was given as (eqn 27, Section 3.2.2):

$$T(r,t) = T_1 + \frac{2(T_0 - T_1)}{R}\left[\sum_{n=1}^{\infty} exp(-\lambda^2\,\alpha^2 t)\,\frac{J_0(\lambda_n\,r)}{(\lambda_n)J_1(\lambda_n\,R)}\right]$$

where r = radius of bed and t = time.

Using MATLAB codes (Appendix B) to solve the equation, the results are shown in Figure 5.8.
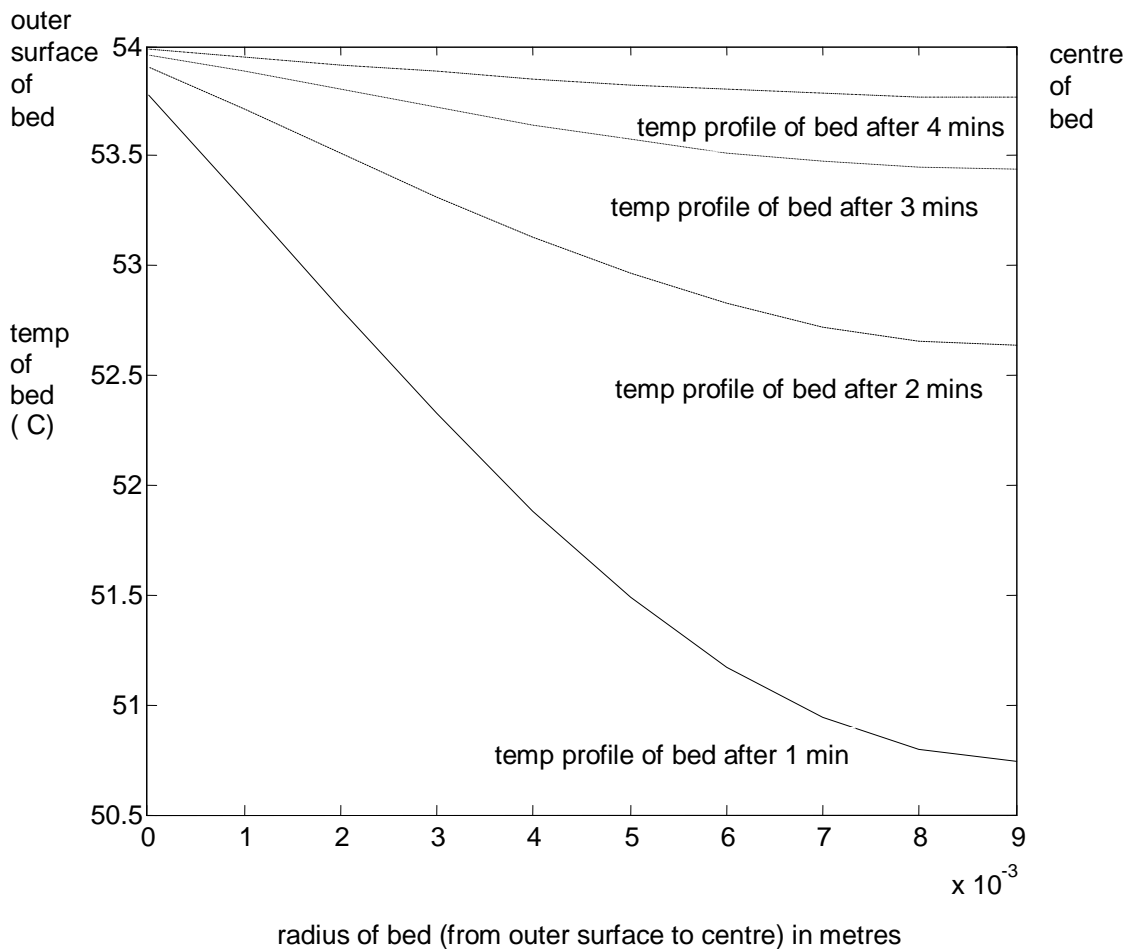
Figure 5.8 Time-Steps of temperature profiles for charcoal/methanol (Desorption) bed with outer surface (copper tube) held at 54°C

The mathematical model of the bed, Figure 5.8, demonstrated that with the outer (copper tube) surface of the bed held at a temperature of 54°C, it took approximately four minutes for the centre of the bed to reach this temperature; starting at 49°C. This time frame was similar to those obtained from the results of the experiments. That is, over a period of four minutes the average surface temperature of the copper tube (bed) was 54°C. At the start of this four minutes period, the centre of the bed was 49°C. At the end of the four minutes period the bed temperature climbed to 53.8^{o}C. This exhibited that the entire charcoal/methanol bed was capable of reaching the required temperature of 52°C for the methanol to desorb (evaporate) from the charcoal pores and migrate to the condenser, once there is sufficient solar irradiance to raise the tube temperature over 54 ^{o}C.

The results of the mathematical model were in close agreement with those of the experiments as is demonstrated in Figure 5.9. It shows both bed-temperature profiles moving in step over the same time period. The difference in the graphs in the first minute could be a result of thermal contact between tube and charcoal, where the model under compensated for the contact. The "Experiment" profile is the average profile taken from Figure 5.7. Further analyses are carried out with this model in Chapter 6.
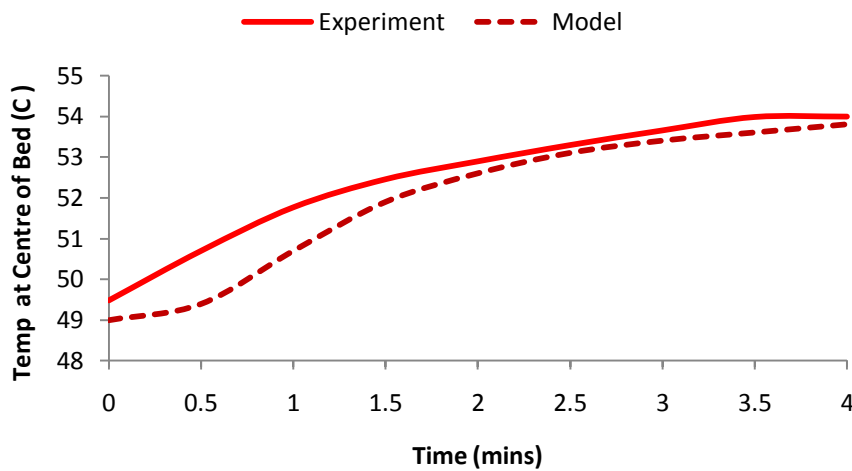
Figure 5.9   Experiment and Mathematical Model Temperature Variations at Centre of Charcoal Bed

5.3.3 Energy Balance on SPAC system

Sections 5.3.1 and 5.3.2 revealed that the charcoal/methanol bed can reach the desorption temperature which is a necessary condition for the methanol to migrate from the pores of the charcoal to the evaporator, via the condenser. Having determined that necessary condition, it was then essential to establish the efficiency of the SPAC system.

To make a determination of the efficiency of the SPAC system, calculations (using MATLAB codes -Appendix C) for an energy balance on the SPAC system were carried out to establish the system's Coefficient of Performance (COP), and, especially, the mass fraction of methanol desorbed from the bed which is a major component of the COP. It has been established that the COPs for these systems are very low, below 1.0 (Sumathy & Li, 1999),

but the fact that the input energy is Solar and totally free makes these systems realistic to build and operate.

The energy balance was necessary to show that all energy issues were accounted for. The aim was for a net balance of zero kilo-Joules (0 kJ) and also a close agreement between the change in evaporator temperature (Δt_w) given by the Calculations and the change in evaporator temperature (Δt_w) measured in the Experiments.

The system of equations needed to achieve the Energy Balance was derived in Chapter 3 and Table 5.7 highlights the summary of the solutions obtained. Appendix C and Nomenclature have the details for the table. Sensitivity analysis for the energy balance is discussed in Chapter 6.

Table 5.7   Summary of Equations for SPAC System

Type of Equation	Formula	Value	Sum Total	Uncertainty
Governing Energy Balance Equation $(E_{net} + E_{gen} - \Delta E_{st} = E_{out})$				
Net Input Energy, E_{net} $(E_{net} = E_{in} - E_{lost})$	$E_{in} = \acute{a}A_{cu}It$ $E_{lost} = UtA_{cu}(T_{tube}-T_{amb})$	361 272.7	88.3(kJ)	5%
Generated Energy, E_{gen}			0 (kJ)	
Stored Energy, E_{st}	$E_{st} = M_{bed}\ C_{P}\Delta T_{bed} +$ $m_{cu}C_p\Delta T_{tube}$	33.7	33.7 (kJ)	0.14%
Output Energy, E_{out}	$E_{out} = h_{des}m_{char}x_m$	54.5	54.5 (kJ)	0.14%

System Net Energy Balance	Net balance = E_{in} -E_{st} - E_{out} $-$ E_{lost}	0.1	0.1 (kJ)	5%
Heat of desorption, h_{des}	$$h_{des} = \mathcal{L}_m \frac{T_{des}}{T_{con}}$$	1180	1180 (kJ/kg)	0.14%
Mass fraction of methanol desorbed, x_m,	$$x_m = x_0 exp\left[-Đ\left(\frac{T_{des}}{T_{con}} - 1\right)^{ń}\right]$$	0.385	0.385	0.1%
System COP	$$COP_{sys} = \frac{E_{evap}}{E_{in}} = \frac{m_w c_{p_w} \Delta t_w}{\acute{a} A_{cu} It}$$	0.1407	0.14	5%
Degree of cooling (measured) from Experiment		9°C	9°C	0.1%
Degree of cooling Calculated:	$$\Delta t_w = \frac{m_{char} x_m \mathcal{L}_m}{m_w c_{p_w}}$$	12.15	12.15°C	0.14%

Degree of cooling (measured) from Experiment:

The recorded average temperature change in the evaporator (chilled water) was 9°C (30°C to 21°C); hence from the results of the experiments: $\Delta t_w =$ **9°C**. This is observed in Figure 5.6 between the hours of 1800 and 2400. The figure shows the temperature of the water in the evaporator (Evap T: red line) falling from 30 °C to 21 °C as the methanol evaporated and migrated back to the bed.

5.3.4 *Application of the SPAC system*

Knowing the degree of cooling that the Solar Powered Adsorption Cooling (SPAC) system gives (Table 5.7), an experimental simulation of this SPAC system was applied to the PV module as described in Section 4.2.4. In the simulation cooling water of temperature 21°C was circulated over the back of the PV module.
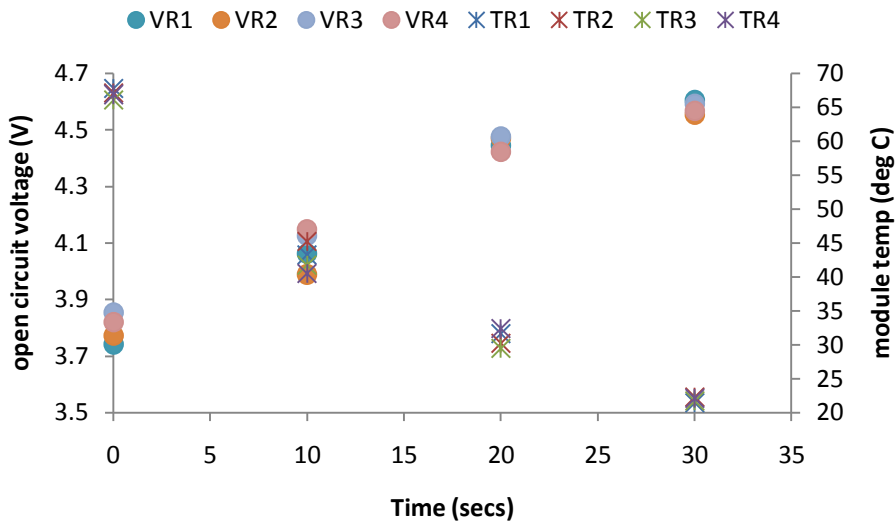
Figure 5.10 Scatterplots of 4 sets of voltage and temperature measurements for the SPAC System
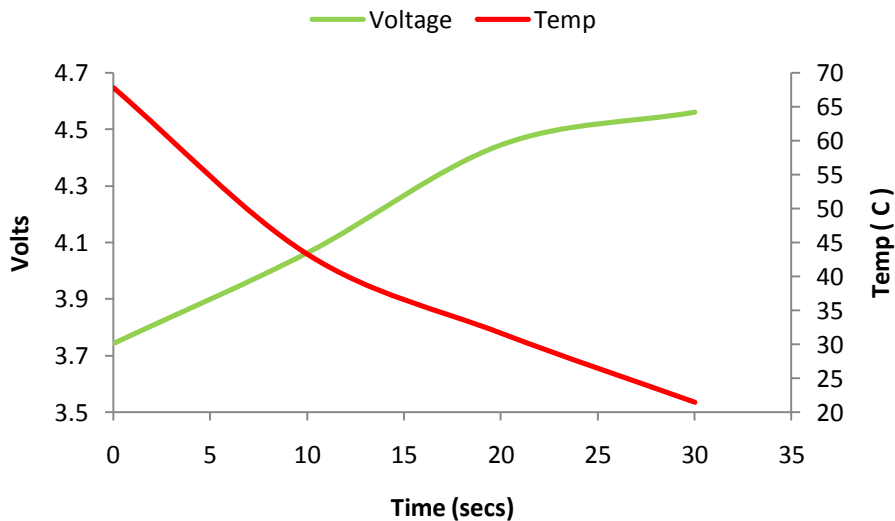
Figure 5.11 Effects of SPAC on Voltage and Temperature profiles of PV module
(averaged values from Figure 5.10)

Figure 5.11 shows the results (Figure 5.10 shows the scatter-plots) of the 8-cell PV module, with rated V_{oc} of 4.5 volts, being exposed to an average solar irradiance of 1000 W/m^2 incident on the front face and the back face held at the cooling water temperature of 21°C. The module temperature was allowed to rise to 67°C before the cooling water was switched on.

The figure shows the module rapidly cooling in seconds, and also highlights the inverse relationship between open circuit voltage and module temperature. The result was very similar to those of the Gravity-Fed profiles shown in Figure 5.4. In essence it is the expansion of Figure 5.4 between times 25.5 minutes to 26.5 minutes but with some interesting differences due to the effects of the SPAC system.

While the effects of the SPAC system were similar to that obtained with the Gravity-Fed Cooling system and showed the rapid cooling of the module, there were two major differences in the results. Firstly, the results of the SPAC system showed that the system was able to bring and keep the module temperature below both the ambient (33°C) and the manufacturer's recommended (25°C) temperatures. Secondly and surprisingly, was that the low module temperature resulted in the module open-circuit voltage rising above the manufacturer's rated voltage. The manufacturer's rating is 4.5 volts but voltage obtained as a result of SPAC system was 4.605 volts. All of this movement of module temperature from 67°C to 21°C and voltage change from 3.75 V to 4.605 V took place within 30 seconds of switching on the water from the SPAC system. This made the effects of the SPAC system superior to that of the Gravity-Fed system. Therefore, in view of the objectives of the research the experimental results from the SPAC system showed that the system also effectively cooled the PV module.

5.4   Hydrogen Production versus Temperature Variation of PV Panel

The second objective in Section 1.2.1.2 seeks to establish the rate of hydrogen production from an electrolyzer, for each cooling technique. To determine the overall effects of a cooled PV module on a PV-Powered Hydrogen Production System, the experiment described in Section 4.3 was executed. In the experiment the PV module temperature moved from $25^{o}C$ to $60^{o}C$ in steps of five degrees. The hydrogen produced and the power output from the module were recorded at each step. Table 5.8 and Figures 5.12 and 5.13 show the results of the experiment.

Table 5.8   **Typical Values from Hydrogen Production Experiments**
(from Nature of Test #7 in Table 4.1)

Effects of Module Temperature on H_2 Production and Power Output						
	Day 1		Day 2		Day 6	
Temp	**H2 Prod**	**Power**	**H2 Prod**	**Power**	**H2 Prod**	**Power**
(deg C)	mL/min	(W)	mL/min	(W)	mL/min	(W)
error 0.1%	uncertainity: 1.4%	uncertainity: 1.2%	uncertainity: 1.4%	uncertainity: 1.2%	uncertainity: 1.4%	uncertainity: 1.2%
25	35	7.05	35.4	6.92	35.2	6.95
30	33.3	6.76	32.9	6.68	33.1	6.77
35	32.7	6.36	32.5	6.29	32.6	6.29
40	31.5	6.07	31.7	5.99	31.5	6.01
45	30.5	5.88	29.9	5.89	29.9	5.89
50	28.1	5.69	28.1	5.71	28.4	5.68
55	27.3	5.32	26.9	5.29	26.8	5.29
60	26.5	5.07	26.5	5.09	26.7	5.14

Table 5.8 represents typical measured values of temperature and hydrogen produced and also calculated values of power out of PV module. The figures in the table show the advantage of thermal management of the PV module. As the module temperature fell, both hydrogen production and power output increased. The uncertainties in the values are also presented. The uncertainties are calculated here due to the compounded effects of the errors in the individual parameters of H_2 Production (flow rate & time) and Power (voltage & amperage). The actual error is usually less than the percentage uncertainty as stated by Wheeler and Ganji (1996).

The following example shows how the uncertainties were calculated using the *Root of the Sum of the Squares* (RSS) formulation: $w_R = \left[\sum_{i=1}^{n} \left(w_{x_i} \frac{\partial R}{\partial x_i} \right)^2 \right]^{1/2}$ (Wheeler & Ganji, 1996).

Example of Uncertainty Calculation for Power

Voltage measured = 3.417 ± 0.003V

Amperage measured = 2.063 ± 0.025A

$$\frac{\partial P}{\partial V} = I = 2.063 \text{ A} \qquad \text{and} \qquad \frac{\partial P}{\partial I} = V = 3.417V$$

$w_v = 0.003V$ and $w_I = 0.025A$

$$W_p = \left[\left(\frac{\partial P}{\partial V} w_v \right)^2 + \left(\frac{\partial P}{\partial I} w_I \right)^2 \right]^{1/2} = [(2.063 \cdot 0.003)^2 + (3.417 \cdot 0.025)^2]^{1/2} = 0.085 \; watts$$

% uncertainty = (0.085/(3.417·2.063)) x100 = 1.2%

Hydrogen Production Rates and Output Power versus Module Temperature
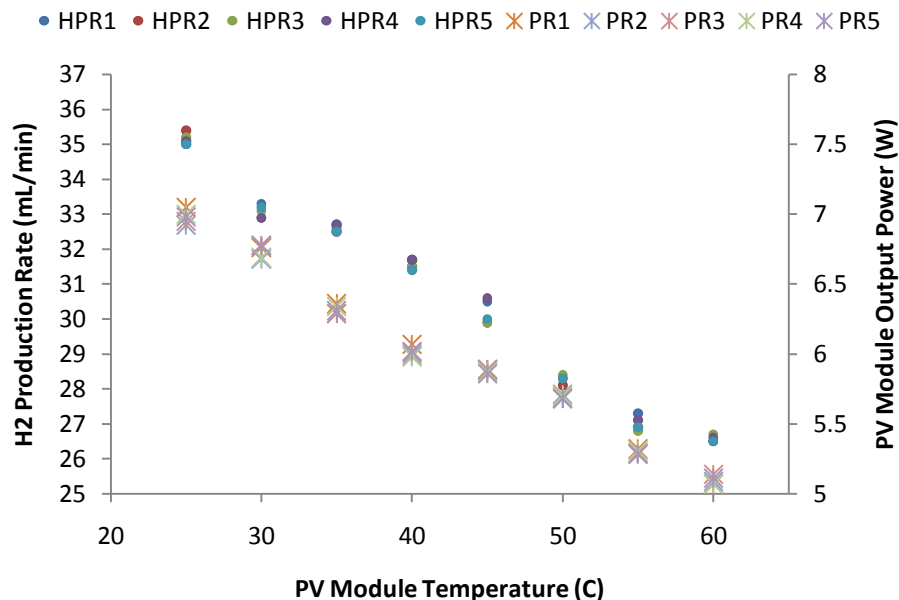
Figure 5.12 Scatter-Plots of Hydrogen Production Rates (HPR) and Output Power (PR) versus module temperature for average solar irradiance of 982 W/m^2
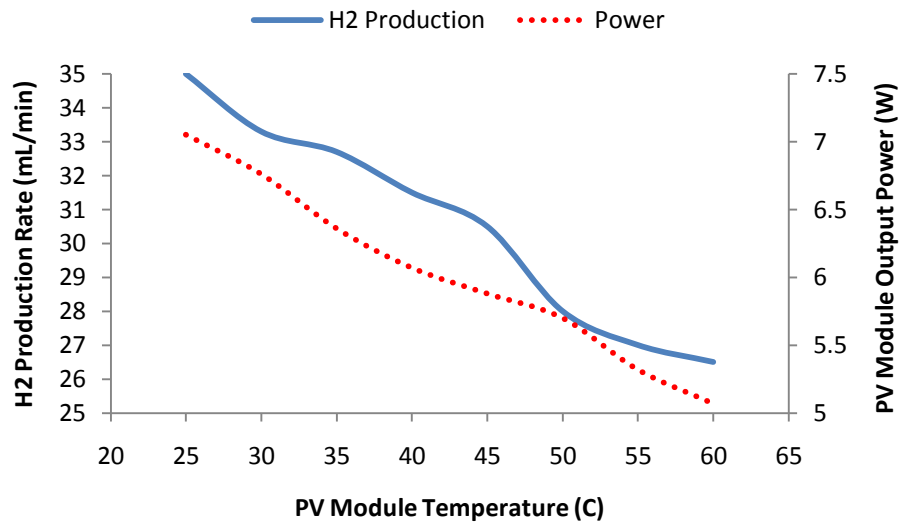
Figure 5.13: H₂ Production Rates and Module Power versus Module Temperature
(profiles extracted from scatter plots in Figure 5.12)

The linear correlation between hydrogen production rates, module output power, and module temperature is evident in Figures 5.12 and 5.13. They show the inverse relationship between elevated temperature of the module and power output of the module and also hydrogen production rate of the electrolyzer. The results showed the production rate falling from 35 mL/min to 26.5 mL/min for a 35 degrees rise in module temperature ($25^{o}C - 60^{o}C$). Correspondingly, the power output to the electrolyzer falls from 7.05 W to 5.07 W.

Figure 5.13 also clearly shows the positive effects of the cooling systems on power and hydrogen outputs, as both outputs climb as the PV temperature falls. The figure also illustrates the superiority of SPAC over Gravity-Fed Cooling. The Gravity-Fed system can bring the module temperature down to only $30^{o}C$ while the SPAC system can take it below $25^{o}C$. This resulted in power output and hydrogen production increasing by 39% and 32% respectively for the SPAC system, in comparison to power output increase of 33% and hydrogen production increase of 26% for the Gravity-Fed system. Nominally, this translates overall to SPAC system being 6% more effective than the Gravity-Fed Cooling (GFC) system.

The results of these tests have proven the hypothesis of this research (Section 1.2.1.1) that: employing Gravity-Fed Cooling (GFC) and Solar Powered Adsorption Cooling (SPAC) techniques for the cooling PV cells, the cells conversion efficiency would improve and also the resulting solar-hydrogen production system would achieve a higher production rate.

5.5   Additional Results and Analyses

5.5.1 Further Analysis of Cooling Systems and Models

It has been demonstrated so far that the GFC system was effective in increasing the conversion efficiency of the PV module and these results also corroborated the results of the mathematical model in Figure 5.5. Of note, though, is the time difference between the model and the experiments for the system to come to steady state in terms of temperature. The model, Figure 5.5, showed the PV module with GFC system reaching steady state within a second while the experiments showed the system reaching steady state within minutes, Figure 5.4.

It can be appreciated that the model is 'ideal' and therefore ignores time dependent effects such as cooling down period of the module. That is, the model 'sees' the back surface of the PV module instantaneously at the cooling water temperature but the experiments accounted for the fact that the back surface was at 60 ^{o}C before the water was applied and thus in real time needed 'time' to fall to the cooling water temperature. Trim (1990) made this point when highlighting boundary conditions in his book, *Applied Partial Differential Equations.* He noted that while mathematically there are no contradictions in instantaneous changes from one value (temperature) to another, especially with respect to Dirichlet boundary conditions, physical these changes are impossible.

It would be of interest to look at a Neumann boundary condition for the back surface, which would explicitly take into account the water flow rates with convective heat transfer, than that of the present fixed temperature Dirichlet boundary condition which implicitly deals with the flow rates and thus requires high flow rates in the experiments for the time frames to reduce to those of the model.

The results of the experiments clearly demonstrated that flow rates of cooling water played an important role, and to this end further tests were carried out to establish the role of the rate of flow of cooling water on the system. Plots from the results, exemplified by Tables 5.4 and 5.5, are presented in Figures 5.14 and 5.15.

5.5.1.1   *Impact of GFC Water Flow Rates on Module Temperature*
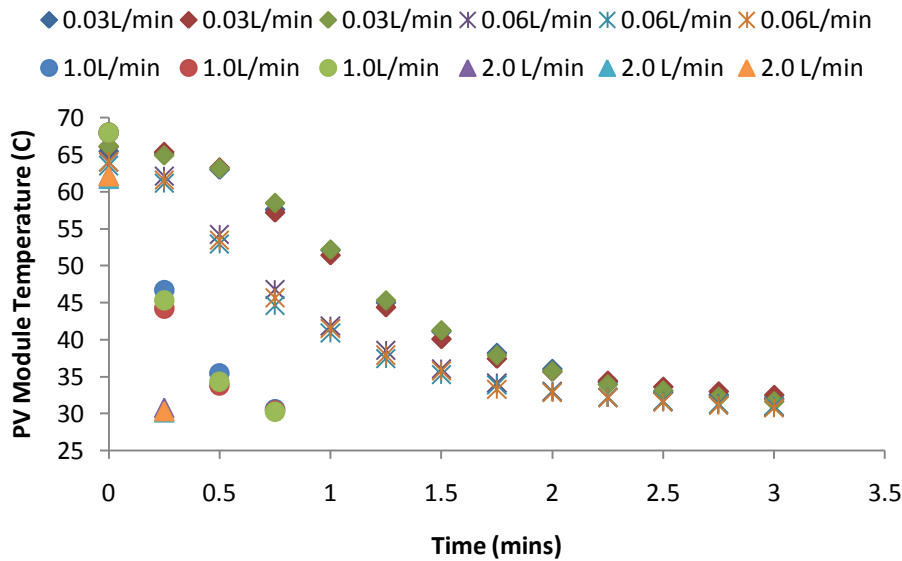
Figure 5.14 Scatterplots of Temperature Profiles for Four Flow Rates of GFC Water
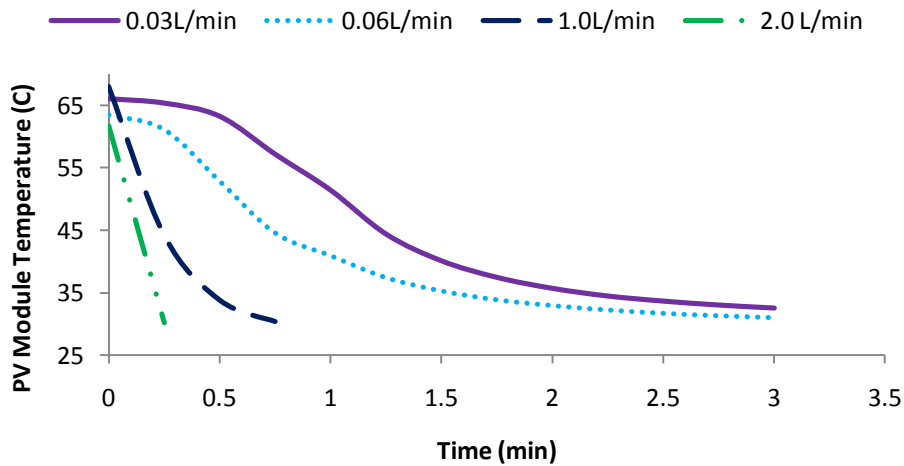
Figure 5.15   Temp profiles of PV module for 4 flow-rates of GFC water
(averaged profiles from scatter plots in Figure 5.14)

Figure 5.15 highlights the time taken for the temperature of the PV module to reach steady state for four different flow rates. The results show that as the flow rates increased, the time the systems took to reach steady state approached those predicted by the model. This corroborates the robustness of the model.

The results also illustrated that for all the flow rates of the cooling water tested, at steady state the module temperature remained within 3 degrees of the cooling water temperature irrespective of how long the solar irradiance stayed at full sun (1000 W/m^2). And

an interesting observation from the experiment was that as long as the cooling water was switched on before the module was exposed to solar irradiance, the module temperature did not rise above 3 degrees of the cooling water for flow rates above 0.5 L/min.

The fact that all flow rates effected the desired degree of cooling in less than three minutes, for a system that was exposed for at least six hours of sunshine, demonstrated that the system can be optimized with low flow rates. That is, three minutes is minuscule in the context of a six hour period, therefore utilizing the low flow rates will not incur a time penalty. The cooling effects of all the flow rates were therefore practically immediate on the PV module.

To further make the point about optimizing with low flow rates, calculations showed that a PV module exposed to full sun(1000 W/m^2), and assuming all light energy is converted to heat, required 7.2 litres per minute per square metre (7.2 L/min·m^2) to cool it. This is with a two-degree rise in the cooling water temperature. Therefore to cool an area of 0.0036 m^2, which is the area of the experimental module, the calculations showed that a flow rate of 0.03 litre/min was required. Figure 5.15 shows that this low flow rate does produce cooling.

5.5.1.2 *Impact of SPACS Water Flow Rates on Module Temperature*

Likewise for the SPAC system, further tests were carried out to better understand the effects of flow rates and correlate the steady rate times with the times given by the Mathematical Model. Figures 5.16 and 5.17 represent the effects. As was seen for the GFC system the "higher" flow rates produced steady-state times approaching those of the Mathematical Model. Note, "higher" in this case is relative since the flow rates for the SPAC system were actually lower than those for the GFC system since less chilled-water was needed to achieve the same level of cooling.

Also, as was noted in Section 2.4, one of the drawbacks of using a circulating water system is the 'parasitic' power required to run the pump. In order to minimize the "parasitic" power needed for the circulating pump, the circulating chilled-water flow needs to be optimized. To achieve this optimization the impact of varying the flow rates needed to be established.

Impact of SPAC Water Flow Rates on Module Temperature

◆0.02L/min ◆0.02L/min ◆0.02L/min ✳0.03L/min ✳0.03L/min ✳0.03L/min
●0.06L/min ●0.06L/min ●0.06L/min ▲0.8L/min ▲0.8L/min ▲0.8L/min
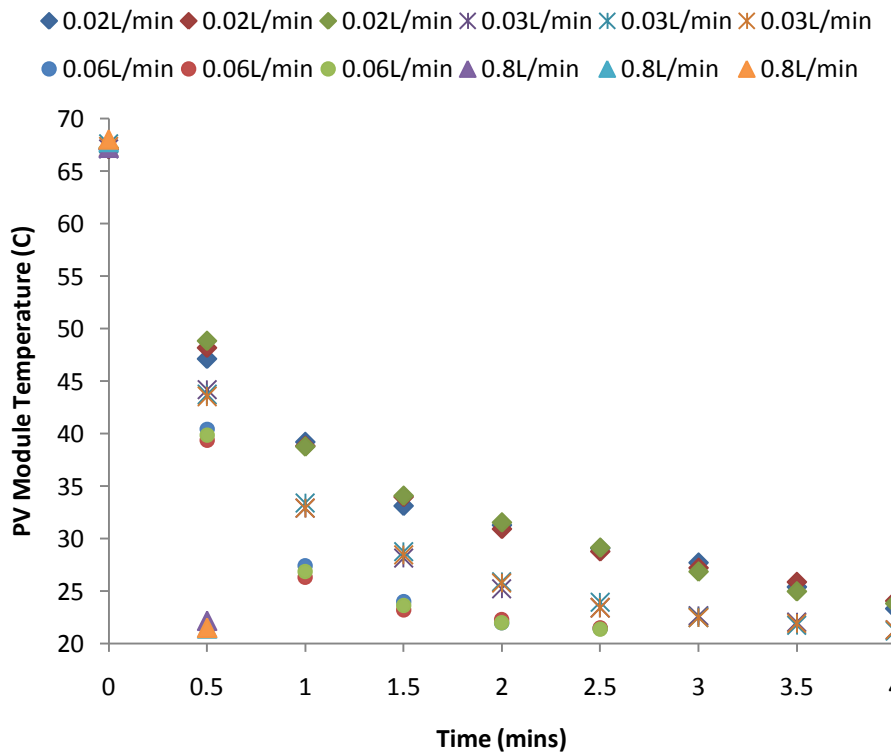
Figure 5.16 Scatterplots of Temperature Profiles for Four Flow Rates of SPAC Water

———0.02L/min ·········0.03L/min ─ ─ ─0.06L/min ─ · ─0.8L/min
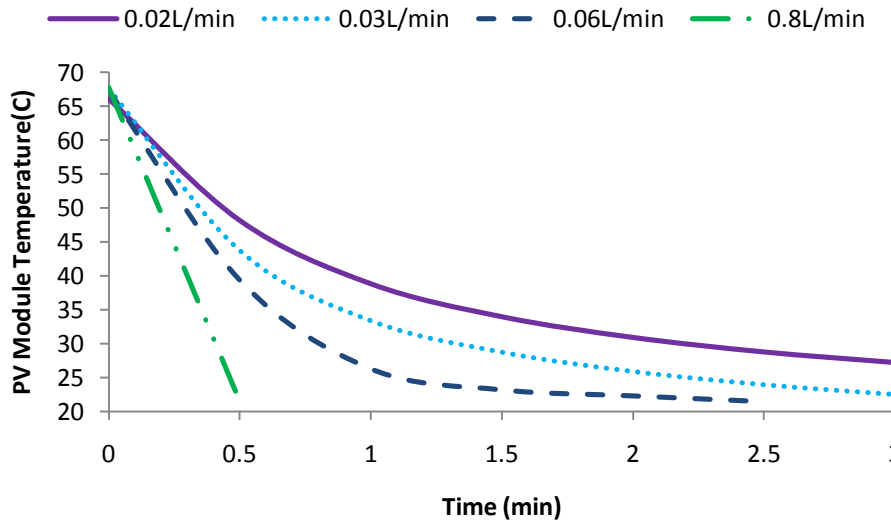
Figure 5.17   Temp profiles of PV module for 4 flow-rates of SPAC water
(averaged profiles from scatter plots in Figure 5.16)

Figure 5.17 presents the time taken for the temperature of the PV module to approach the cooling water temperature of 21 ^{o}C for four different flow rates. Within three minutes all profiles are below 30 ^{o}C. The results also showed that for all the different flow rates of the SPAC water tested, at steady state the module temperature fell and stayed below the

manufacturer's rated temperature of 25°C irrespective of how long the solar irradiance remained at full sun (1000 W/m^2).

The profiles in Figure 5.17, when compared to those in Figure 5.15, also exemplify the greater impact of the SPAC system over the Gravity-Fed Cooling (GFC) system. That is, the profiles in Figure 5.17 curve downward more quickly than those for the GFC system illustrated in Figure 5.15, indicating a faster cooling rate.

The sub-cooling (temperature below 25°C) ability of the SPAC system which resulted in flow rates as low as 0.02L/min suggested that that the system would require a smaller than normal circulating pump. This then would reduce the 'parasitic' power required to circulate the chilled water from the evaporator and therefore satisfy one of the objectives of the research.

5.6   Systems Costs Calculations

After examining the effects of the cooling systems on PV power generation, the cost of producing Hydrogen with a PEM Electrolyzer System and those of the Cooling Systems were considered. In addressing the costing, a small scale hydrogen generator (HG30) was used as the reference for the calculations. The overall system cost is presented in Chapter 6.

5.6.1 Background to Costs Calculations

The first step in the calculation was to determine a base unit (litre per minute per unit area of PV module – L/min·m^2) for cooling water required. This base unit was chosen so that comparisons can be made between cooling systems.

The results from the experiments employing a GFC system showed that a PV panel of area 0.0036 m^2 and an area of 0.11 m^2 took 0.03 L/min and 0.6 L/min, respectively, of cooling water to keep the panel temperature within 3 degrees of cooling water temperature; and that was with a solar irradiance of 1000 W/m^2 exposure. This extrapolated to 3.5 L/min (1 gal/min) of cooling water for each square metre (1 m^2) of PV panel and further translated to 35 L/min (10 gal/min) of cooling water for each kW of power produced (1 kW = 10 m^2).

The results of the SPAC system further demonstrated a one-third decrease in usage of cooling water when compared to the Gravity-Fed system. That is, the SPAC system utilized 1.2 L/min (0.3 gal/min) of cooling water for each square metre of PV panel.

As stated before, the costs calculations were based on a HG30 PEM Generator with specifications given in Table 5.9 (Heliocentris Energy Systems Inc).

Table 5.9   **PEM Hydrogen Generator Specifications**

ITEMS	UNITS
PEM Hydrogen Generator	HG30
Media Hydrogen Flow Rate	0….30 std. l/h
Hydrogen Purity	6.0 (99.9999%)
Hydrogen Delivery Pressure	0.1…..10.7 bar g (1…155psi g)
Water Quality	Deionized or Distilled
Power Mains	120 V AC, 50/60 Hz; 240 V AC, 50/60 Hz
Power Consumption	260 W max

5.7   Summary

From the results of the experimentations for both Gravity-Fed and Solar Powered Adsorption Cooling systems the chapter concluded that the objectives of the research were met. The Mathematical Models developed were in close agreement to the results of the experiments. The chapter also highlighted the energy balance on the Solar-Powered Adsorption Cooling (SPAC) system and gave the resulting coefficient of performance (COP) for the system. In addition, descriptions of the effects of elevated module-temperature on system productivity are given. The chapter closed with the background to the costing of a small Solar-Hydrogen Plant utilizing the cooling systems.

CHAPTER 6

ANALYSES of MODELS

The overall objective of this investigation is to increase the conversion efficiency of a PV module by reducing module temperature using two proposed types of cooling techniques; namely Gravity-Fed Cooling (GFC) and Solar-Powered Adsorption Cooling (SPAC) systems. The outcome is to quantify the impact that the cooling techniques have on the conversion efficiency of the module. While Chapter 5 gave the overall results of the investigation, in this chapter the results from the Mathematical Models developed are further scrutinized by means of parametric analyses to establish that objectives 1 and 2 are met; and also to corroborate the 'predictive' nature of the models and therefore demonstrate their contribution to the wider community.

The chapter also extends the analyses to the specific outcomes which seek, in general, to establish hydrogen gas as a practical renewable-alternative to fossil-fuel-based "cooking" gases, such as propane. To this end, the chapter goes on to analyse the results of the experiments carried out to determine how easy it is for hydrogen to be used as a "cooking" gas. The chapter covers:

- Parametric Analyses of Porous Bed Isosteric Heating Model
- Parametric Analysis of Gravity-Fed Cooling (GFC) Model
- Analyses of Hydrogen Production System
- Analyses of Hydrogen as a 'Cooking' Gas

6.1 Analyses of Porous Bed Isosteric Heating Model

6.1.1 Statistical Validation of Model for Porous Bed Temperature Profile

To measure the temperature profile in an adsorption bed in a practical system is not an easy task, as any insertion runs the risk of compromising the vacuum seal. Therefore, to provide a tool that can show the isosteric temperature profile of the bed without any insertion of instruments, a model was developed (eqn 27, Section 3.2.2) and given as:

$$T(r,t) = T_1 + \frac{2(T_o - T_1)}{R} \left[\sum_{n=1}^{\infty} exp(-\lambda^2 \, \alpha^2 t) \, \frac{J_o(\lambda_n \, r)}{(\lambda_n) J_1(\lambda_n \, R)} \right]$$

Also, in Chapter 5, Figure 5.9 showed the close agreement between the results of the experiments and those of the model. But to further validate the model as a practical tool which may be used beyond the scope of this research, Statistical verification is firstly determined. A combination of Student's t and Snedecor's F tests are employed.

6.1.1.1   *Statistical Inference Analysis: Student's t and Snedecor's F Methodologies*

Students's t methodology utilizes hypothesis testing and according to Gregory (1963) it gives one of the most stringent test for the acceptance/rejection of the null hypothesis. For the two-sample (experiment and model) test the hypotheses are:

Null Hypothesis, H_0 = there are no significant differences between the values of the samples

Inverse Hypothesis, H_1 = there are significant differences between the values of the samples

Where the null hypothesis, H_0, is rejected if

$$t_{stat} > t_{critical \; two \; tailed}$$

Student's t is given as:

$$t = \frac{|\bar{x}_1 - \bar{x}_2|}{\sqrt{\dfrac{\hat{\sigma}_1^2}{n_1} + \dfrac{\hat{\sigma}_2^2}{n_2}}} \qquad\qquad (28)$$

Where $\bar{x}_1$ = experiment sample average

$\bar{x}_2$ = model sample average

$\hat{\sigma}$ = best estimate of standard deviation

n = size of sample

Using MS Excel Data Analysis programme, the following results were obtained:

Table 6.1   t-Test: Two-Sample Assuming Equal Variances

	Exp Temp	Model Temp
Mean	52.47333	51.944444
Variance	2.438025	3.3452778
Observations	9	9
Pooled Variance	2.891651	
Hypothesized Mean Difference	0	
df	16	
t Stat	0.659778	
P(T<=t) one-tail	0.259391	
t Critical one-tail	1.745884	
P(T<=t) two-tail	0.518782	
t Critical two-tail	2.119905	

The result shows that $t_{stat} < t_{critical\ two\ tailed}$ which implies that the null hypothesis cannot be rejected at the 95% confidence level. But to further consolidate the results a variance test must be conducted to determine if there's any statistical difference between the variances of the samples. Snedecor's F test is now engaged.

Null Hypothesis, H$_0$ = there is no significant difference between the variances

Inverse Hypothesis, H$_1$ = there is significant difference between the variances

Where the null hypothesis, H$_0$, is rejected if

$$F > F_{critical\ upper\ one\text{-}tailed}$$

$$Snedecor's\ F = \frac{greater\ variance}{lesser\ variance} \tag{29}$$

Using MS Excel Data Analysis programme, the following were obtained:

Table 6.2   F-Test Two-Sample for Variances

	Model Temp	Exp Temp
Mean	51.94444	52.47333
Variance	3.345278	2.438025
Observations	9	9
df	8	8
F	1.372126	
P(F<=f) one-tail	0.332579	
F Critical one-tail	3.438101	

Here, it is also seen that the null hypothesis cannot be rejected at the 95% confidence level.

Therefore, according to both Student and Snedecor statistically the data generated by the model and those recorded from the experiments are equivalent. This implies that the model can replace experimentations and thus be used in situation beyond the scope of this research, within the limitations given for the model.

6.1.2 Sensitivity Parametric Tests on Model for Porous Bed

Having established that the model is statistically sound, sensitivity tests were executed on the critical parameters of the model.

6.1.2.1   Effects of Combined Radius (R) and Thermal Conductivity (Ke) on Speed of Isosteric Heating

Crucial to the function of the SPAC system is the temperature of its desorption bed. Designing the bed as cylindrical, as oppose to the more traditional rectangular, and also the treatment of the Effective Thermal Conductivity of the bed, K_e, raise the issue of functionality. That is, will this design allow the entire bed to reach desorption (evaporation) temperature (isosteric/sensible heating), and if so, how quickly? The speed at which the bed reaches desorption temperature can be significant to the efficiency of the system. Regions with great cloud variations, even on a very sunny day, have immense variation in solar

irradiance intensity also, and therefore when there is the need for direct radiation, time becomes important. Hence, the time taken for the bed to reach desorption is a factor of import. As stated by Li et al. (2004), an effective bed must have good heat and mass transfer. Heat transfer is time dependent. Critoph and Turner (1994) went further and remarked that to improve the power output per mass of carbon required rapid isosteric (sensible) heating/cooling of desorption/adsorption bed.

The Mathematical Model set out to determine how quickly the bed, as designed, attains the temperature (pressure) required for the evaporation of the methanol. Therefore, to further analyze the predictive ability of the model the combined roles of Effective Thermal Conductivity, Ke, and Radius of bed (R) are examined (the effective thermal conductivity is embedded in the exponential function in equation 27).
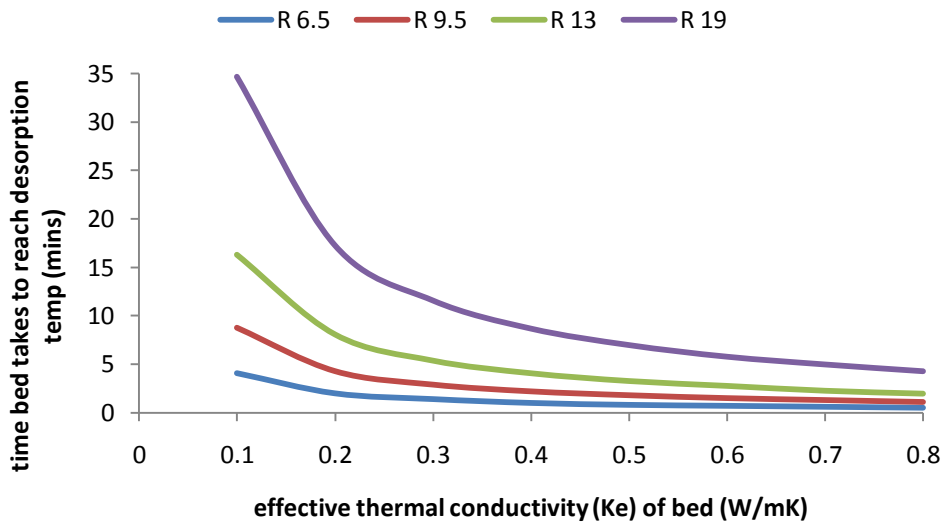
Figure 6.1   Sensitivity of Desorption time/temp to Combined Ke & R variations
Where R9.5, $K_e0.244$ = reference

The profiles in Figure 6.1 demonstrate that desorption time/temp is sensitive to effective thermal (Ke) in the range of $0.1 - 0.3$, as can be seen by the slopes of the graphs. But the sensitivity is greatly impacted by the radius (R) of the bed. As the bed radius increases desorption time/temp becomes more sensitive to Ke especially in the 0.1-0.3 range.

The interpretation of the effects of interaction between R and Ke on desorption time/temp is that increase Ke reduces the time the bed takes to reach desorption temperature while increase R increases the time. So, which parameter is desorption time/temp more sensitive to? As evident by the rate of change in slopes of the profiles, it is Ke in the range of

0.1-0.3 that is most sensitive. This conclusion is derived from the fact that changes in the slopes of the profiles reflect the effects of Ke while changes in the gaps between profiles reflect the effects of R.

Note, Figure 6.1 shows the time-profiles for the four bed radii (mm) when the outer surface of the bed was held at 54°C, initial temperature of bed 25°C, and void fraction of bed 0.476. Also, results of the inverse relationship between times taken to reach desorption temperature and values of Ke is supported by Demir et al. (2008) who found that the lower the thermal conductivity of the bed, the longer desorption process takes.

6.1.2.2 *Influence of Combined Radius (R) and Void Fraction (VF) on Speed of Isosteric Heating*
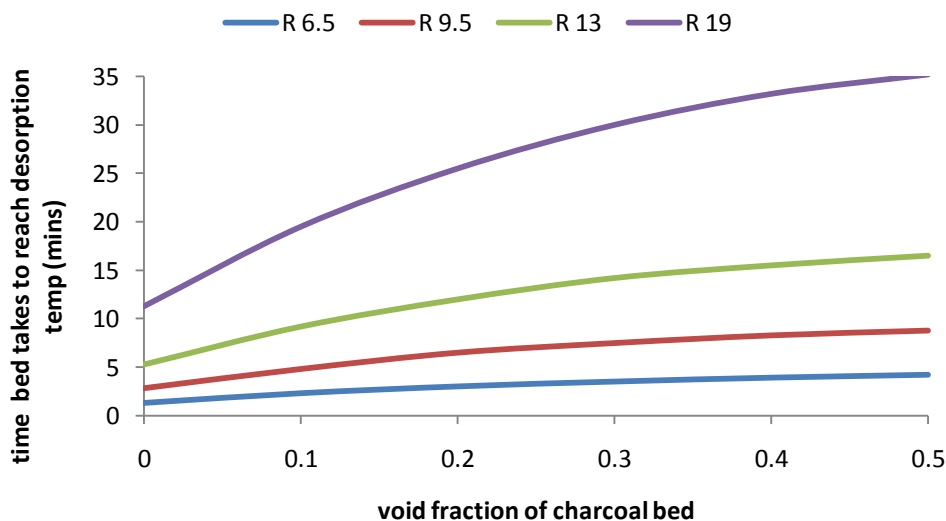
Figure 6.2   Sensitivity of Desorption time/temp to Combined VF & R variations
Where R9.5, Void 0.476 = reference

With the gaps-between- profiles being indicative of the effects of R and slope-of-profiles the effects of VF, it is clear that with this combination desorption time/temp is more sensitive to R, as is observed from the profiles of Figure 6.2. The profiles show increases in R from 6.5-19mm resulted in desorption times with ranges of 1-11 minutes at zero void fraction to 2.5-35 minutes at 0.5 void fraction; increase in R negatively affects the system.

The results concurred with the understanding that increase in void fraction increases the time taken for bed to reach desorption temperature. Void fraction (inter granular void) is

the fraction of bed space that is not occupied by charcoal. Its influence on the speed of isosteric heating of the bed is such that, according to Wang and Oliveira (2005), for the internal heat transfer of the bed to improve the most suitable option is the use of consolidated adsorbents. This simply means zero void fraction. This sentiment is also supported by Critoph and Turner (1995) who noted that the higher the porosity (void fraction) of the bed the lower the conductivity. Banker et al. (2004) went further and stated that ideally there should be no void fraction in a thermal compressor (desorption bed).

But while void fraction reduces heat transfer in the bed it does increase mass transfer of the methanol through the bed. Wang and Oliveira (2005) noted that consolidated (zero void fraction) adsorbents do have lower mass transfer properties than granular ones. The question that arises is what then is the "ideal" void fraction that maximizes both heat and mass transfer? Section6.1.3 seeks to answer the question.

Also, from Figure 6.2 it can be inferred that tube radii of 6.5 – 13 mm (¼" – ½") are more suitable for bed construction.

6.1.2.3   *Indicative Optimum Design Parameters for Adsorption Bed*

Since bed radius (R), effective thermal conductivity (Ke) and void fraction (VF) are parameters that critically influence the speed of isosteric (sensible) heating of the charcoal bed and hence the desorption process, it would be useful to optimize these variables. The model developed for the isosteric heating was used to generate Figure 6.3 as an indicative design aid.
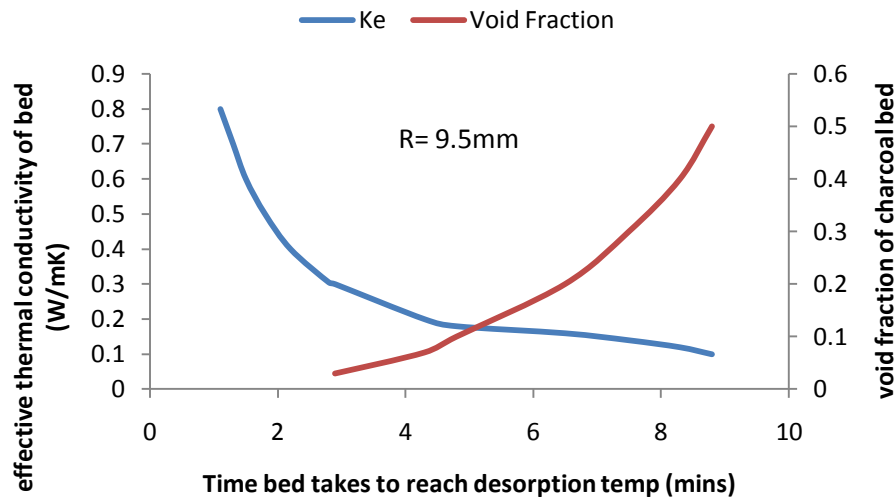
Figure 6.3   Optimization of Desorption Bed Parameters R, Ke & VF

Where R9.5, Ke0.244, VF0.476 = reference

For an adsorption/desorption bed comprised of methanol/granular-charcoal pair, with copper tube of radius 9.5 mm being held at an average temperature 54°C and initial bed temperature 25°C, Figure 6.3 indicates the values for the effective thermal conductivity and void fraction that will optimize the time taken for the bed to reach desorption temperature. The figure shows a void fraction of 0.12 and effective thermal conductivity of 0.18 will optimize the time to 5.2 minutes for the given temperature range.

Matching the optimized parameters against the experimental and original (reference) model results, where the initial bed temperature was 49 ^{o}C and average tube temperature 54 ^{o}C, Figure 6.4 highlights the results.
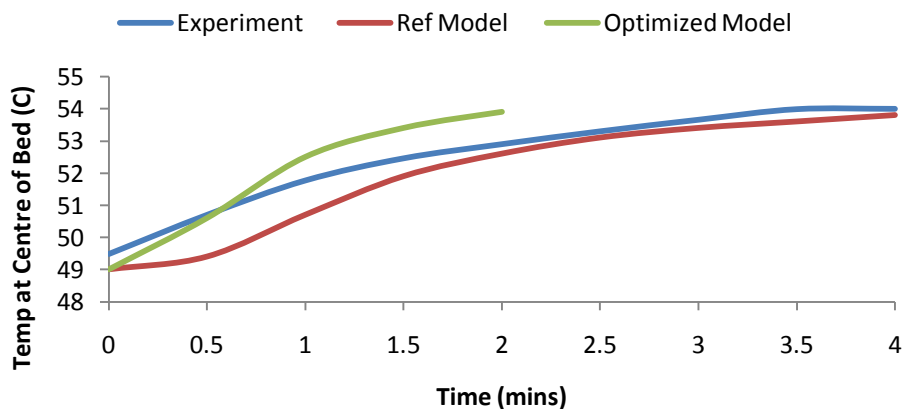
Figure 6.4   Effects of Optimized Parameters on Bed-Centre Temp Profile

Figure 6.4 shows that the optimized parameters caused the bed to reach steady state in half the time the non-optimized conditions used. It would be interesting to carry out further experiments with these data.

6.1.3 *Sensitivity Tests on Solar Powered Adsorption Cooling (SPAC) System*

Analyses of the coefficient of performance (COP) obtained from the energy balance on the SPAC system (Table 5.7) showed that the most influential parameters are solar irradiance, temperature of the charcoal bed and the condenser temperature. The sensitivity of the COP to these variables is highlighted in Figures 6.5-6.8.
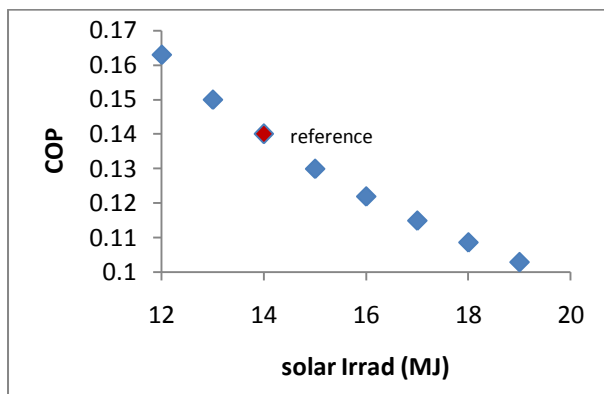
Fig 6.5   Sensitivity of COP to Sol Irrad
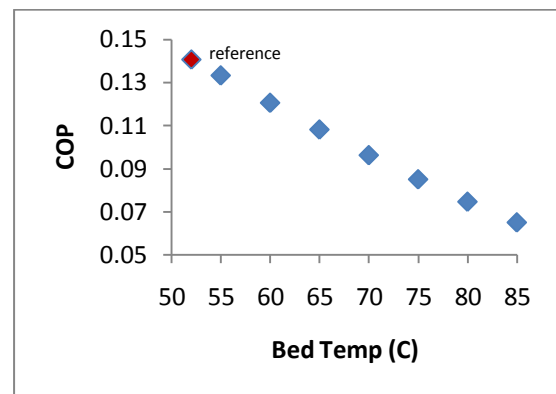
Fig 6.6   Sensitivity of COP to Bed Temp
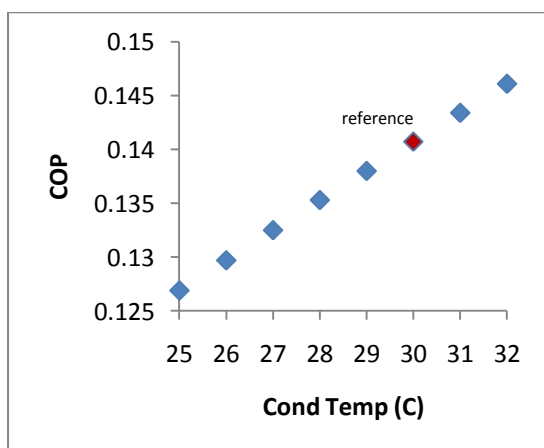
Fig 6.7 Sensitivity of COP to Cond Temp
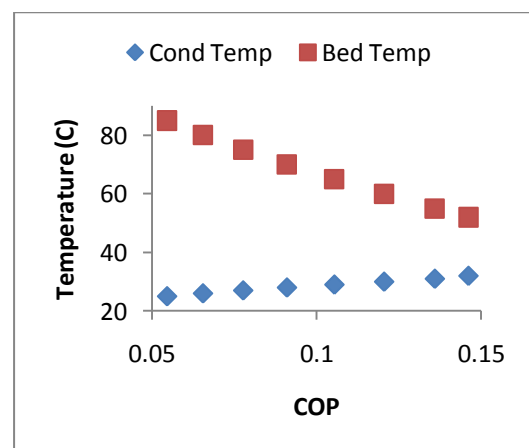
Fig 6.8   Sensitivity of COP to Simultaneous Changes in Bed & Cond Temps

Figure 6.5 shows that the system COP reduces with increases in solar irradiance. This can be explained by the fact that once the energy needed for desorption is attained, any additional energy is wasted; hence reduction in COP with increased irradiance. From the figure it can be shown that COP reduced by 37% for an 58% increase in irradiance. This implies a 0.1 sensitivity index (negative) for each percentage rise in irradiance above desorption requirement. It must be noted that the referenced value was well aligned with the trend of the COP profile. This, according to Boubakri, et.al (2000), implies that the system was well balanced.

As condenser temperature increased, surprisingly, the COP increased also, according to Figure 6.7. This may be explained by the fact that as condenser temperature rises so too its corresponding pressure. The bed temperature will increase accordingly thereby desorbing more methanol. This increase in methanol will definitely increase the COP, since more methanol means more effective cooling.

The effects of condenser temperature on system COP resulted in a sensitivity index (positive) of 0.07 for each percentage rise in condenser temperature. The results revealed a 15% increase in COP for 28% increase in condenser temperature. The reference value was again in alignment with the profile trend.

The most interesting trend is the sensitivity of the COP with respect to increases in bed temperature as seen in Figure 6.6. As bed temperature increased it presented a sensitivity index (negative) of 0.12 for each percentage rise in bed temperature. In other words, a 63% rise in bed temperature gave a 54% fall in COP. This inverse relationship between bed temperatures above desorption value and COP can be explained by the compounded effects of the bed temperature on the entire system.

The bed temperature needs to rise above evaporation temperature for the refrigerant to desorb from the bed. The COP of the system is directly proportional to the amount of refrigerant desorbed. But the COP is also directly proportional to the amount of refrigerant re-adsorbed into the bed. The amount of refrigerant re-adsorbed is very dependent on bed temperature. So, the more the bed temperature rises above the evaporation temperature the less the bed is able to re-adsorb in the second phase.

To further explore the bed and condenser temperatures phenomena, both were simultaneously changed in their increasing COP trends, and plotted in Figure 6.8. The combined positive effects resulted in a 4% increase in COP above the reference value.

In terms of sensitivity, the system COP is most sensitive to Bed Temperature, then Solar Irradiance, and least sensitive to Condenser Temperature.

6.2   Parametric Analyses of Gravity Fed Cooling (GFC) Model

The results in Section 5.2.3 showed that the GFC model predicted the rapid cooling of the PV module in every instant when compared with the experimental results. But to further test the robustness of the model, sensitivity analyses were undertaken on the four most significant parameters; namely: cell material, cell thickness, solar irradiance and cooling water temperature and flow rate.

6.2.1 Sensitivity of Cell Surface Temperature to Changes in Material and Thickness

While Silicon (Si) is the most common material used for PV cell construction, Section 2.2 explained that Germanium (Ge), Gallium arsenide (GaAs) and Cadmium sulfide (CdS) are commonly used too. To get an understanding of the impact that variations in construction material (thermal conductivity) and cell thickness play in the temperature profile of the cells Figure 6.9 is used for this analysis.

The results of the GFC Model have already shown, Section 5.2.3, that with the application of the cooling water, the 3 mm thick silicon cell rapidly reached thermal equilibrium with the water. Figure 6.9 shows the temperature profiles of the front-face of the cells after one second of applying the cooling water versus changes in cell thickness. All cells were at 60°C at the start of the cooling process. The front surface is chosen because it is furthest from the cooling water and would be the last area to be affected by the cooling.
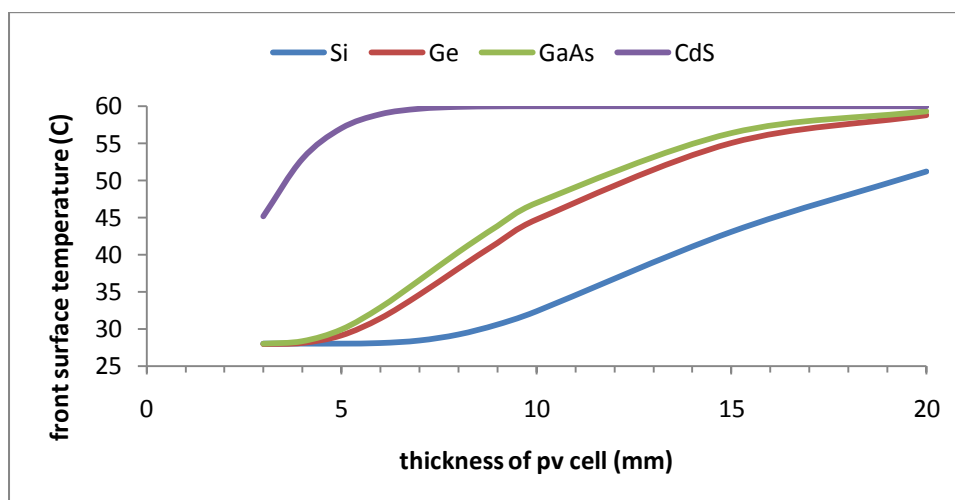
Figure 6.9   Sensitivity of Cell Surface Temperature to Cell Thickness/Material after the application of cooling water

Figure 6.9 indicates that for cell thicknesses less than 5 mm all materials, except Cadmium sulfide, cool equally rapidly. But as thickness increases there are marked differences in the effects of the cooling water. Germanium and Gallium arsenide are similarly affected as their thickness increase, but Cadmium sulfide, with thickness above 5 mm, is practically unaffected by the cooling water. Silicon is the material that is mostly affected through its range of thickness and therefore this Mathematical Model suggests that Silicon would be one of the most promising semiconductor materials suited for the application of thermal management. Also, the analysis implies cell thicknesses of less than 5mm are more amenable to thermal management.

6.2.2 Sensitivity of Cell Surface Temperature to Changes in Solar Irradiance

The information portrayed by Figure 6.10 suggest that once the GFC system is employed, its impact reverses and negates all influence of solar irradiance on cell temperature. The simulations were carried out with three thicknesses of silicon cell where all cells were initially at 60°C and the readings of the front surface temperature taken after one hundredth of a second of the application of the cooling water. The cooling water was at a temperature of 30°C. The cells temperatures immediately dropped to the values shown, and afterwards they were independent of the intensity of solar irradiance.
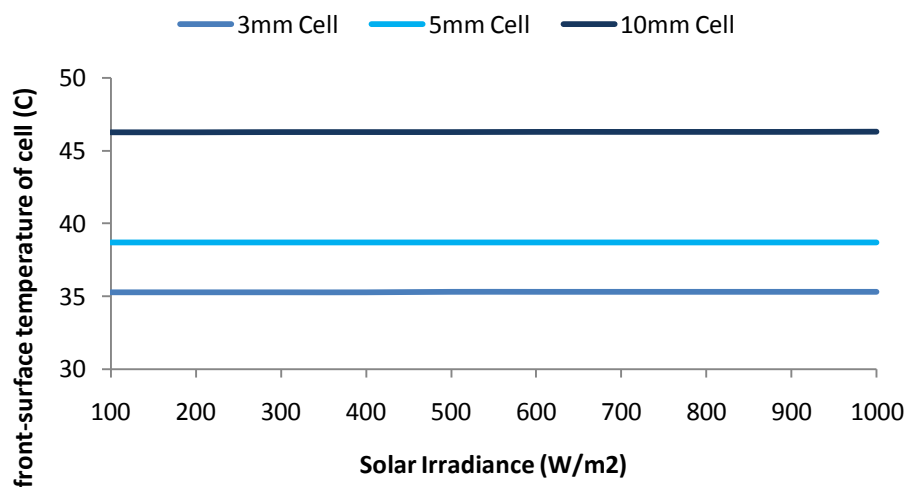
Figure 6.10   Sensitivity of Cell Surface Temperature to Changes in Solar Irradiance after the application of cooling water

This portrayal of the temperature profiles given by the GFC Model was verified by the results from the experiments conducted, as reported in Section 5.2.2. The experiments had shown that once the GFC system was applied, the cell temperature dropped to the cooling water value and stayed there irrespective of the variations in, and duration of, the solar irradiance intensities. This is another demonstration that the model can be applied to practical fieldwork designs.

6.2.3 *Sensitivity of Cell Surface Temperature to Changes in Cell Thicknesses and Cooling Water Temperatures*
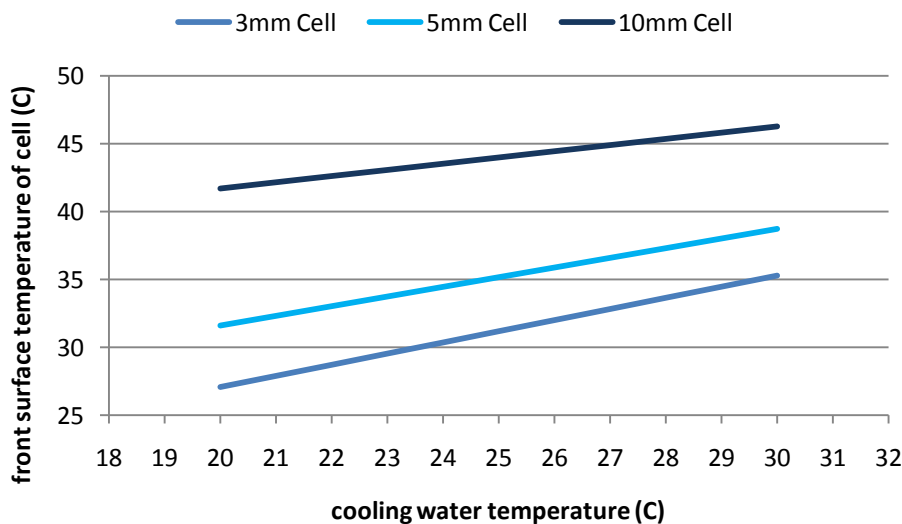
Figure 6.11   **Sensitivity of Cell Surface Temperature to Changes in Cooling Water Temperature**

From Figure 5.5 it was shown that for thin cells, complete cooling of the cell took just a fraction of a second. Therefore, to generate Figure 6.11 with some variation in the temperature readings, a small time frame of one hundredth of a second was applied to the model. All cells were initially at 60°C at the start of the cooling process and the analyses were done for silicon material with the three cell thicknesses shown.

Figure 6.11 illustrates the effects of using sub-cooled (temperature below 25$^{\text{o}}$C) water in the cooling process. In the cases of 3mm and 5mm thicknesses, cooling water temperatures below 25 brought the cell temperature from 60$^{\text{o}}$C to below 35$^{\text{o}}$C instantaneously. The effects that sub-cooled water has, augurs well for regions where the ambient temperature is below 25$^{\text{o}}$C. This implies that the application of a cooling system such as Gravity-Fed Cooling in such regions would give good returns in terms of improvement in cell efficiency.

6.3   Indicative Optimal Design of PV Power System with Thermal Management

In terms of application in the wider community, utilizing the results from the parametric analyses to design a PV power system with thermal management for optimal outputs implies the following design parameters:

- Semiconductor material: Silicon
- Thickness of cells: $\leq$ 5mm
- Cooling water temperature: $\leq$ 25$^{\text{o}}$C
- Range of Solar Irradiance: 500-1000 W/m^2

The indications are that a PV power system that incorporates thermal management allows for a wider range of operating conditions with optimal outputs. The Gravity-Fed Cooling (GFC) system with its simple design, adds to the increase in outputs benefits.

6.4   Analyses of Hydrogen Production System

The true test of the cooling systems is their effects on the productivity of any system to which they are attached. To this end the experiments were developed and executed to ascertain the effects of the cooling systems on a Solar-Hydrogen Production System. The analyses of the results of the experiments described in Section 5.3 are now presented.

6.4.1 System Operational Performance Analyses

Table 6.3 presents a concise overview of comparative performances of the Solar-Hydrogen Plant under varying operating conditions.

Table 6.3 Solar-Hydrogen Plant Parameters Performance for 3 Operating Conditions

Plant Parameters	Un-Cooled	GFC	SPAC
PV Module Tempeature (C)	62	30	25
Module Power Output (W)	5.07	6.76	7.05
Module Conversion Efficiency (%)	12.8	14.7	15
Hydrogen Production (mL/min)	26.5	33.3	35
Cooling Water Rate (L/min)	-	9.1	3.03

The table shows the performances of the Solar-Hydrogen Plant parameters, in absolute values, for three operating conditions. It illustrates the increase gain in productivity when a PV power generator operates with a cooling system. The values in the table demonstrate that the Solar-Powered Adsorption Cooling (SPAC) system performed better than the Gravity-Fed Cooling (GFC) system. This was as a result of the SPAC sub-cooling (cooling below 25 ^{o}C) capabilities. The results here also underscore the possible benefits the wider community can gain from utilizing the cooling systems.

6.5   Analyses of Hydrogen as a 'Cooking' Gas

The specific outcome of the research is to present Hydrogen as a 'regular' cooking gas that is ready to supplement or replace propane gas. Analyzing the results of the demonstration of hydrogen being used as cooking gas, as described in Section 4.4.2, the following observations were made.

(a)   Hydrogen "Cooking' System   (b) Egg Boiling with Hydrogen "Cooking" System

Figure 6.12   **Cooking with Hydrogen Gas**

The analyses showed that hydrogen behaved like a 'regular' cooking gas (Figure 6.12) with the exception that it brought the water to boiling much quicker than propane would and therefore cooked quicker than propane. In other words, it took less hydrogen gas to achieve the same results as propane. This supports the fact that hydrogen has a higher calorific value, 2.8 times, than that of propane (Engineering ToolBox, ret. 2008)

The demonstration illustrated that hydrogen gas can be used as a cooking gas as long as safety regulations are in place. This augurs well for tropical regions where the solar insolation is high and the countries are looking for alternatives to fossil fuel.

6.6 Cost of Solar-Hydrogen Plant with Cooling Systems

Chapter 5 and Sections 6.1- 6.5 all demonstrated that a Solar-Hydrogen Plant with Thermal Management is technologically feasible. This determination was a central objective of this research. What now needs to be established is the economical feasibility of such a plant.

To establish a small plant with an HG30 hydrogen generator (electrolyzer) with Cascading Storage (developed by this investigation), and employing the Gravity-Fed and Solar-Powered Adsorption cooling systems, the associated capital costs are presented in Table 6.4. (NB: The Cascading Storage System is 1/8 the cost of a Metal Hydride Storage Canister-HS760).

Table 6.4   Capital Cost for Solar-Hydrogen Plant with Cooling System

ITEMS	SPACS (US$)	GFCS (US$)
Electrolyzer (HG30)	14,750	14,750
Cascading Storage System	200	200
PV Module	2,035	1,455
Cooling Water	10	0
Cooling Water Storage Tank (insulated plastic)	350	-
Solar-Powered Circulating Pump	545	-
Balance of Plant (BOP)	3,524	300
TOTAL CAPITAL COST	**21,414**	**16,705**

Table 6.4 lists the major cost components associated with a Hydrogen Plant utilizing the Cooling systems. Along with showing the complexity of the SPAC system, the table highlights the relatively high capital cost of the SPAC system balance of plant (BOP) in comparison to that of the GFC system. The BOP for the SPAC system costs almost 1200% more than that of the GFC system. The table also shows the low cost of the Cooling Systems in contrast to the cost of the Hydrogen Plant. The table underscores the point that the Plant using the SPAC system cost 28% more than the one using the GFC system.

What also must be highlighted is that the Electrolyser is the single most expensive item in the system. Any reduction in its cost would bring the system in the reach of small businesses.

6.7   Summary

Chapter 6 dealt with analyses performed on the results from chapter 5. It covered:

- Parametric Analyses of Porous Bed Isosteric Heating Model
- Parametric Analysis of Gravity-Fed Cooling (GFC) Model
- Analyses of Hydrogen Production System
- Analyses of Hydrogen as a 'Cooking' Gas

It showed effects, such as those of material types and thickness of cells, on the temperature profile of a PV module. It indicated optimal design parameters for the cooling systems. It highlighted the greater impact of the SPAC Technique over those of the GFC Technique. But went on to show that the SPAC system is more expensive to build and operate. The chapter also illustrated that hydrogen gas functioned easily as a "cooking" gas, and ended with the contributions the research made to the wider community.

CHAPTER 7

DISCUSSION, CONCLUSION and RECOMMENDATION

This chapter discusses the overall objectives and original outcomes that were proposed by the investigation. The chapter also revisits the findings of other researchers to evaluate the results of this research with regard to theirs. It then gives its conclusion, recommendations and also proposed papers to be submitted to International Journals.

7.1 Discussion on Objectives of Research

7.1.1 Effectiveness of Cooling Systems

An objective of the research was to establish the effects of the cooling systems on the Conversion Efficiency of photovoltaic cells. The instruments used in this determination were the mathematical models created under objective 2, results from experiments conducted and also results obtained by other researchers. Using the given instruments, it is shown that the cooling systems are effective.

The mathematical models showed that cooling of a PV module can be achieved with water flowing over the back of the module. The question was how efficiently this can be done in practice. The Gravity-Fed Cooling (GFC) system demonstrated its effectiveness by keeping the PV module operating continuously at 100% of the open-circuit voltage given by the manufacturer, whilst keeping the module within 3 ^{o}C of the cooling water temperature.

In comparison, the Solar-Powered Adsorption Cooling (SPAC) system established its superior effectiveness in assisting the PV module to operate continuously at 103% of rated open-circuit voltage by keeping the module at 3 ^{o}C degrees below the manufacturer's recommended temperature.

The literature showed that researchers in general have not definitively quantified the increases in Conversion Efficiency they obtained from their cooling systems, except for Krauter (2004) who obtained an 8.8% increase from his system. But King, et al. (1997), Sweelem, et al. (1999) and Hu and White (1983) translate the impact of the GFC the SPAC

systems of this research as an absolute increase of 12.8% and 14.8%, respectively, in the Conversion Efficiency of the module.

In addition, Radziemska (2003) obtained from his experiments a temperature coefficient of -0.65%/K for Power Output for a PV cell. This translates to an increase of 20-23% in Power Output for a temperature reduction of 30-35 $^{\circ}$C. The results of this research show that the effects of the cooling system give an increase of 33-39% in Power Output for the same degree of temperature reduction in the PV module.

Also in comparing cooling system designs, the GFC system has achieved simplicity and lower costing than that of the SPAC system and some of those by other researchers. That is, water tube welded on to the back of the module by Brogren and Karisson (2002); increasing thermal mass of modules by attaching them to small water filled tanks by Ronnelid, et al. (1999); and employing evaporative cooling based on the theory of heat pipes by Farahat (2004), all seem more complex and costly than the GFC system. In addition, the water used by the GFC system is returned to its source thus making the cost for water practically zero; and for the whole process no circulating pump is employed.

7.1.2 *Production Rate of Hydrogen by an Electrolyzer for each Cooling System*

The first objective of this thesis was to establish the production rate of hydrogen under each cooling system. This determination was accomplished by engaging an off-the-shelf Hydrogen Production System and subjecting it to the GFC and SPAC systems (Section 4.3). (It must be stated that during the experiments when the hydrogen system was placed under the manufacturer's specifications, the output of hydrogen obtained was only 54% of that stated by the manufacturer. This raises the question of the system being over-rated by the manufacturer. Further investigation is need here).

From Section 6.3 the superiority of SPAC over GFC is evident in the rate of hydrogen produced. The effects of the SPAC system resulted in a production rate of 35mL Hydrogen per minute in comparison to 33 mL Hydrogen per minute for the GFC system. This translates to the SPAC system being 6% more effective than the Gravity-Fed Cooling (GFC) system. But what should be highlighted is that the key to the SPAC system is its sub-cooling abilities; that is, keeping the cooling water temperature below 25 $^{\circ}$C. This then suggests that for regions where water temperature is normally below 25 $^{\circ}$C, the GFC system will achieve the

same level of output as the SPAC system without the complexity and costs associated with the SPAC system.

7.2   Discussion on the Original Outcomes of the Research

From the original outcomes, the investigation was to establish the robustness of the mathematical models created and exhibit that the cooling systems improved conversion efficiency of the PV cells. Also, an objective was to demonstrate the practicality of producing hydrogen as a renewable fuel source from a renewable energy sources (water/sunlight), and use the hydrogen as domestic cooking gas. This was to be achieved by utilizing matured, enhanced, system-level devices. Section 7.1 dealt with the results from enhancing the matured system-level device of Photo Voltaic module which is coupled to the also matured technology of Electrolysis. This section now discusses the practical issues that need addressing before Hydrogen can be used as a 'cooking' gas.

The first issue that came to the fore was that of safety. But on examination of all the literature it was found that hydrogen poses no greater risks than those of gasoline, methane, natural gas, propane, etc. The major drawback with it is that it burns with almost an invisible flame and in addition it is also odourless and colourless. It therefore means that for domestic application flame-colouring and smell detecting additives need to be explored. But researchers like Booth and Pyle (1993) are already experimenting with "flame-colouring" by employing simple designs such as placing Stainless Steel Wool around the burner nozzeles. These make tackling the safety tasks that much easier.

The second issue that arose was the type of stove-burner required to accommodate burning of hydrogen gas. From the literature and the experiences in this research it was found that a typical gas stove will need retrofitting to accommodate hydrogen gas. This need presents opportunities for local communities. It is shown (Booth and Pyle, 1993) that the retrofitting and burners require only local materials and expertise. These simplify the process and thus make easier the accommodation of hydrogen as a cooking gas.

The third, and maybe the most significant, issue was gas storage. The fact that the bulk density of hydrogen gas is very low compare to the liquid bulk densities of the present cooking gases makes the issue of storing hydrogen gas a challenging one. Metal hydride

(hydrogen gas is absorbed) is the preferred choice of storage right now but the cost and handling (reheating of the cylinder for desorption) does not make it fit into the "simple" operation that this research is aiming for. This investigation found that a Cascading Storage System (CSS) is simpler to fashion. The CSS takes hydrogen from the electrolyzer at elevated pressure and stores it in a high pressure cylinder. The high pressure cylinder is connected to a standard low pressure cooking-gas cylinder, via a pressure reducing valve. The low pressure cylinder is connected to a stove. Refilling (topping up) of the low pressure cylinder can be accommodated automatically or manually while still connected to the stove. This removes the need for specialized equipment and personnel associated with the refilling of metal hydride cylinders.

With the practical issues taken into account, it can be said that producing hydrogen from a renewable source and using it as a cooking gas is practical. But this brings into question the issue of cost. So, to put the capital costs given in Section 6.4 in proper perspective, assuming a 25 year life cycle for the systems, the expenditures translate to $153/kg hydrogen and $120/kg hydrogen for the Hydrogen Plant that utilizes SPAC system and GFC system, respectively. This is in comparison to $40/kg hydrogen for other solar-hydrogen system (electrolyzer size unknown) as reported by Gibson and Kelly (2008) or $1.63/kg propane (Clearwater Gas System). This makes the project, for the given size electrolyzer, uneconomical and therefore the issue of economies of scale is now brought to the fore. Hence, to address the issue of economics, medium to larger plants that produce on a commercial level seems the more realistic route to take. All this, though, raises the need for more research into the technology of Proton Exchange Membrane (PEM) Electrolyzers; the single most costly item in the production of hydrogen from a renewable source!

Finally, as this research project sought to demonstrate the feasibility of self-sustained small to medium solar-hydrogen plants with thermal management, especially suitable for the Equatorial Belt regions of the world, it is evident that with the present cost of PEM electrolyzers small, home-run, solar-hydrogen plants are technically but not economically feasible. Medium to large commercial plants, due to economies of scale, are feasible.

7.3   CONCLUSIONS

The motivation for this study was to address the question of: Why not utilize Photovoltaic Power by day and Hydrogen Power by night? The question arose, in part, due to the dwindling reserves and extremely wild swings in the price of oil (high of US$148/barrel, low of US$59/barrel, all this in one year, 2008; on the upward swing it has ravaged many small oil-importing economies) and therefore the need to replace or reduce it.

In answering the question the research looked at the factors that militate against both PV Power and Hydrogen Power. The factors were found to be low conversion efficiency of the PV cells and the present hydrogen production processes that are deleterious to the environment. In proposing possible solutions to the problems, this project has contributed to pool of knowledge by demonstrating that the militating factors have been minimized by a focus on System-level Design and Optimization of Direct Photovoltaic Hydrogen-Generation through the adoption of cost-effective technologies such as Gravity-Fed and Solar-Adsorption cooling to improve system efficiency.

From the particulars of the proposed solutions and with regard to the objectives and original outcomes that were established, it has been concluded that the research has achieved the following:

- The two mathematical tools to represent specific aspects of the proposed systems that were created were shown to be robust and had their resilience verified by experimental and statistical results.

- The two proposed innovative thermal managements cooling systems (GFC/SPAC) both improved the conversion efficiency of the PV system.

- The Gravity-Fed Cooling (GFC) system increased the conversion efficiency of the PV system by 12.8% and power output by 33% compared to a non cooled system.

- The Solar-Powered Adsorption Cooling (SPAC) system increased the conversion efficiency of the PV system by 14.8% and the power output by 39% compared to a non cooled system.

- The proposed, coupled, PEM Solar-Hydrogen plant with GFC/SPAC thermal management increased hydrogen production by 32% compared to a non-thermally managed plant.

The general conclusion from this study is that the proposed system of Solar-Hydrogen Fuel Generation with either GFC or SPAC Thermal Management can help significantly developing, oil imported countries to reduce their dependence on imported fossil fuel because

of the capabilities of the system and its improved efficiency compared to non-thermally managed systems.

7.4   Original Works Produced from Research

This research has contributed to the wider community by producing the following original pieces of work:

1. The utility of GFC or SPAC for Thermal Management of Photo Voltaic Power Systems is original.

2. Increasing Hydrogen Production through PEM electrolyzer powered with PV system cooled by GFC or SPAC is original.

3. Low pressure application of hydrogen gas from solar energy, <u>with cascading storage,</u> for domestic cooking is original.

4. Mathematical "Tools" developed are original.

7.5   RECOMMENDATIONS

Whilst the research work demonstrates that it is possible to move towards Renewable and Environmentally friendly Energy Carriers, it also clearly highlights the struggle of keeping this energy cost-effective enough to compete with Fossil Fuel. This points to the need for sharper focus to be placed on PEM Electrolyzer Technology. For, as soon as more resources are poured into this technology then cost reduction is inevitable. It is recommended that future work concentrates on PEM Technologies.

Also, it is recommended that design consideration be given to PV modules to accommodate the flow of cooling water over the back surface. Presently, all the electrical connections are accessed from the back of the modules. This presents a challenge to the smooth flow of the cooling water.

Finally, it was surprising to find that sub-cooling (below 25 $^{\circ}$C) the module produces a voltage that was higher than what the manufacturer's specified. It would be interesting to investigate, further, the effects of sub-cooling on PV cell output.

7.6   Proposed Publications

As a way of engaging the wider community in the finding of this research, the following are papers submitted and to be submitted to the International Journal of Renewable Energy:

1. Theoretical and operational thermal performance of a 'wet' crystalline silicon PV module under Jamaican conditions.
(Status: Accepted, Int. Journal of Renewable Energy, Vol.34, pp. 1655-1660, 2009)

2. Impact of a Solar-Powered Adsorption Cooling System on a PV Module
(Status: Submitted, Int. Journal of Renewable Energy, August, 2009)

3. Effects of Thermal Management on a Solar-Hydrogen Fuel Generation Plant
(Status: Revising; to be submitted September, 2009)

APPENDICES

APPENDIX A: MatLab Codes for Heat Conduction in a PV Cell

```matlab
syms x
L  = 0.003;          %m
p  = 0.0015;  %position of in slab
al = 9.07e-5     %thermal diffusivity of silicon, m2/s
k  = 130;         %thermal conductivity of silicon, W/m.degC
t  = 0.1; %input('input the value of t = ')   %sec
fx = 60;  %initial temperature
UL = 28;  %temperature of cooling water,degC
qr = 1000;  %solar radiation, W/m2
Qx = UL + (qr*(L-p)/k)   %Steady state temperature,degC
sum = 0;         % initializing Iteration

% Iteration Process
xL = [0:0.0001:p];
for n = 1:10;
    Fn = (2/L)*int(((fx-Qx)*cos((((2*n)-1)*pi*x)/(2*L))),x,0,p);
    ep = exp(-al*((((2*n)-1)*pi/(2*L))^2)*t)
    cs = cos((((2*n)-1)*pi*xL)/(2*L));
    sum =sum + eval(Fn)*ep*cs

end


%Final temperature of PV Cell at any point(x)and time(t)
 Uxt = (Qx + sum)'         %Temperature of cell

a = xL;
b  = double(Uxt);

plot(a,b,'b');
hold on;
```

APPENDIX B: MatLab Codes for Heat Conduction Through a Porous Medium

```
R = .0095;                          % outer radius of bed
t = 240;                            % time, sec
T0 = 41;                            % tmperature of bed at time = zero; degC
T1 = 48;                            % temperature of copper surface; degC
Ks = .3;                        % thermalconductivity of charcoal (W/mK)
Kf = 0.19;                          % thermalconductivity of methanol (W/mK)
e = 0.476;                          % void fraction of bed
Ke = Ks*(1+ (((3*e)*(1- (Ks/Kf)))/((1-e)+ (2+e)*(Ks/Kf)))); %effective
thermal conductivity of bed (W/mK)


Rhof = 791.3;                       % density of methanol kg/m3
Rhos = 190;                         % density of charcoal (kg/m3)
Spf = 2550;                         % specfic heat capacity of methanol J/kgK
Sps = 1000;                         % specific heat capacity of charcoal J/kgK
RhoCpe = (e*Rhof*Spf + (1-e)*(Rhos*Sps)); %effective (density x specific
heat capacity)
AlSq = Ke/RhoCpe;                   % Alpha square
FinT = [];


%Development of Bessel Function
Joz = [2.4048 5.5201 8.6537 11.7915 14.9309]; %first five zeroes of J0
lamda = Joz/R;
for r = [0:0.001:R];                % arbituary radius
ep = exp(-(lamda.^2)*AlSq*t);
b = besselj(0,lamda*r);
c = lamda.*besselj(1,lamda*R);
U = sum((ep.*b)./c);
FinT = [FinT;T1 + (2*(T0-T1)*U)./R];
end


r = [0:0.001:R];
plot(r,FinT,'b');
hold on;
```

APPENDIX C: Energy Balance on SPAC System

```
alpha = 0.87;          % absorption coefficient of copper, range (0.87 - 95)
D = 13.38;             % coefficient of D-A eqn: Wang L.W. et. al.
e = 0.476;             % void fraction of bed
Itot = 13.9e006;       % total solar radiation over period (J)
L = 1.0;               % length of tube (m)
Lmet = 11e005;         % latent heat of vaporization of methanol (J/kg)
Mbed = 0.167;          % combined char/methanol mass (kg)
MCu =  1.6;            % mass of copper (kg)
Mchar = 0.12;          % mass of charcoal (kg)
Mwat = 1.00;           % mass of water (kg)
n =1.5;                % coefficient of D-A equation: Wang L.W et.al
pi = 3.142;            % pi
r = 0.0095;            % radius of tube(m)
Spf = 2550;            % specfic heat capacity of methanol (J/kgK)
Sps = 1000;            % specific heat capacity of charcoal (J/kgK)
SpCu = 385;            % specific heat capacity of copper (J/kgK)
Spwat =4180;           % specific heat capacity of water (J/kgK)
t = 25200;             % overall time (sec)
Tamb = 23;             % ambient temperature (C)
Ttube = 64;            % temperature of tube (C)
Tbed = 325;            % temperature of desorption bed (K)
%Tdes = Tbed           % desorption temperature of bed
Tcond = 303;           % temperature of condenser (K)
Tevp = 21;             % temperature of water in evaporator (C)
U = 10.4;              % tube heat-loss coefficient (W/m2K)
Xo = 0.5;              % max mass concentration of methanol (kg met/kg char)


% desorption energy J/kg
hdes = Lmet*Tbed/Tcond;


% combined char/methanol specific heat capacity J/kgK
ComCpe = (e*Spf) + ((1-e)*Sps);


%D-A Equation: mass of methanol desorbed (kg)
Xm = Xo*exp(-D*((Tbed/Tcond)-1)^n)*Mchar;


% Input Energy, Ein (J)
Acu = pi*r*L;
Ein = Acu*alpha*Itot


%Energy Lost from system, Elost (J)
Elost = U*t*Acu*(Ttube - Tamb)


%Stored Energy, Est (J)
Est = (Mbed*ComCpe*(52-23)) + (MCu*SpCu*(64-23))


%Energy Desorbed from Bed, Eout (J)
Eout = hdes*Mchar*Xm


%Temperature change in evaporator water (C)
TempDropWater = (Xm*Lmet)/(Mwat*Spwat)


%System COP:
COPsys = (Xm*Lmet)/Ein
% System Energy Balance (J)
balance = Ein -Est - Eout - Elost
```

APPENDIX D: Instrumentation

The instruments used in the execution of the experiments are listed here along with their degree of precision.

Pyranometer - Kipp and Zonen CM1

ISO classification; used for solar irradiation measurements with the following specifications:

- Non stability (change/year) — 0.5%
- Non linearity (0 - 1000 W/m2) — 0.6%
- Directional error (at 80 ° with 1000 W/m^2 beam) — $\pm$ 10 W/m^2
- Temperature dependence of sensitivity — $\pm$ 1% (-10 to 40 ^{o}C)
- Operating temperature — -40 to +80 ^{o}C

Data-Logger - Campbell's CR23X

used to record all measurements

Thermocouple - T Type

- Accuracy — $\pm$ 1 ^{o}C

PEM Electrolyzer StaXX2

- Electrode area — 2 cells of 16 cm^2 each
- Power — 15 W at 4 Vdc
- Permissible voltage — 3.0 – 4.0 Vdc
- Permissible current — 0 – 4.0 Adc
- Gas production (H_2) — 65 mL/min

PV Module 1

- Eight cells
- Rated voltage — 4.5 V

PV Module 2

- Model — SUN-13
- Rated Power — 13 W
- Rated Voltage — 4.8 V
- Rated Current — 2.7 A

- Open Circuit Voltage   5.9 V
- Short Circuit Current   3.06 A

Standard Test Conditions: 1000 W/m^2, AM 1.5 and 25 $^{\circ}$C – Made in China

Calibrated Sieves

- USA Standard Testing Sieve
- A.S.T.M   E-11
- Number 18   1.00 mm

- Canadian Standard Sieve Series
- Tyler Equivalent   12 mesh
- Number 14   1.40 mm

Electronic Scale

- Manufacturer   Sartorius
- Model   CP2202S
- Accuracy   ±0.01% - ISO 9001 standard

Multimeter

- Manufacturer   Kosmos
- Model   RE830B   CAT II

Voltage Divider

- Manufacturer   Campbell's
- Model   VDIV 10 - 1

Current Shunt

- Manufacturer   Fluke

- Model   80J-10
- Rated   10 amp 100 mV
- Accuracy   ±0.25%

APPENDIX E: Physical Parameters for Simulations

Main Input Data for Simulations

Symbol	Parameter	Value	Unit
Heat transfer in PV cell			
α	Thermal diffusivity of silicon	9.07e-5	m^2s^{-1}
k	Thermal conductivity of silicon	130	$Wm^{-1}K^{-1}$
L	Thickness of PV cell	0.003	m
q_o	Solar irradiance	1000	Wm^{-2}
U_L	Temperature at back surface	28	^oC
Heat transfer in porous medium			
C_{pf}	Specific heat capacity of methanol	2550	$Jkg^{-1}K^{-1}$
C_{ps}	Specific heat capacity of charcoal	1000	$Jkg^{-1}K^{-1}$
e	Void fraction of bed	0.476	
K_f	Thermal conductivity of methanol	0.19	$Wm^{-1}K^{-1}$
Ks	Thermal conductivity of charcoal	0.3	$Wm^{-1}K^{-1}$
R	Outer radius of bed	0 .0095	m
ρ_f	Density of methanol	791.3	kgm^{-3}
ρ_s	Density of charcoal	190	kgm^{-3}
Energy Balance on SPAC System			
ά	Absorption coefficient of copper	0.87	
c_o	Orientation factor	466.3	$Wm^{-2}K^{-e}$
Ð	Coefficient of D-A eqn	13.38	
E_{tube}	Emissivity of copper	0.03	
h_w	Wind heat transfer coefficient	16.8	$Wm^{-2}K^{-1}$
I_{total}	Total solar irradiance	13.9e006	J
$\mathcal{L}$	Heat of vaporization of methanol	11e005	Jkg^{-1}
n	Power coefficient of D-A equation	1.5	
n_{pls}	Number of plastic wrap	1	
T_{amb}	Ambient temperature	296	K
T_{tube}	Temperature of tube (C)	337	K
T_{bed}	Temperature of desorption bed	325	K
T_{con}	Temperature of condenser	303	K
T_{evap}	Temperature of water in evaporator (C)	294	K
U	Overall heat-loss coefficient	10.4	$Wm^{-2}K^{-1}$
Xo = 0.5;	Max. mass concentration of methanol	0.5	$kgkg^{-1}$

LIST OF REFERENCES

REFERENCE LIST

Aghbalou F., Mimet A., Badia F., Illa J., El Bouardi A., Bougard J. *Heat and Mass Transfer During Adsorption of Ammonia in a Cylindrical Adsorbent Bed: Thermal Performance Study of a Combined Parabolic Solar Collector, Water Heat Pipe and Adsorber Generator Assembly*. Applied Thermal Engineering. Vol.24, pp.2537-2555, 2004.

Abdolzadeh M., Ameri M. *Improving the effectiveness of a photovoltaic water pumping system by spraying water over the front of photovoltaic cells.* Renewable Energy, Vol 34, pp 91-96, 2009.

Angrist S. *Direct Energy Conversion*. Boston: Allyn and Bacon; 1982.

Anyanwu E.E. *Review of Solid Adsorption Solar Refrigerator 1: An Overview of the Refrigeration Cycle*. Energy Conversion and Management. Vol. 44, pp.301-312, 2003.

Anyanwu E.E. *Review of Solid Adsorption Solar Refrigerator II: An Overview of the principles and theory*. Energy Conversion and Management. Vol. 45, pp.1279-1295, 2004.

Anyanwu E.E., Oteh U.U., Ogueke N.V. *Simulation of a solid adsorption refrigerator using activated carbon/methanol adsorbent/refrigerant pair.* Energy Conversion and Management. Vol. 42, pp. 899-915, 2001

Araki K., Uozumi H., Yamaguchi M. *A Simple Passive Cooling Structure and its Heat Analysis for 500 X Concentrator PV Module*. In: Conference Record of the Twenty-Ninth IEEE Photovoltaic Specialists Conference, pp.1568-71, 2002.

Badwal S.P.S., Giddey S., Ciacchi F.T.(2006). *Hydrogen and Oxygen Generation with Polymer Electrolyte Membrane (PEM)-based Electrolytic Technology*. Retrieved February 6, 2008 from www.springerlink.com/index/V**7**13T860J131L243.pdf.

Banker N.D., Srinivasan K., Prasad M. *Performance analysis of activated carbon + HFC-134a adsorption coolers.* Journal Carbon. Vol 42, pp. 117-127, 2004.

Booth D., Pyle W. (1993) *Hydrogen* as a *Heating Fuel*. Lecture #28. *www.mae.ufl.edu/NasaHydrogenResearch/h2webcourse/L28-Heatingfuel2.pdf*

Boubakri A., Guilleminot J.J., Meunier F. *Adsorptive Solar Powered Ice Maker:Experiments and Model*. Solar Energy. Vol. 69, pp.249-263, 2000.

Bourgeois R. (2006). *Advanced Alkaline Electrolysis.* GE Global Research Center. Retrieved February 6, 2008 from www.hydrogen.energy.gov/pdfs/review06/pd_8_bourgeois.pdf.

Brogren M., Karlsson B. *Low-Concentrating Water-Cooled PV-Thermal Hybrid Systems for High Latitudes*. In: Conference Record of the Twenty-Ninth IEEE Photovoltaic Specialists Conference, pp.1733-36, 2002.

Carabe J., Gandia JJ. *Thin-Film-Silicon Solar Cells*. Opto-Electronics Review, Vol. 12, No.1, pp.1-6, 2004.

Centurioni E., Iencinell D., Rizzoli R., Zignani F. *Silicon Heterojunction Solar Cell: A New Buffer Layer Concept With Low-Temperature Epitaxial Silicon*. IEEE Transactions on Electron Devices. Vol. 51, No. 11, 2004.

CIA – World Fact – Jamaica 2006. Retrieved June 23, 2007 from https://www.cia.gov/library/publications/the-world-factbook/print/jm.html

Clearwater Gas System. Retrieved November 14, 2008 from http://www.clearwatergas.com/bill/propane.asp

Conibeer G., Green M., Cho E.C., König D., Cho Y.H., Fangsuwannarak T., Scardera G., Pink E., Huang Y., Puzzer T., Huang S., Song D., Flynn C., Park S., Hao X., Mansfield D. *Silicon Quantum Dot Nanostructures for Tandem Photovoltaic Cells*. Thin Solid Films, 2008 (Elsevier-Article in Press).

Crabtree G.W., Dresselhaus M.S., Buchanan M.V. (2004). *The Hydrogen Economy.* PhysicsToday.Org. Retrieved July 15, 2007 from http://www.physicstoday.org/vol-57/iss-12/p39.html#bio

Critoph R.E., Turner L. *Heat Transfer in Granular Activated Carbon Beds in the Presence of Adsorbable Gases*. Int. J. Heat and Mass Transfer. Vol.38, No.9, pp.1577-1585, 1995.

Dahl J., Buechler K., Finley R., Stanislaus T., Weimer A., Lewandowski A. et al. *Rapid Solar-thermal Dissociation of Natural Gas in an Aerosol Flow Reactor*. Proceedings of the 2002 U.S. DOE Hydrogen Program Review NREL/CP-610-32405.

Demir H., Modedi M., Ulku S. *A review on adsorption heat pump: Problems and solutions*. Renewable and Sustainable Energy Reviews. Vol. 12 pp. 2381-2403, 2008.

DOE Hydrogen Program Progress Report (2005). *Low-Cost, High-Pressure Hydrogen Generator*. Retrieved February 10, 2008 from http://www.hydrogen.energy.gov/pdfs/progress05/iv_h_1_cropley.pdf

Duffie J.A., Beckman W.A. *Solar Engineering of Thermal Processes*. A. Wiley- Interscience Publication, 1991.

Durisch W, Bitnar B, Mayor J, Kiess H, Lam K, Close J. *Efficiency model for photovoltaic modules and demonstration of its application to energy yield estimation*. Solar Energy Materials & Solar Cells 2007; 91:79-84

EarthTrends (2001). World Resources Institute. *Share of Woodfuels in National Energy Consumption.* Retrived November 08, 2008 http://earthtrends.wri.org/text/energy-resources/map-219.html

Electrolytic Processes (2006). *HFCIT Hydrogen Production: Electrolytic Processes Reform*. Retrieved February 7, 2008 from http://www1.eere.energy.gov/hydrogenandfuelcells/production/electro_processes.html.

Engineering ToolBox. *Fuels and Higher Calorific Values*. Retrieved October 31, 2008 from: http://www.engineeringtoolbox.com/fuels-higher-calorific-values-d_169.html

Farahat M.A. *Improvement the Thermal Electric Performance of a Photovoltaic Cells by Cooling and Concentration Techniques*. In: 39th International Universities Power Engineering Conference, UPEC, Conference Proceedings 2, pp. 623-28, 2004.

Furushima K., Nawata Y. *Performance Evaluation of Photovoltaic Power-Generation System Equipped With a Cooling Device Utilizing Siphonage*. Solar Energy Engineering Vol.128, pp.146-51, 2006.

Gibson T.L., Kelly N.A. *Optimization of solar powered hydrogen production using photovoltaic electrolysis devices.* Int. Journal of Hydrogen Energy, Vol. 33, pp 5931-5940, 2008.

Goetzberger A., Knobloch J., Vob B. *Crystalline Silicon Solar Cell*. Chichester: John Wiley & Sons; 1998.

Graff K., Fischer H. *Carrier Lifetime in Silicon and Its Impact on Solar Cell Characteristics*. In: Seraphin BO, editor. Topics in Applied Physics-Solar Energy Conversion-Solid-State Physics Aspects, New York: Springer-Verlag Berlin Heidelberg, pp. 173-211, 1979.

Gregory S. *Statistical methods and the geographer.* London and New York: Longman; 1963.

Hamzaoui H., Bouazzi A.S., Rezig B. *Theoretical Possibilities of $In_xGa_{1-x}N$ Tandem PV Structures*. Solar Energy Materials & Solar Cells. Vol. 87, pp. 595–603, 2005.

Hauch A., Jensen S.H., Ebbesen S.D., Mogensen M. Durability of Solid Oxide Electrolysis Cells for Hydrogen Production. Retrieved, February 12, 2008 from http://www.risoe.dk/rispubl/reports/ris-r-1608_327-338.pdf.

Heliocentris Energy Systems Inc.
http://www.heliocentris.com

Hu C., White R. *Solar Cells: From Basic to Advance Systems*. New York: McGraw-Hill; 1983.

Huslage J., Rager T., Schnyder B., Tsukada A. *Radiation-Grafted Membrane/Electrode Assemblies with Improved Interface.* Electrochimica Acta Vol.48, pp. 247- 254, 2002

Hydrogen Economy Fact Sheet (2003). Retrieved June 30, 2007 from www.whitehouse.gov/news/release/2003/06/20030625-6.html

Hydrogen Fact Sheet-Hydrogen Production, Hydrogen Production – Steam Methane Reforming (SMR) . Retrieved March 22, 2009 from www.getenergysmart.org/Files/HydrogenEducation/6HydrogenProductionSteamMethaneReforming.pdf

Hydrogen Production and Delivery (2007). DoE Hydrogen Program. *Summary of Annual Merit Review Hydrogen Production and Delivery Subprogram*. Retrieved February 11, 2008 from www.hydrogen.energy.gov/pdfs/review07/42072-03_prod_delivery.pdf

Hydrogen Production lecture #6 (2005). Retrieved February 6, 2008 from www.mae.ufl.edu/NasaHydrogenResearch/h2webcourse/L06-prod2.pdf

Incropera F.P.; DeWitt D.P. *Fundamentals of Heat and Mass Transfer (5th Ed, pp. 68).* New Jersey, John Wiley & Sons, 2002.

Jing H., Exell R.H.B. *Adsorptive Properties of Activated Charcoal/Methanol Combinations*. Renewable Energy, Vol.3, No. 6-7, pp.567-574,1993.

Jing H., Exell R.H.B. *Simulation and sensitivity analysis of an intermittent solar-powered charcoal/methanol refrigerator*. Renewable Energy, Vol.4, No. 1, pp.133-149,1994.

Kaviany M. *Principles of Heat Transfer in Porous Media(2nd Ed).* Mechanical Engineering Series. Springer-New York, 1995.

King D., Kratochvil J., Boyson W. *Temperature Coefficients for PV Modules and Arrays: Measurement Methods, Difficulties, and Results*. In: Conference Record of the Twenty-Sixth IEEE Photovoltaic Specialists Conference, pp.1183-6, 1997.

Knier Gil. *How do Photovoltaics Work.* Science @NASA.
Retrieved February 12. 2008 from:
http://science.nasa.gov/headlines/y2002/solarcells.htm

Krauter S. *Increased Electrical Yield Via Water Flow Over the Front of Photovoltaic Panels*. Solar Energy Materials & Solar Cells , Vol.82, pp.131-37, 2004.

Kroposki B., Levene J., Harrison K. *Electrolysis: Information and Opportunities for Electric Power Utilities.* Technical Report, NREL/TP-581-40605. September 2006.

Lehman P. *Development of a PEM Electrolyzer: Enabling Seasonal Storage of Renewable Energy*. California Energy Commission. Energy Innovations Small Grant Program. CEC-500-2005-085, 2005.

Lemmini F., Errougani A. *Experimentation of a solar adsorption refrigerator in Moroco*. Renewable Energy, Vol.32, pp.2629-2641, 2007.

Li M., Sun C.J., Wang R.Z., Cai W.D. *Development of No Valve Solar Ice Maker*. Applied Thermal Engineering. Vol.24. pp.865-872, 2004.

Li M., Wang R.Z. *Heat and Mass Transfer in a Flat Plate Solar Solid Adsorption Refrigeration Ice Maker*. Renewable Energy. Vol.28, pp. 613-622, 2003.

Li Z., Sumathy K. *A Solar-Powered Ice-Maker with the Solid Adsorption Pair of Activated Carbon and Methanol*. Int. Journal of Energy Research. Vol. 23, pp 517-527, 1999.

Low-Cost Membrane Electrode Assemblies (2001). Advanced Manufacturing. Techniques and New Catalyst. Substrates Reduce Costs**.** Retrieved February 8, 2008 from www.eere.energy.gov/vehiclesandfuels/pdfs/success/membraneelect3_28.pdf.

Luque A., Sala G., Arboiro J.C. *Electric and Thermal Model for Non-Uniformly Illuminated Concentration Cells*. Solar Energy Materials and Solar Cells. Vol.51, pp. 269-290, 1998.

Markvart T., Castaner L. *Practical Handbook of Photovoltaics Fundamentals and Applications.* Elsevier Ltd. Oxford 2003.

Maycock P., Stirewalt E. *A Guide to the Photovoltaic Revolution*. Pennsylvania: Rodale Press; 1985.

Momirlan M., Veziroglu T.N. *Current Status of Hydrogen Energy*; Renewable and Sustainable Energy Reviews. Vol.6, pp.141–179, 2002.

Natural Gas Reform (2006). *HFCIT Hydrogen Production: Natural Gas Reform*. Retrieved February 10, 2008 from http://www1.eere.energy.gov/hydrogenandfuelcells/production/natural_gas.html

Ni M., Leung M.K.H, Leung D.Y.C. *Parametric Study of Solid Oxide Steam Electrolyzer for Hydrogen Production*. Int. Journal Hydrogen Energy Vol.32, No.13, pp.2305-2313, 2007.

Ni M., Leung M.K.H, Leung D.Y.C. *Energy and exergy analysis of hydrogen production by solid oxide steam electrolyzer plant*. Int. Journal Hydrogen Energy Vol.32, pp.4648-4660, 2007.

Panorama 2005: *Energy Consumption in the Transport Sector*. Retrieved June 28, 2008 from www.ifp.com/content/download/5751**6**/1274819/file/IFP-**Panorama**05_09-ConsommationVA.pdf

Poirier M.G., Sapundzhiev C. *CATALYTIC DECOMPOSITION OF NATURAL GAS TO HYDROGEN FOR FUEL CELL APPLICATIONS.* J. Hydrogen Energy, Vol.22, No. 4, pp.429-433, 1997.

Power Trip Energy Corp. *Photovoltaic History.* Retrieved Jan 14, 2008 from http://www.powertripenergy.com/pv_hist.htm

Properties of Fuels
Retrieved August 2, 2008 from
www.methanol.org/pdf/FuelProperties.pdf

Radziemska E. *The Effect of Temperature on the Power Drop in Crystalline Silicon Solar Cell*. Renewable Energy, Vol. 28, pp.1-12, 2003.

Rifkin J. 2003. *The Hydrogen Economy-After Oil*, Clean Energy from a Fuel-Cell-Driven Global Hydrogen Web. Emagazine.com January/February 2003Vol. XIV, no. 1. Retrieved July 3, 2007 from http://www.emagazine.com/index.php?toc&issue=8

Ronnelid M., Perers B., Karisson B., Krohn P. *Cooling of PV Modules Equipped with Low-Concentrating CPC Reflectors*. *ISES Solar World Congress, 1999.*

Rosen M.A., Scott D.S. *Comparative Efficiency Assessments for a Range of Hydrogen Production Processes*. Int. Journal Hydrogen Energy, Vol.23, No.8, pp. 653-659, 1998.

Rosen M.A. *Advances in hydrogen production by thermochemical water decomposition: A review.* Energy, pp 1-9, 2009.

Royne A., Dey C.J., Mills D.R. *Cooling of Photovoltaic Cells Under Concentrated Illumination: A Critical Review*. Solar Energy Materials & Solar Cells. Vol.86, pp. 451–483, 2005.

Sakoda A., Suzuki M. *Fundamental Study on Solar Powered Adsorption Cooling System*. Journal of Chemical Engineering of Japan. Vol.17, No.1, 1984.

Solomon B. D., Banerjee A. *A Global Survey of Hydrogen Energy Research, Development and Policy.* Energy Policy 34 (2006) 781–792

Spath P.L., Mann M. K. *Life cycle assessment of Hydrogen Production via Natural Gas Steam Reforming*. NREL/TP-570-27637 Revised February 2001.

Sumathy K., Li Z. *Experiments with Solar-Powered Adsorption Ice-Maker*. Renewable Energy. Vol. 16, pp. 704 – 707, 1999.

Sweelem E., Fahmy F., Abd-EI Aziz M. *Increased Efficiency in the Conversion of Solar Energy to Electric Power*. Energy Sources, Vol.21, pp.367-77, 1999.

The Jamaica Energy Policy Analysis 2005 (Web site) CABINET OFFICE. Retrieved June 23, 2007 from http://www.cabinet.gov.jm/docs/pdf/The%20Jamaica%20Energy%20Policy%20Analysis%202005.pdf

Trim D.W. *Applied Partial Differential Equations*. University of Manitoba. PWS-Kent Publishing Company, Boston, 1990.

Tropics. Retrieved June 20, 2007 from http://en.wikipedia.org/wiki/Tropics

Wang L.W., Wang R.Z., Lu Z.S., Chen C.J., Wang K., Wu.J.Y. *The performance of two adsorption ice making test units using activated carbon and a carbon composite as adsorbents*. Carbon, Vol. 44, pp. 2671-2680, 2006.

Wang R.Z., Oliveira R.G. *Adsorption Refrigeration-An Efficient Way to Make Good Use of Waste Heat and Solar Energy*. International Sorption Heat Pump Conference. Denver, Co, USA, June 22-24, 2005.

Wang W., Huang Y., Jung S., Vohs J.M., Gorte R.J. *A Comparison of LSM, LSF, and LSCo for Solid Oxide Electrolyzer Anodes*. Journal Electrochemical Society, Vol.153, No.11, pp A2066-A2070, 2006.

Waugh D. *The New Wider World*. Chelteham, UK. Thomas Nelson & Sons Ltd, 1998.

Wen J.C., Mason D.M. *Electrocatalysis on Solid Oxide Electrolytes*. Journal of Applied Electrochemistry Vol.8, pp.81-85, 1978.

Wheeler A.J., Ganji A.R. *Introduction to Engineering Experimentation*. Prentice Hall, N.J, 1996.

Yurum Y. *Hydrogen Energy System: Production and Utilization of Hydrogen and Future Aspects*. North Atlantic Treaty Organization Scientific Affairs Division in association with Kluwer Academic Publishers, Boston, 1995.

Zhang X.J., Wang R.Z. *Design and performance simulation of a new solar continuous solid adsorption refrigeration and heating hybrid system.* Renewable Energy. Vol. 27, pp.401-415, 2002.